UNIVERSITY OF NAIROBI

EVALUATION OF GROUND CONDITIONS FOR OPTIMAL SELECTION OF COAL MINING METHODS FOR MUI COAL DEPOSITS, KITUI COUNTY, KENYA

BY

NORBERT KINYUA MAMBO

I56/63949/2010

A research project dissertation submitted for examination in partial fulfilment of the requirements for award of the degree of Master of Science in Geology (Engineering Geology) in the Geology Department in the University of Nairobi

2015

DECLARATION

This research project dissertation is my original work and has not been presented for a degree in any other university.

Signature……..Date……..

Norbert Kinyua Mambo (I56/63949/2010)

This research project dissertation has been submitted for examination with our approval as university supervisors:

Signature……..Date……..

Dr. Edwin Dindi

Department of Geology, University of Nairobi

eedindi@uonbi.ac.ke

Signature……..Date……..

Prof. Eliud M. Mathu

Department of Geological Sciences, South Eastern Kenya University

emathu@seuco.ac.ke

DEDICATION

This research project is dedicated to my family; my daughters; Vanessa and Shirleen and their mother Margaret, my mum Margaret and my dad Cyril.

ACKNOWLEDGMENTS

First, I thank the Ministry of Energy and Petroleum for financially supporting me to undertake this Master Degree program. The University of Nairobi facilitated my admission to facilitate these studies.

Gratitude goes to my supervisors at the University, Dr. Edwin Dindi of Geology Department at the University of Nairobi and Professor Eliud Mathu of the Department of Geological Sciences at South Eastern Kenya University for their guidance during the entire period of this project. Professor Justus Barongo and Mr Aaron Waswa of the Geology Department at the University of Nairobi also offered valuable project advice.

Special regards go to Messers Musakhala and Njoroge Mbitu, both of Chemistry Department at the Ministry of Transport and Infrastructure, Messers Muchina and Nicholas, both of Civil Engineering Department at the University of Nairobi for advice into best practices with various laboratory procedures. Also, thanks go to Mr Peter Maingi of Kenya Soils Survey for the assistance to prepare the soils map for project area.

A vote of thanks go to Dr. Loke M.H., the developer of RES 1-D for offering his software as a freeware and for the direct advice on how to source and use the scientific input file format for the software.

Finally but importantly, I thank all the members of my family, my daughters Vanessa and Shirleen and their mother Margaret for their invaluable continual support and patience in this academic endeavour.

Above all, thank the Almighty God for all the innumerable blessings.

ABSTRACT

It is vital to establish scientific methods towards optimally mining coal to increase efficiency in knowledge and profitability. This project aimed to determine the ground conditions for coalmines development at Block C. Block C (an exploration area that covers about 131Km^2) is the contemporary coal frontier in Kenya that spans from Kateiko (North) to Yoonye (South) in Kitui County, Kenya. This coal, once mined will be used to harness national development which requires much electrical power energy to maintain.

In this project, known geological information and studies involving X-Rays fluorescence (XRF), apparent resistivity (VES) and unconfined compressive strength (UCS) were used to determine the ground conditions. Based on these studies, the challenges of coal mining and the applicability of open cast and subsurface mining methods at project sites were assessed.

Rock specimens that were used in this project were retrieved from coal boxes which are stored in a shed in Mathuki, Kitui County. Uniform compressive forces were used to press these specimens at constant rates. Measurements were recorded at failure points for the specimens and used in UCS computations. The harder specimens were analysed using the Dennison 2000kN Compression machine while the softer specimens were analysed in the UNESCO 50kN flexural loading/transverse frame loading machine. Next, the same specimens were dried in an oven at about 105°C for one hour and analysed for major elemental oxides contents using Shimadzu's energy dispersive XRF spectrometer and its proprietary FP software. Also, VES data (earlier acquired using SARIS Terrameter) were analysed using RES 1-D software.

The findings from this study shows that mudstones are the weakest rocks with UCS values ranging from 82.504 to 3,490.92kN/m^2. Shales are the strongest with UCSs ranging from 1,218.09 to 37,211.91kN/m^2. XRF analysis enabled the reclassification of majority of the specimens into muddy sandstones and two unique classifications. These are marlstones (previously silty sandstones) and shaley ironstones (previously muddy shales). The VES results revealed that the Commissioning Well's area has the largest stratum with the highest apparent resistivity (457m layer with 50,000Ω-m). On the other hand, Yoonye well's area has the largest stratum with the lowest apparent resistivity (492.5m layer with 0.45Ω-m). The isotropy of strata at Commissioning Well and FP 2 suggested that the optimal coal mining method here can be subsurface tunnelling. The anisotropy at FP 3, Katz. 3 and YO 2 suggested that large scaled open cast mining method can be suitable at these sites.

***Keywords*:** Coal, XRF, VES, UCS, Mining

TABLE OF CONTENTS

CHAPTER 2: LITERATURE REVIEW

CHAPTER 3: METHODOLOGY

CHAPTER 4: DATA ANALYSIS, RESULTS AND DISCUSSION

LIST OF FIGURES

LIST OF PLATES

LIST OF TABLES

LIST OF ACRONYMS

AAS	Atomic Absorption Spectrometry, in Geochemistry
CBM	Coal bed methane
CCT	Clean Coal Technologies
CMRR	Coalmine Roof Rating; in Coal Mine Design Procedures Engineering Geology
DTS	Diametral Tensile Strength, in CMRR procedures
EDX	Energy Dispersive X-ray, in Fluorescence Spectrometry
GoK	Government of Kenya
HQ/NQ/BQ	Notations for standard drill-well cores; Φ=63.5mm, Φ=47.6mm and 36.5mm, respectively
MMB	Mozambique Mobile Belt, in Tectonics
MoEP	Ministry of Energy and Petroleum, in Kenya Government
MoTI	Ministry of Transport and Infrastructure, in Kenya Government
NCAPD	National Coordination Agency for Population and Development, Kenya
NDMA	National Drought Management Authority, in Kenya
RMR	Rock Mass Rating; in Coal Mine Designs, Engineering Geology
SARIS	Scintrex's Automated Resistivity Imaging System, in VES survey
UoN	University of Nairobi, Kenya
UCS	Unconfined Compressive Strength; also Uniaxial Compressive Strength, in CMRR procedures
UCG	Underground Coal Gasification, in Coal Mining
VES	Vertical Electrical Sounding, in Geophysics
WRA	Whole Rock Analysis
XRF	X-Ray Fluorescence Spectrometry, in Geochemical

CHAPTER 1: INTRODUCTION

1.1 BACKGROUND

1.1.1 GENERAL INTRODUCTION

The key to mine coal resources successfully from any location lies in proper scientific and professional investigations the ground conditions. Some of these ground conditions include rock classifications, occurrences of aquifers, strata thickness, and strength distribution. Various geological tools are available to conduct investigations into such ground conditions. The aim of such initiatives is to find the applicability and optimal selection of coal mining methods (open cast or subsurface mining).

Recently, exploration confirmed the occurrence of economically viable coal deposits in Kitui County, Kenya. Kitui County lies between the equator and 3°0' 0"S and longitudes 37°30' 0"E and 39°0' 0"E and covers an area of about 30,496.5Km^2 (Infotrack, 2014).

Figure 1.1 show the administrative location of the project area within which the coal deposits have recently been discovered. The map legend indicates that the major rivers are given as black coloured lines while the blue coloured line indicates the new Kitui County boundary.

This study set out to investigate the subsurface rock conditions in the project area. The data that were used in the determination of subsurface conditions were obtained through subjecting rock samples to X-rays fluorescence spectrometry (XRF) and unconfined compressive strength (UCS) testing. In addition, vertical electrical sounding (VES) survey data for selected sites in the project area were used. A synthesis of these data was carried out in order to assess the applicability of selected mining methods (open cast or tunneling) as well as identification of the optimal mining methods for use at each of the selected mining method for the project sites.

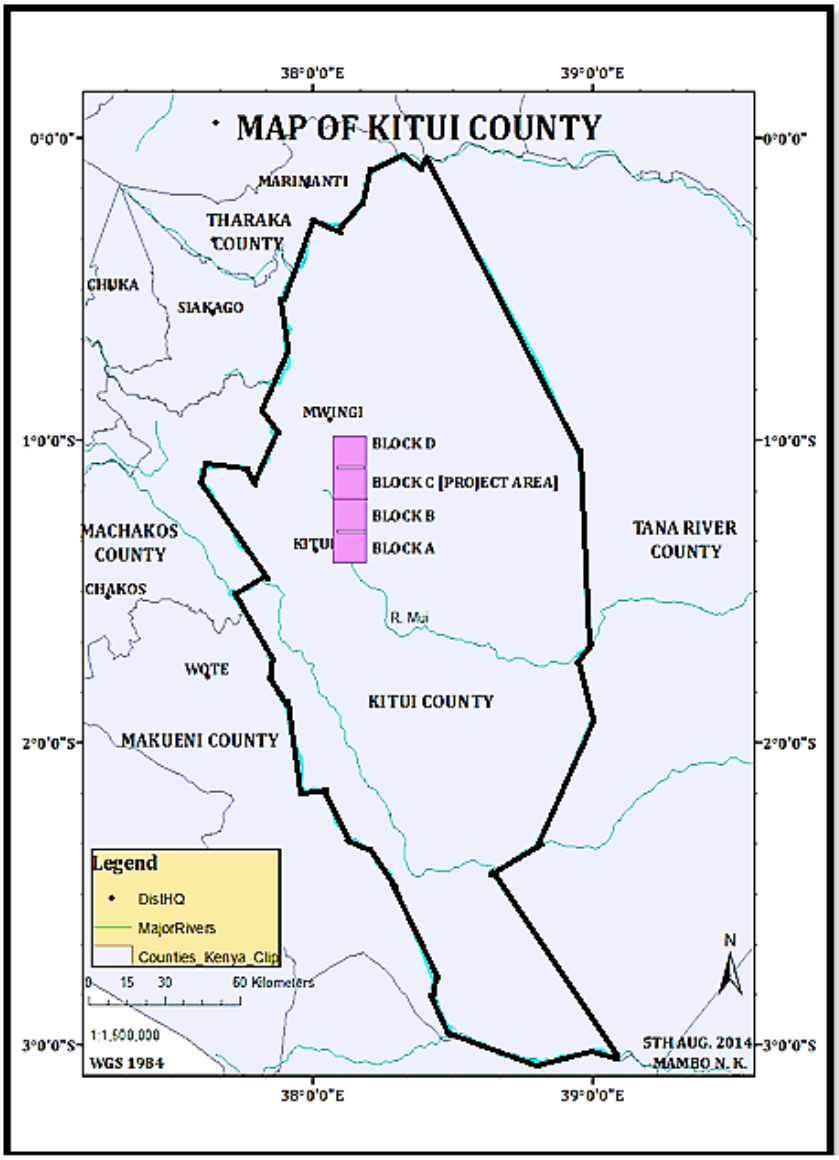

Figure 1.1: Map illustration of Block C, at relative location and administrative areas in Kitui County

1.1.2 WEATHER, CLIMATE AND VEGETATION

Weather, climate, and vegetation information for Block C is important to coalmining. Weather and climate helps the engineering geologist to understand ground water recharge system which influences ground water levels, which if high due to high rainfall trends then will need pumping out in the coal access tunnels. Similarly, for example if vegetation cover is scarce at the coal sites, will mean that natural ecosystems will be adversely interfered with minimally.

Block C falls under Kenyan regions classified as arid and semi-arid land (ASAL). This is because semi-arid vegetation (acacia trees and the like) thrive here. We also have a

persistently dry and hot weather pattern that hardly supports life in this region. Rainfall normally, is about 900mm per annum with potential evaporation highs of 1800 to 2000mm per annum (Droogers & Van loon, 2006). Figure 1.2 shows rainfall patterns in the project area.

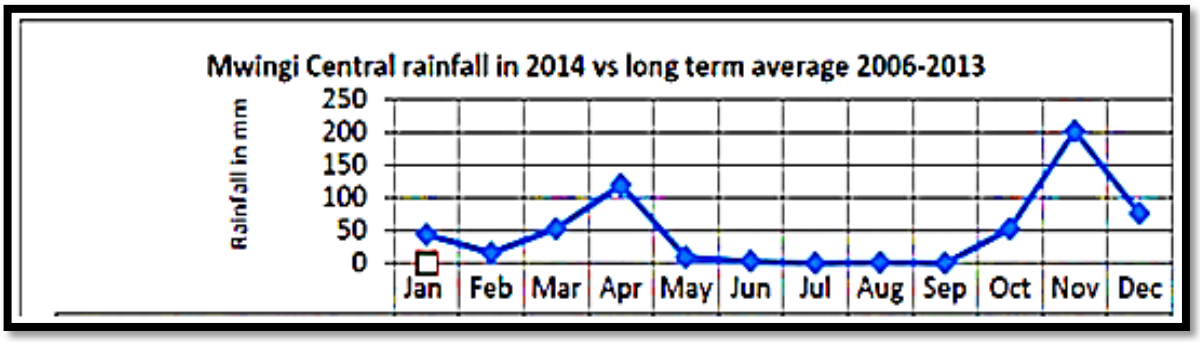

Figure 1.2: Depiction of rainfall patterns for Mwingi Central (near Block C, Mui Basin) after (NDMA, 2014)

1.1.3 PHYSIOGRAPHY AND DRAINAGE

A good example to consider is if the gradient of the ground surface at a coal site is very high, then coalmining will be more complex and costs will be high. Therefore, it is important to have basic physiography information in readiness. Also, traverses of the coal site by rivers can be of adverse effects especially during coalmining, which cannot be done if the tunnels are flooded with river water.

Mui Basin (Figure 1.3**)** is a sedimentary, Palaeogene, peneplain that is about 570m ASL, at Zombe in the South and about 680m ASL, at Mui Market. This area is enveloped between the Nuu hill ranges in the East and the Mutito-Andoa hill ranges in the West. These ranges are probably parts of the Palaeogene peneplain with inlier inselbergs forming some of the highest parts within them, (Sanders, 1954). Mui, an intermittent major river, is fed by numerous intermittent streams to form a dendritic river pattern from North East towards the South West in this region.

1.1.4 SOCIO-ECONOMICS

Socio-economic data can be used to project the cost and acceptability of mining coal in Mui Basin. For example, if the poverty levels are low, then this implies that land value can be also low and hence land compensation will be low which makes the project profitable. Large numbers of disabled children can benefit from a welfare project also known as corporate

social responsibility (CSR) and thus further cooperation and cohesion among the stakeholders.

A measure of wealth for the population at Mwingi for the year 2000 is shown in Table 1.1. The figures are relevant in that they reflect the high degree of need for the dissidents living in the project area towards improved and alternative means of livelihood, which in this case is coal mining.

Table 1.1: Socio-economic indicators (2000) after (NCAPD, 2005)

Total no. of households	60,099
Average households size	5.3
Number of female headed households	19,621
Number of children headed families	589
Children needing special protection	1,983
Number of disabled children	16,119
Absolute poverty (rural and Urban)	60%
Income from agriculture	75%
Income rural self-employment	6%
Wage employment	15%
Urban self-employment	2%
Number of unemployed	98,452

1.1.5 GEOLOGICAL SETTING

Geological information about coal sites can be directly helpful in the determination of which the optimal coalmining can be. For, example if a coal seam of economic value occurs between two hard sandstone formations, then tunnelling can be a viable option to mine if the depth of occurrence is great. In addition, if the coal occurs in highly fracture and faulted region, then due high levels of anisotropy, then open cast mining may be selected to safely mine the coal.

Four distinct rock units previously were mapped in Mui Basin. Mozambique Mobile Belt (MMB) rock outcrops reveal that the rocks comprise mainly of gneisses, granulites, and schists, (Mathu, 1980). Then there are lacustrine sediments in Mui Valley that mainly comprise of sands, carbonaceous clays, thin shales, and Neogene coal beds. Next, occur Neogene superficial deposits, which, mainly comprise of red low humus to brown residual soils, deposits of ironstones and dolomites and dark clay soils. There also are igneous intrusions that comprise of porpyhyric trachytes and some lamprophyres as found at Endau area, south of Mui Basin, (Sanders, 1954).

Nyamai et al (2003) have further studied the geology of this area. They have described this area to consist of MMB rocks that include gneisses, migmatites, diorites, gabbros, anorthosites, granites, limited andesitic volcanics and ultramafic bodies. These rocks are set in folds superposed into domes and basins, which are characteristic of *island*-arc assemblages. This is a common feature in the MMB. Major fault found in project area included the Mutito Fault, (Mathu, 1992).

The outcrops of Precambrian crystalline rocks occur in the surrounding hill ranges of Mutito to the West, Nuu Hills to the East, Endau Hills in the South East and Mathuki/Lundi area highlands in the North. Otherwise, the vast low-laying land enveloped by the hill ranges comprise mainly of Palaeogene sediments is known as Mui Basin.

Figure 1.3 gives the geology of the study area. Also shown on the figure is the exact extent of the study area (square box) and geological cross-section.

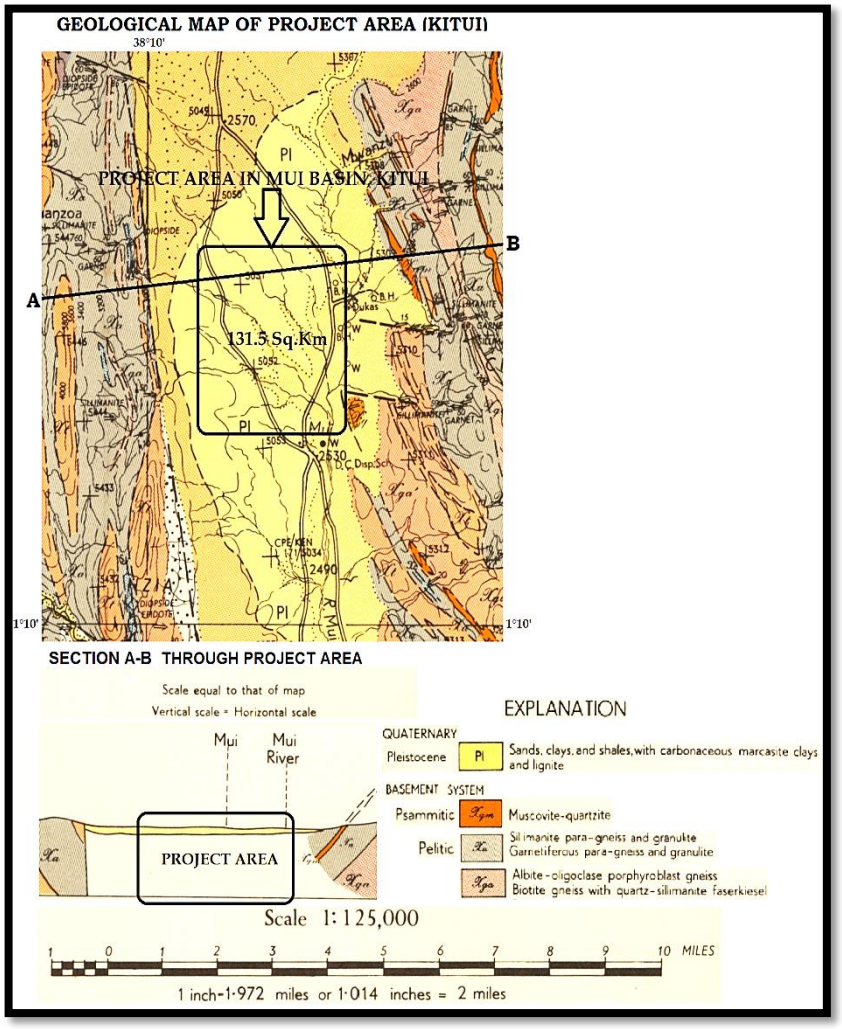

Figure 1.3: Geological map of Kitui County area. Delineated on the map is the location of the project area (box) after (Sanders, 1954)

Figure 1.4 shows the predominant soils in the project area. These are well drained, deep to very deep, dark red to strong brown, friable, sandy clay-to-clay soils (ferral sols). Relatively minor humic cambisols, lithisols/regosols, and luvisols occur to the W and NW. while feral sols with arenosols and luvisols occur in the SW of the project area.

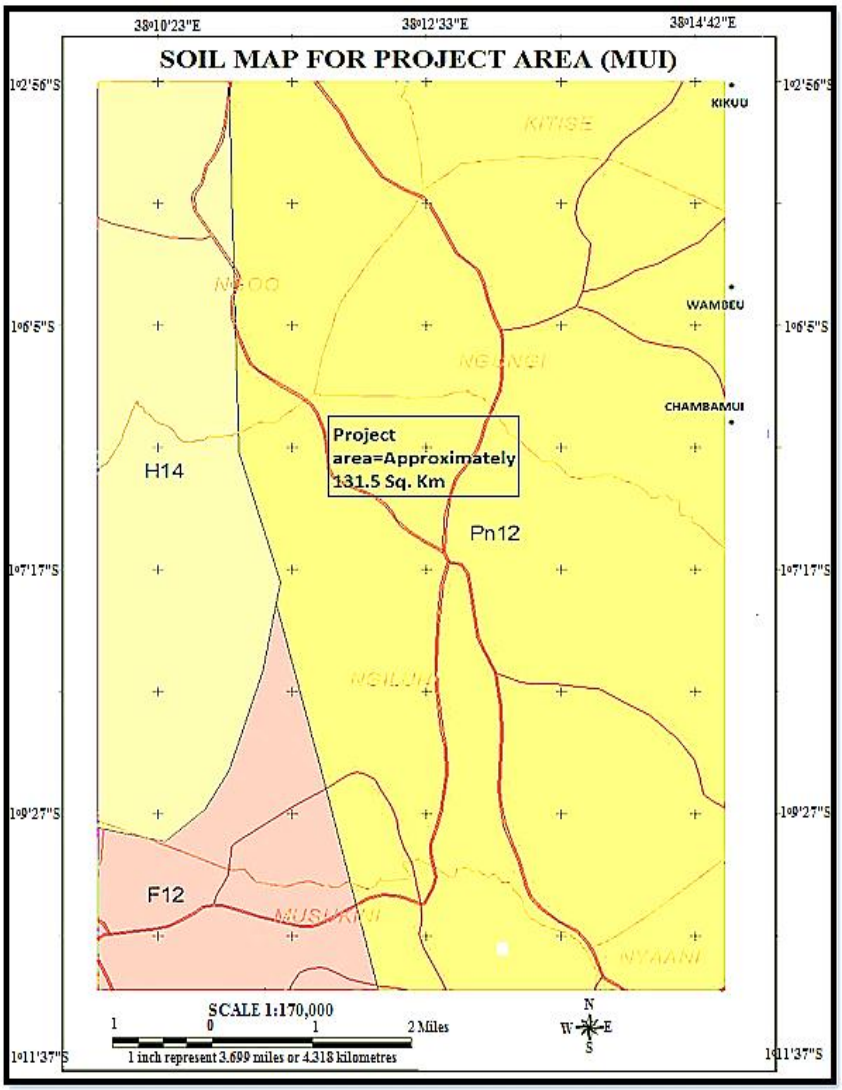

Figure 1.4: Soils map of Project area (Kitui) Modified to scale by Peter Maingi of Kenya Soils Survey; below is the map legend

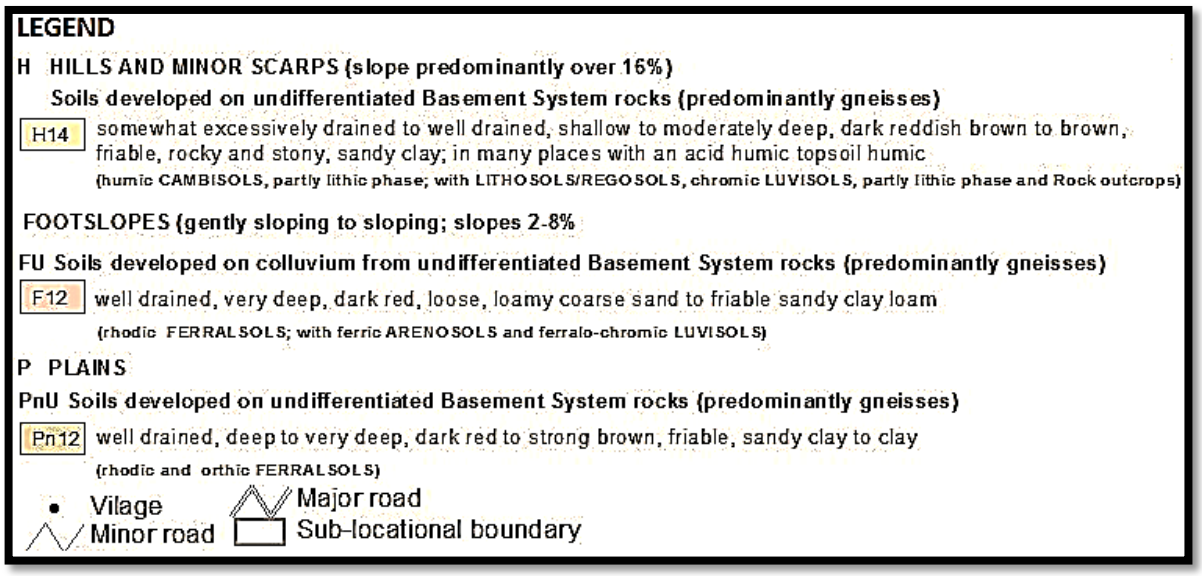

1.1.6 LITHOSTRATIGRAPHY

The generalized schematic litho-stratigraphic succession is sufficient to describe the subsurface in Block C. Just below the top soils at the top of the geological column are loose sediments, then, semi-lithified to lithified sediments (that include shales, sandstones, mudstones, siltstones and claystones; all of varying thicknesses) and, MMB system rocks at the bottom (Chebet, 2009; Chebet, 2009; Chebet & Otieno, 2009; Mutunguti, 2003; Mutunguti & Ndogo, 2007).

Coal formations also occur in this litho-profile mainly as intercalations within carbonaceous mudstones and shales, and as coal seams. The coal seams range in thickness from 0.3m to 13m and occur at depths of 20m to 320m bgl (Ndogo & Omenge, 2012).

1.1.7 STATUS OF COAL EXPLORATION AT PROJECT SITES

Currently, Kenya imports an average of 150,000 metric tons of coal and coke annually at a cost of about Ksh. 3 Billion. The Government has plans to put up a 600MW coal-fired power plant in Kilifi that will rely on imported coal until Kenya can produce her own indigenous coal (MoEP, 2011). As a country, Kenya has attained the milestones to have successfully explored and found coal and coal bed methane (CBM). The coal is mainly bituminous and sub bituminous with calorific value of about 18MJ/Kg. Exploratory works undertaken for a period spanning from 1999 to 2014 helped find these deposits. Subdivision of the approximately 500Km^2 of sedimentary Basin into four exploratory blocks was done as

illustrated in Figure 1.5 to ease this work. These were designated as Block A (Zombe-Kabati), Block B (Mutito-Itiko), Block C (Kateiko-Yoonye) and Block D (Karunga-Isekele) and measures 121.5Km^2, 117.5Km^2, 131.5Km^2 and 120Km^2 respectively (MoEP, 2011).

Block C is so far the most promising coal exploratory area within Mui Basin. This area has about 56 coal exploration wells drilled to depths of 75m to 445m. Coal and carbonaceous mudstone are strata of greatest interest in terms of coal reserves in Mui Basin as a whole (MoEP, 2011). In addition, these coal seams are of bituminous and sub bituminous quality, have the longest traceable continuity and therefore bear the greatest relative coal tonnage (Foundation Piling, 2010).

So far, Block C and D are concessioned to a Chinese company and Blocks A and B are also in a similar process.

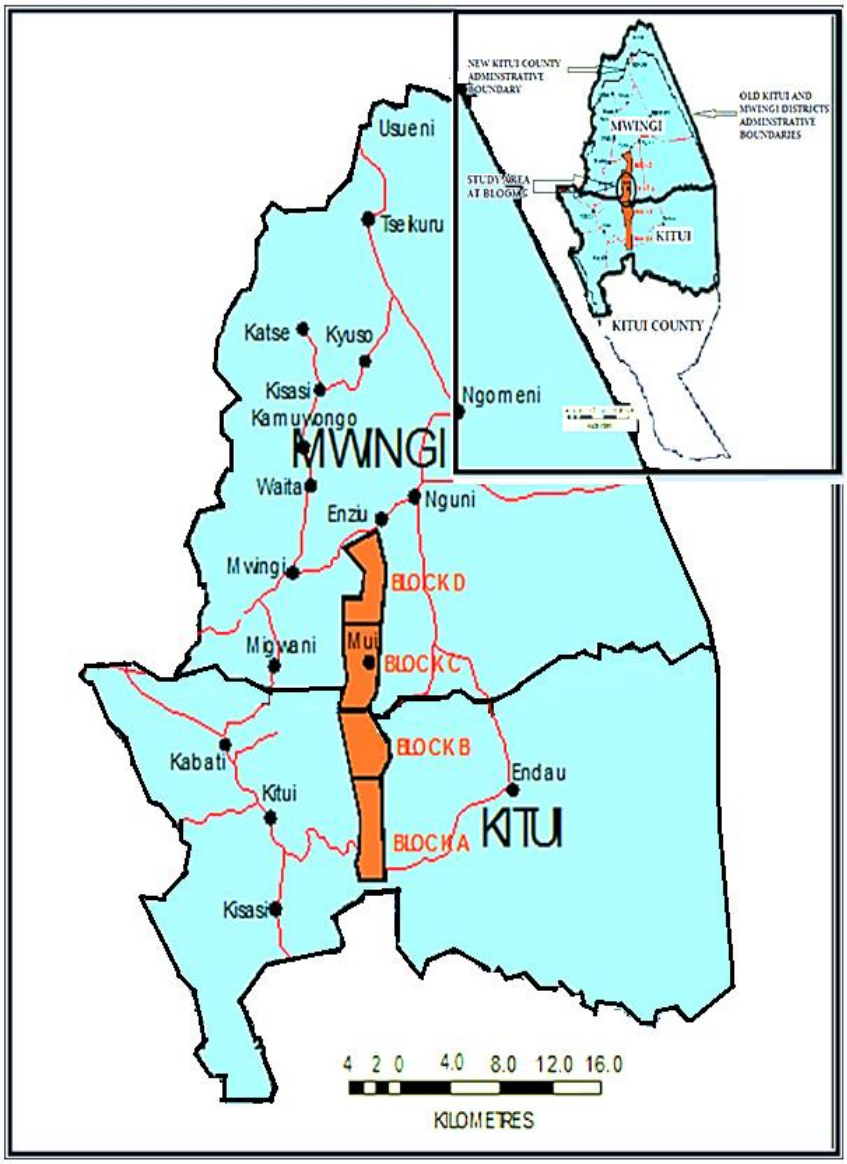

Figure 1.5: Map of Kitui coal exploratory Blocks A, B, C and D in Northern sections of the Kitui County, modified from (Ndogo & Omenge, 2012). Inset map shows approximate extension boundary of new Kitui County

1.2 STATEMENT OF PROBLEM

Coal describes clean, affordable, and reliable thermal source of electricity. The use for coal rates as safe, if used under clean coal technologies (CCT). CCT manages the potentially dangerous emissions (including carbon and sulphur gases). Subsequently, coal is competitively suitable to complement the use of alternative electrical power sources such as hydro, solar and wind and is safer than nuclear sources.

Kenya as a country has prioritized to find, develop, and harness coal for electrical power production. During the extensive exploration program dating from the year 1999 to 2012, the Ministry of Energy and Petroleum managed to drill 76 exploratory wells in Kitui County. Of

these, 42 wells indicated coal seam interceptions of various thicknesses and at different depths. At Block C (the project area), coal reserve estimates are to a tune of about 400 million tons. Power production projections expect 2000MW electrical power by 2017 and about 4500MW by 2030 (MoEP, 2015).

One major shortcoming towards the achievement of this goal has been identified as the lack of ready technical data for use by developers to enable secure coal production. Information on suitable coalmining methods is lacking. This information must be able to offer choices between open cast and subsurface tunnelling technology. To provide these choices, geological information is required.

This project uses XRF, VES and UCS to establish ground conditions at Block C in Mui basin. Plates 1.1 and 1.2 highlight some of the dominant problems experienced in the project area that reflect the subsurface conditions. Plate 1.1 depicts high intensity cracking that many structures erected in the area suffer, while Plate 1.2 demonstrates the abrupt changes in the soil characteristics with changes in moisture conditions in the area. In plate 1.1, it is apparent that the majority of the cracks run approximately perpendicular to the ground level. One possible explanation of this is that at least each major crack was produced by arching-up force that lie immediately below. If these buildings were affected a single crack prominently cutting across them, then it would be safe to say that the causant force was of a tectonic origin. Poor workmanship cannot be a major cause since there also would occur a mix of cracks that include those that run parallel to the ground level. This reasoning subsequently supports the theory that the most viable cause would be unstable soily foundations. These foundations need to be studied to suitable depths to adequately support all coalmining infrastructure.

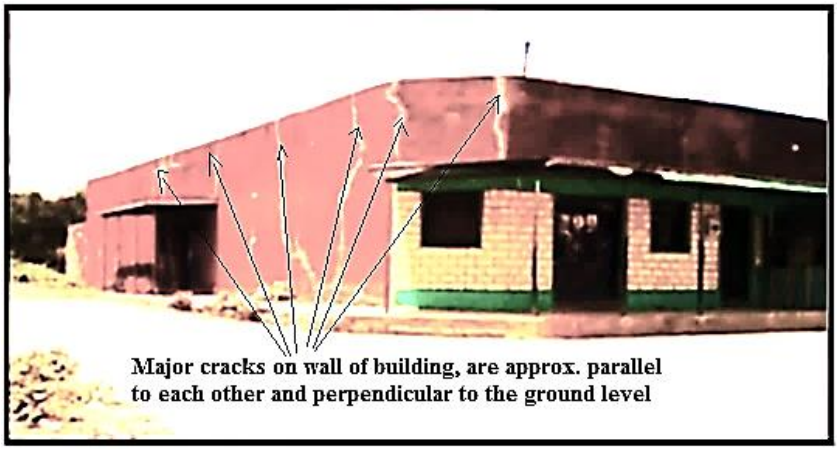

Plate 1.1: Photographic illustration of a cracks-infested prime building at Mutito-Andoa market centre in Mui Basin, can be an indication of challenging subsurface geological conditions

Plate 1.2: Photographic illustration of the problematic soils whose characteristics change drastically in response to changes in moisture conditions–an indicator of challenging subsurface conditions

1.3 AIM AND SPECIFIC OBJECTIVES

1.3.1 AIM

Excavations for mining coal deposits, either through open cast or tunnelling must be stable and safe. This can maximize coal production and increase financial profits. Almost all instances of natural ground are unstable in one way or another.

The main objective of this project was to determine site characteristics and the applicability of selected coal mining methods for use in Mui Basin. Key determinants included variation in rock types, strata thicknesses and subsurface strengths. In addition, studies on rock electrical properties and groundwater conditions were required.

1.3.2 SPECIFIC OBJECTIVES

The specific objectives for this project were to:

i. Determine the ground conditions through use of existing geological information and studies involving XRF, apparent resistivity and UCS.
ii. Determine the applicability of selected mining methods for the sites investigated.
iii. Identify the optimal mining methods for use at each of the five key sites in Mui basin.

1.4 JUSTIFICATION AND SIGNIFICANCE

It was important to undertake this study and especially at this particular time because the results are required in the ongoing coal mining plans in Kitui County. The Kenya Government has already issued the coal concession license for Block C, Kitui County to potential international companies. This collaboration of stakeholders requires information on how to start mining the coal. This study attempts to provide these valuable insights into how the coal in Kitui can be scientifically conducted, which is a major justification. It is envisaged that recommendations based on the findings of this study can help secure coal mining at Kitui County, which in turn can hasten the much-required national development.

In addition, this whole report can be valuable to the academia and other scientists in that it contributes to new research-based knowledge in the fields of engineering geology and mining.

To details, in this project, the author studies how the principles of geochemical classification, vertical electrical sounding, and unconfined compressive strength can be used to determine the suitability of open cast or tunnelling in coal mining in Kitui County.

Geochemical classification using X-rays fluorescence spectrometry was applied on soil samples drilled from the subsurface at the project area. This methodology was important to this study because high accuracies in soil classification were achieved. Visual classification and earlier classification by the Ministry of Energy and Petroleum personnel were used to add credibility to the classification results using XRF spectrometry. These classification results are important in that they were used in conjunction with other criteria to determine the most suitable coal mining methods per each site.

Electrical resistivity properties of the subsurface at the project area were also studied. Vertical electrical sounding was used to determine the thicknesses and apparent resistivities of the strata at the project site. The VES results were vital in the determination of which strata are critical in terms of isotropy and reflect the level of strengths. In addition, VES informs about ground water saturations and determines the thicknesses of strata, which include the overburden thicknesses. This information in turn can be used in the determination of the more suitable coal mining method, between open cast and tunnelling.

Of importance also were the unconfined compressive strengths results in the project area. These results showed which strata were either isotropic or anisotropic. This is very important in making choice as to which strata can form the roof or the floor of the coalmines at Kitui County. An example is that if the results are high then such strata are rigid enough to serve as the floors or roofs of the coalmine tunnels.

CHAPTER 2: LITERATURE REVIEW

2.1 LITERATURE REVIEW

2.1.1 COALMINES DEVELOPMENT CHALLENGES

Many challenges have been documented in the history of coalmines development. These challenges led to the misconception that coal mining is dangerous and almost an impossible activity. However, it is now generally appreciated that with proper scientific and technical measures coal mining can be accomplished successfully and safely. Some of the aspects in coalmines development that are challenging include how to avoid coalmines induced subsidence, coalmines sinkholes and coalmine floods (Ndogo & Omenge, 2012). Sinkholes are large dissolution cavities that open to the Earth's surface (Nelson, 2012). Mine subsidence is the downward movement of the ground surface due gravity in response to a loss of support at mine level (Knott, 2012). Coalmines floods involve the infilling of the mines with water mostly from natural sources either in the ground or at the surface. Good examples of coal mining hazards that were witnessed at various famous collieries include the subsidence at Shaanbei Jurassic Coalfields in China where an area of about 43.33km^2 had subsided by end 2006 (Xueyi *et al*, 2008). In addition, there are cases of sinkholes that occurred in 2003 in the currently abandoned lignite mines of Yamoto town (presently Higashi-Matsushima City) in Japan (Aydan & Tano, 2011). An example of coalfield floods is that witnessed at the Carboniferous and Permian Durham Coalfields in the Northeast of England. At this site, ground water levels initially at 150m bgl rose significantly from 1994-2004 (Culshaw *et al*, 2006).

A review of existing literature reveals that various case studies of coalmines exist. However, most of these studies are from countries with histories of coalmining. Thus, there are no such case studies in Kenya. This is true because there has never been any significant coal finds in Kenya in the past. Thus, the only information available on Kenya is on the recent finds in Mui Basin in Kitui County.

2.1.2 LITERATURE REVIEW ON XRF

Geologists from the Ministry of Energy and Petroleum (MoEP) have in the past attempted to classify the rocks of Block C, Mui Basin. This is documented in drill-well log reports. The rock classification method in their works involved visual observations of rock properties (rock fabrics and mineral grains).

Sanders (1954) also largely used visual observation of rock properties and fabrics during his classification of outcrop rocks from the larger Kitui area including Block C, Mui Basin.

Nyamai *et al* (2003) have classified metamorphic rocks below the sediments of Block C, Mui Basin. Their works suggested that the geology of a larger area of which Block C, Mui Basin was part of, comprises mainly of mica (biotite, muscovite) and /or hornblende schists and gneisses that occasionally showed the presence of staurolite, almandine garnet, kyanite, and sillimanite. Present also, are amphibolites (±garnets), migmatites, granitoid gneisses and granites, intrusive and meta-intrusive mafic and ultramafic rocks that included diorites, gabbros, anorthosites, peridotites and picrites. These metamorphic rocks underlie sediments at Block C, Mui Basin that were parent/ source to these sediments.

Agioutantis & Komnitsas (2004) demonstrated that rock classification for drill-core specimens was possible and gave worked examples from Florina and Elassona coal Basins, West Macedonia in Greece. These two researchers' works further suggested that the oxide per centage compositions for four drill-well core specimens from the two-mentioned coal basins be analysed using two modern geochemical methods. These two modern geo-chemical methods were atomic absorption spectroscopy (AAS) and inductively coupled plasma atomic emission spectroscopy (ICP-AES). Major elements results obtained by these two researchers are shown in Table 2.1.

Table 2.1: Range per centages oxide compositions for rocks from four coal basins in Greece, after (Agioutantis & Komnitsas, 2004)

	Oxide Type	Range in per centage composition
1.	SiO_2	41.81 to 58.08
2.	Al_2O_3	13.97 to 18.99
3.	Fe_2O_3	6.33 to 8.31
4.	TiO2	1.00 to 14.80
5.	CaO	7.95 to 14.80
6.	MgO	3.10 to 4.97
7.	K_2O	1.00 to 2.56
8.	Na_2O	0.05 to 0.43
9.	MnO	0.1 to 0.21
10.	P_2O_5	0.09 to 0.22
11.	SO_3	5.97 to 12.72

The two authors used data in Table 2.1 to infer: (i) the geology regarding basinal parent rocks and: (ii) how to monitor the environment during coal mining activities and, (iii) to discern if any other-types of mineral enrichments occurred within the coal Basins in West Macedonia, Greece. Similar studies generally recommended the use geochemical methods to classify

rocks. In addition, they recommended use of X-Rays fluorescence spectrometry method (XRF). One example of this is in a study to measure the thicknesses of ash deposits suspected to have erupted from Utah, Nevada where ancient supervolcanoes suspected to exist (Best *et al*, 2013).

2.1.3 LITERATURE REVIEW ON VES

As VES was one of the methods used in this study, the author conducted literature review on the concept of VES and its applications in coal mining within the sedimentary basins.

VES is a method in geophysics that entails the study of the subsurface to reveal the apparent resistivity of each significantly unique stratum and the corresponding stratum thicknesses (Rahim, 2013). This is true especially for sedimentary formations whereby the subsurface comprises of uniquely heterogeneous rock materials in significantly thick strata such that the two ambiguities of 1-D VES interpretation described as the principle of equivalence and the principle of suppression are minimal.

The principle of equivalence explains that different layered models can yield the same response. On the other hand, the principle of suppression explains the detectability of a relatively thin stratum depends on its apparent resistivity, such stratum can only be detected if its apparent resistivity value is significantly higher than that of the background strata, (Sqaysi, 2015; Thaxton & Courtier, 2015).

VES is one of the various methods in exploratory electrical resistivity methods and one of the most common. It entails the injection of low frequency alternating currency (AC) or direct current (DC) into the subsurface through a pair of steel electrodes and then measuring the potential difference (PD) in the closed circuit using another pair of steel electrodes plugged into the ground. The operator critically determines the distances of electrodes in correspondence with the intended depths of survey. Increment in depth of survey can be accomplished through successive increment in spacing of both pairs of electrodes. This is known as Schlumberger configuration. There are several arguments as to what the depth approximation coefficient should be. One-third of [AB] in a four-electrode array has been misused while one-sixth of [AB] has been favoured through theoretical derivations and practical tests (Barker, 1992).

Electrical resistivity methods including the VES method are based on Ohm's law. Ohm's law states that the current in a DC circuit is directly proportional to the applied voltage and inversely proportional to the resistance.

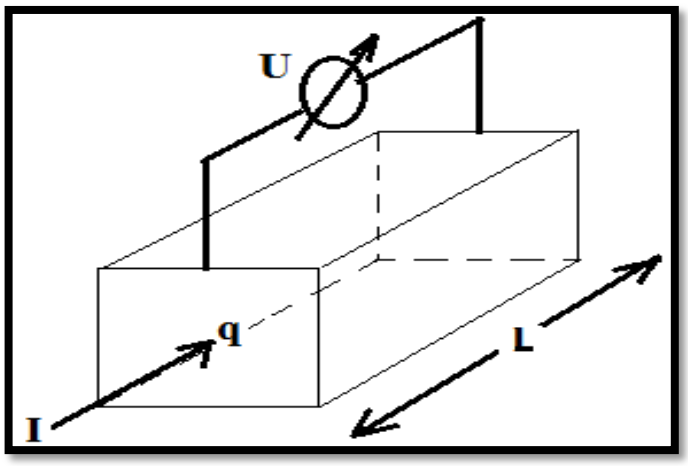

Figure 2.1: Graphical representation of Ohm's Law

Ohm's law is usually formulated as equation 2.1,

$V \alpha IR$.....equation 2.1

Where, V is the potential difference (Volts),

I is the current (amperes) and,

R is the resistance (ohms).

This equation can also be written as equation 2.2,

$\rho = k\Delta V/I$……...equation 2.2

Where, ρ is resistivity,

k is geometrical factor,

ΔV is change in potential difference and,

I is current.

The geometrical factor that applies to collinear arrays including the central symmetrical Schlumberger can be expressed as equation 2.3 (Rahim, 2013).

$k=2\pi/\{(1/AM)-(1/MB)-(1/AN)+(1/NB)\}$……equation 2.3

Where, AM, MB, AN and NB are electrode separation distances.

Rhett (2001) explains that whether a material obeys Ohm's law or not, its resistance is temperature related and can be described in terms of its bulk resistivity. The electrical resistivity of a finite length of wire is also dependant on its length and cross-sectional area. At constant temperature and using DC (not low AC as in this study), this relationship can be expressed as equation 2.4.

$R=\rho L/A$……....equation 2.4

Where, R is the resistance (ohm),

ρ is the resistivity (ohm-meter),

L is the length (meters) and,

A is the cross-sectional area (square-meters).

The inverse of resistivity is known as conductivity.

The recordings made in VES method are surface measurements of the potential field distribution due to the current passing through the ground. This potential is a solution to Poisson's equation; equation 2.5,

$\delta^2 V = 0$.....equation 2.5

Where, δ^2 is a second derivative operator and,

V is the potential difference.

For the potential (V) at a distance (r) from the current (I) on the surface of the earth (an infinite half space below), the solution is given in Rhett (2001) as equation 2.6,

$\rho = 2\pi r(V/I)$……equation 2.6

Where, ρ is the resistivity

V is potential difference

r is distance from current source and,

I is current.

And for (a finite half space) below, then,

$\rho = \pi V b\ (b+a)/Ia \sim \pi V b^2/Ia$.....equation 2.7

If a<<b

Where, a is distance between the potential electrodes and,

b is the distance between the current electrodes

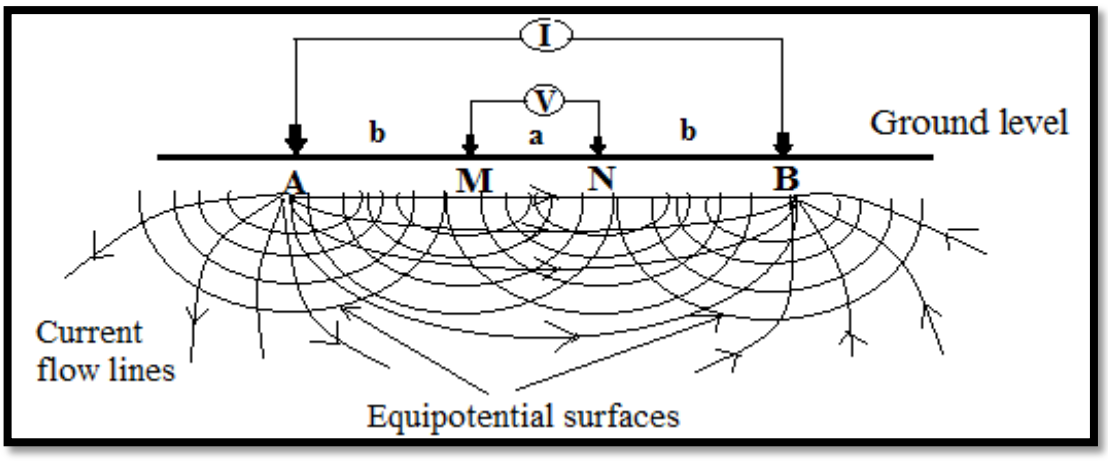

Figure 2.2: Representation of Resistivity parameters in Schlumberger configuration

The solution to Poisson's equation for each pair of current and pair of potential electrodes would give a general form for a measured potential with electrodes placed anywhere on the

surface. In practice, however, the current and potential electrodes are arranged most often in a collinear pattern including the Schlumberger configuration, (Rhett, 2001).

The resulting equation for the measured potential (voltage) difference is given in equation 2.8,

$$\delta V = I\rho/2\pi\{[(1/AM)-(1/MB)]-[(1/AN)-(1/NB)] \quad \text{.....equation 2.8}$$

Where, δ is a first derivative operator,

V is potential difference,

ρ is resistivity

I is current,

AM, MB, AN and NB are electrode separation distances.

By solving the above equation for ρ, the resistivity of the subsurface region can be determined. A homogeneous and isotropic half-space is assumed when deriving the above equation. Because the earth is neither homogeneous nor isotropic, a measured potential difference yields a resistivity value that is an average over the path length the current follows. Thus, we can determine only apparent resistivity, given by equation 2.9 (Rhett, 2001).

$$\rho_a = (2\pi\Delta V/I)\{1/[(1/AM)-(1/MB)-(1/AN)+(1/NB)]\} = \Delta V/I\ G(r) \quad \text{.....equation 2.9}$$

Where, G(r) is the geometric factor for Schlumberger array for this study.

The interpretation of VES has been achieved by use of master curves or in modern times computer algorithms namely inversion and forward modelling (Barker, 1992; Cardimona, 2002; Rahim, 2013).

To apply the concept of apparent resistivity, two case studies, one from Nigeria, and the other from India are considered. In the Nigeria case, Adekoya *et al* (2012) gave a range of 32 to 1775 Ω-m for coal seams at Ute area, South Nigeria using VES method. A lone drill-well made these observations possible.

On the other hand, Lokhande *et al* (2004) gave a range of 989 to 1632 Ω-m for a coal seam at northern part of Dharia coalfield at Dhanbad District in India using 2-D pole-dipole imaging in an experimental study.

Several other researchers (Abraham *et al,* 2013; Eke & Igboekwe, 2011; Lar *et al*, 2014) have reported on the use of VES for coalmines development.

2.1.4 LITERATURE REVIEW ON UCS

Foundation Piling Company Limited (2010) was the first company to be involved with coal in Mui Basin. The company conducted a feasibility study for coal mining at Block C in Kitui County. Recommendations from the study by the company provided part of the motivation for the current project. These included the need to measure soil/rock parameters for the reason that the behaviour of surrounding/host rocks after evacuation needed to be determined. This is with the understanding that surpassing of the magnitude of the resulting stresses to that which the ground can sustain often results in ground failure. The recommended tests were expected to provide information on how the subsurface can support the geo-design, including sizes of pillars and drifts to be constructed. In addition, protection from the ingression of unacceptable flow of ground water must be in place for under-ground coal mining. Rates of such ground water inflows are subject to permeability of rocks measured *in situ*. Therefore, the delineation of potential aquifers was vital.

Another significant study that related to the current project though not directly is that by Onyancha *et al* (2011). These researchers used UCS to calculate the allowable bearing capacities of the sub-surface in Nairobi area. In addition, Price (2009) proved that UCSs were vital representations of tentative amounts of pressure exerted by the built structures upon soils and, which the soils can support with respect to their shear failure and without appreciable settlement.

Lack of literature on coalmines development in Kenya resulted in the selection to study three case studies from the global library for review. These case studies were selected from among some of the most-renowned coalmine sites around the world. These were examined especially in regards to the methodologies that were and are still in use in the geo-design of coalmines and associated infrastructure around the world.

The first case study reviewed was a report on numerical modelling procedures for practical coalmines design (Zipf, 2006). These works suggested the derivation of two key inputs into the geo-design of coalmines from drill-well core specimens. These two key inputs are; (i) the isolation of strata of same geological properties, and, (ii) the determination of strata' strengths (either point load or unconfined compressive strengths (UCSs)). The processing of these two inputs assisted in the estimation of suitable strengths for use to design the rock-bolt anchorage system for the specific geological strata types.

Another notable work is that by Debasis *et al* (2001). Their study proposes that the important factors to consider in coalmines geo-design include rock mechanics procedures that are enacted into professional regulations, for example in the United States of America. Most, if

not all of these rock mechanic procedures rely on coalmine roof rating (CMRR). CMRR in principle, firstly, considers in situ weaknesses of mine roof due to discontinuities that are present within the rocks for example, joints, bedding planes and laminations. This team of researchers proceeded to explain that the study of geological discontinuities in rocks as opposed to the study of the intactness of rock via fabric observation, which makes a stable rock mass, is of key importance. Therefore, CMRR evaluated the inherence of bolted intervals, which also use a number (0-100), to depict the weakest to a solid roof. Again, in CMRR procedure, uniaxial compressive strength (UCS) and the diametral tensile strength (DTS) are determined. Further, the values of CMRR are broken down to strength equivalents, that is, (CMRR=0-45, means weak, 45-65, means moderate and >65 means strong). It is possible, using this strength classification scheme to come up with appropriate coalmine roof support requirements, mine layout, and an opening design for coalmines.

In yet another study report on UCS, are works by Van Der Murwe (2001). The viewpoints expressed in Van Der Murwe's report are derived from discussions from an international workshop that worked on coalmines' pillar design methodologies. The reason for this is that prior to the times of the workshop there existed diverse theories on how to tackle this matter. The end of the conference achieved no firm conclusions. From Van Der Murwe's report, it was clear that most of the coalmines' pillar design methodologies consider strength of pillars as a key parameter. The pillar strength should couple with other associated geo-parameters in an effort to find universally accepted coalmines' design formula or equations.

Two other studies also have been documented in the support of the use of UCS to design coalmines (Aryberk *et al,* 2015, Liayang, 2010). These two sets of authors recommended the use of UCS (or point loads, which produce similar results) in sub-surface infrastructural developments using rock quality designation (RQD) and rock mass rating (RMR) methods.

CHAPTER 3: METHODOLOGY

3.1 BASIC CONCEPTS

The methodology used to achieve the objectives in this project comprised mainly of three scientific methods. These are XRF, VES and UCS methods.

A brief revisit of the basics of these methods is given in Sections 3.1.1, 3.1.2 and 3.1.3.

3.1.1 CONCEPT OF XRF METHOD

The basic principle behind ED-XRF spectrometry test method is that the interaction between X-Rays (a beam of high-energy electrons fired from anode in the X-rays tube source) and a specimen cause emission of energy (in KeV) at a definite emission rate (in cps). This source is able to vary excitation energy and filters to tailor source profiles for lower detection limits. The energy dispersive multi-analyser, uses a super-cooled (liquid nitrogen at about -186°C) solid-state detector to monitor both the energy and number of photons over a pre-set measurement of time. A digital pulse processor (in the analyser software) automatically converts the spectral data (cps verses KeV) direct into read-outs of results (concentration/per centage verses type of element) using proprietary analytic software incorporated in Shimadzu's EDX-800HS system as shown in Figure 3.1.

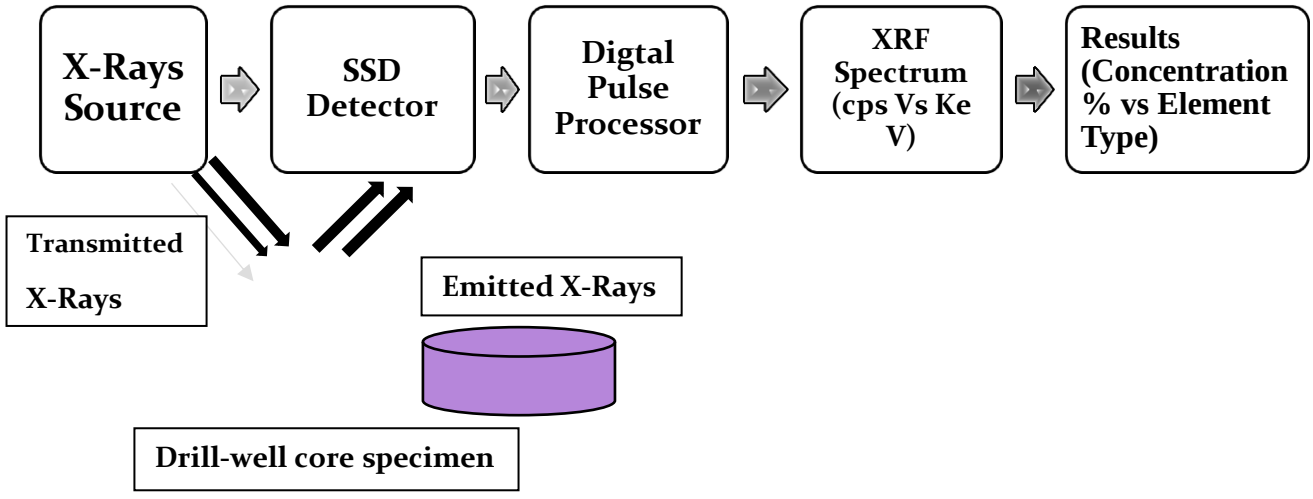

Figure 3.1: A schematic flow-chart to illustrate the principles of ED-XRF spectrometry

Refined results are then auto-printed, in table forms as shown in Shimadzu (2011). Theoretical calculations for quantization are used achieve the refinement. The modernized design of the EDX-800HS fluorescence spectrometry system by nature does not require the use of standard samples. Instead, the special primary X-Rays filters incorporated therein, are effective tools to automatically cutting out of the unnecessary background scatter of continuous X-Rays from the X-Rays tube. In the past, this scatter made it difficult to detect target peaks and its riddance consequently improved the detection sensitivity. This was especially the case with trace element analysis, for example, in the case of chlorine (Cl) whereby characteristic X-Rays from the X-Rays tube normally but unfavourably interfere and overlap with a target peak as shown by Shimadzu (2011). Theoretical filtering in Table 3.1 shows a number of representative measurement elements that remove X-Rays absorption. Rousseau (2013) recommends the classification of geological materials by use of Fundamental Principle (FP) method in XRF analysis.

In this project, the analysed data were obtained directly from the EDX-800HS fluorescence spectrometer system alongside their corresponding standard deviations.

Table 3.1: Five types of filters in FP software for EDX-800HS spectrometer by (Shimadzu, 2011)

Filter number (#)	Representative measurement elements
1	Cl
2	Cr
3	Hg, Pb, Br and Bi
4	Rh and Cd
5	Cd

Reconstruction of the mineralogies is possible from the provided clusters of elemental oxides obtained from ED-XRF analyses. This is done using the CIPW norm.

CIPW norm is one of the methods in normative mineralogy in geochemistry. Normative mineralogies attempt to calculate the idealised mineralogy of a rock specimen using the principles of geochemistry. CIPW norm was invented in 1931 by petrologists Cross, Iddings, Pirrson and a geochemist, Washington (Myron, 2002).

In spite of many assumptions/errors, CIPW norm method can be applied appropriately to assess silica saturation levels in rock specimens (Hess, 1989) and hence sand content in sedimentary rocks. Also, other closely associated chemical oxides in sedimentary rocks can be estimated including alumina, Fe_2O_3, TiO_2, K_2O, P_2O_5 and SO_3, each when coupled with

geological knowledge can be worked to reflect actual minerals and therefore the basic composition of a sedimentary rock as will be shown in Chapter 4 on data analysis.

Since this is a purely mathematical approach, the CIPW norm has been made simpler to calculate using computerised models. Such analytical program has been used in this project as written in MS Excel by Professor Kurt Hollocher, Geology Department at Union College in Schenectady, NY, 12308.

3.1.2 CONCEPT OF VES METHOD

VES is a method in geophysics, which allows for predictive detection of anomalous geological phenomena in the subsurface using electrical resistivity as the physical property. This state-of-the-art technology is applied commonly in various developmental projects including coalmining projects.

1-D VES survey data were used in this project to predict the strata thicknesses at Block C.

Equations 3.1 to 3.3 were specifically used in the measurement of apparent resistivity such that the, apparent resistivity is given by,

$(\rho_a)=kR$….....equation 3.1

Where, ρ_a is apparent resistivity,

k is geometrical factor,

R is resistance.

Moreover, resistance is given by,

$R=\Delta V/I$ ……equation 3.2

Where, R is resistance,

ΔV is change in potential difference,

I is current.

In addition, the geometrical factor for Schlumberger array, which was used in this project, is given by,

$k=2\pi/\{(1/AM)-(1/MB)-(1/AN)+(1/NB)\}$……....equation 3.3

Where, AM, MB, AN and NB are electrode separation distances, Figure 2.2.

Detailed information has been mentioned in Section 2.1.3.

3.1.3 CONCEPT OF UCS METHOD

UCS is a methodology in Geomechanics, which links Geology and Engineering. It deals with the analysis of soil and rock for their properties, under motion, with an aim to use them safely in developmental construction projects. In this project, the rock mechanics property, which was calculated, was the UCS.

UCS is regarded as one of the basic engineering properties from which the mining engineer can tell if geological materials are suitable for use as construction materials and specifically in coalmines development in this project.

UCS test is a special case of triaxial compression test where no lateral pressure/confining pressure is applied such that, $\sigma_2=\sigma_3$=zero. In addition, the volume of specimen is assumed to remain unchanged because this quick test allows no drainage. Compression machine presses the specimens at uniform rate of strain while taking measurements of lateral deformation and corresponding axial compressive force. The maximum compressive stress that is resisted by a specimen just before its failure is the UCS (q_u) and is given by Equations 3.4 to 3.6.

$q_u=F/A_c$ …...……Equation 3.4

Where, F is the deviator force and Ac is the corrected area of cross-section of specimen at failure.

$A_c= A_0/(1-\epsilon)$ …...…….Equation 3.5

Where, A_0 is the initial area of cross-section of specimen while,

$\epsilon=\Delta L/L0$…...……...Equation 3.6

Where, ϵ is the modulus of elasticity,

ΔL is change in length and,

L0 is the initial measurement of length.

Moreover, this is the axial strain at failure point (Ramamurthy & Sitharam, 2011).

For soils that fail with no or very small amounts of friction the result is that the undrained shear strength can be obtained from parameters C_U (cohesion) and ϕ_U (angle of friction) after plotting the Mohr-Coulomb model (Gainouscr, 2008) as shown in Figure 3.2.

Equations 3.7 and 3.8 are used to obtain the undrained shear strength.

$q_U/2$…..……Equation 3.7

Where, q_U=UCS……..Equation 3.8

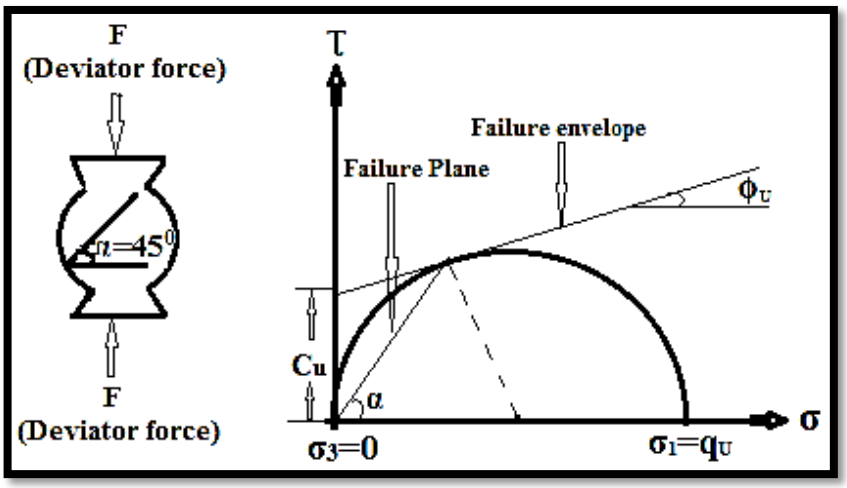

Figure 3.2: Schematic illustration of brittle failure at 45^0 during unconfined compression test (for $\phi \approx 0$ and c-ϕ soil) using a graph of shear stress verses normal stress, prepared from Mohr-Coulomb models in the internet

Calculations using standard formula/mathematical equations then were used to analyse the collected data sets.

Using compression, Equations 3.9 and 3.10 in Figure 3.2 it is trigonometrically correct that,

$\sin 2\alpha = \text{Opposite/Hypotenuse} = [\tau/(\sigma_1+\sigma_3)/2]$…..……Equation 3.9

Therefore,

$\tau = [(\sigma_1+\sigma_3)/2] \sin 2\alpha$…..…….Equation 3.10

In addition, for τ (maximum), $2\alpha = 90^{\circ}$. Moreover, $\sigma = 45^{\circ}$, hence brittle failure normally occurs at approximately 45° to the horizontal plane (Verwaal, 2004).

In this project, both professional procedures and scientific methods were applied. This combination helped to solve complex problems normally encountered in the course of UCS testing, as was the case with this project.

This combined method approach considered a number of essential factors. Firstly, that the sizes (diameters and lengths) of specimens did not influence deformation and UCS results in this project as in agreement with Sakamoto & Shogaki (2003). A check was made to ensure that the quantities of ratio of diameter-to-length ranged within scientifically acceptable margins (1:4) as shown in Figure 3.3. Secondly, that no index properties, such as water content, dry density, degree of saturation and others, the project specimens were to be

determined in this project. These were considered optional which was in agreement with Vulcanhammer (2001). Figure 3.3 presents the range of actual ratios data used for this project as indicated, (FP 3.3' 1.67 to Comm. Well's 2.90).

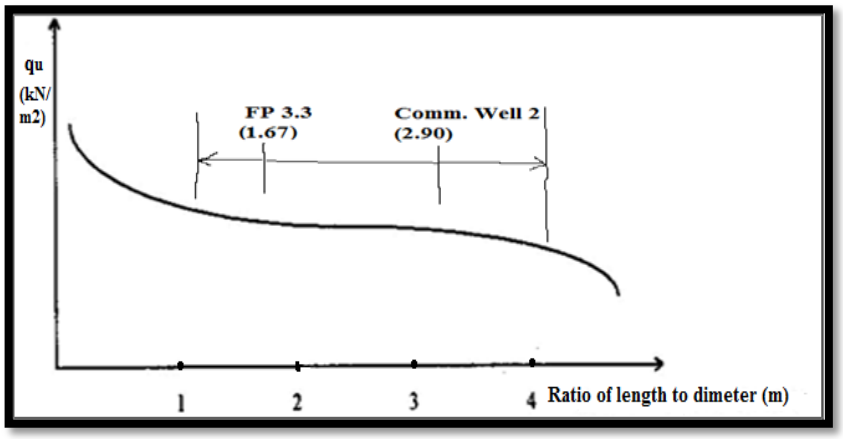

Figure 3.3: A schematic line-graph to illustrate the effects of varying specimens' length-to-diameter ratios verses UCS values and the range that is used in this this project, modified from (Lai & Olson, 2004)

Also, considered under UCS concept method are the effects of ages of these specimens (since their retrieval dates during drilling up to time of testing) as shown in Table 3.2. Debasis *et al* (2008), proved this phenomenon as quite influential towards the final UCS. This groups' works revealed that UCS values increased by about 60%, if the specimens dried in natural atmospheric humidity and in the process lost about 40% of the moisture content within approximately the first two weeks. Weak coal measure rocks of Pittsburgh coal-beds in Greene Co., PA revealed this inverse trend (Debasis *et al,* 2008). Increased atmospheric humidity during hot and wet seasons registered only slight increases in UCS at about 11%. This project applied this information in UCS method.

Table 3.2: Ages of specimens, from retrieval-date to test-date for Block C, Mui Basin

Name of drill well	Names of MoEP authors for well log reports	Date for drill core recovery from well (approximate)	Date for drill core specimens testing for UCS	Age of drill core specimen at time of test (approx.)
FP 2	Chebet Z. K.	February 2009	April 2013	Four (4) years, two (2) months
FP 3	Chebet Z. K.	April 2009	April 2013	Four (4) years
Katz. 3	Chebet Z. K. and Otieno J.C.O	September 2008	April 2013	Four (4) years, eight (8) months
Comm.Well	Mutunguti F. and Ndogo J.M.	December 2006	April 2013	Six (6) years, five (5) months
YO 2	Mutunguti F.	April 2003	April 2013	Ten (10) years

3.2 FIELDWORK METHODS

Project work included the choice of suitable research design and research-site selection methods as explained in Sections 3.2.1 and 3.2.2.

3.2.1 RESEARCH DESIGN METHOD

Research design method means either the structure (Kombo & Tromp, 2011), a scheme, an outline, or a plan (Orodho, 2003), or the blueprint for the collection, measurement and analysis of data, (Kothari, 2003).

The design for this project used both descriptive and correlational survey schemes. Descriptive design is a method of collecting information and reporting the findings while correlational design is a method that enables the assessment of the degree of relationship that exists between two or more variables, (Kombo & Tromp, 2003).

In this project, descriptive method involved investigations that focused on measurement of UCSs for the selected drill-well specimens. These data were used to map the subsurface source locations at suitably selected depth intervals using VES under the Schlumberger array. In the latter case, correlation of acquired data using geochemical results from XRF with the existing drill-well logs was done. The primary data obtained from the above tests were used to complement other secondary data retrieved and compiled from journals, books and the internet. This combination assisted in the production of a subsurface VES models enriched with UCS and corresponding XRF data. These then formed the partial design of coalmines development at Block C, Mui Basin.

3.2.2 RESEARCH SITE SELECTION METHOD

It was purposeful to focus on an area, which currently serves as the coal-energy development frontier in Kenya. Block C, Kitui County in South Eastern Kenya serves this purpose. Block C was the most researched into, at time of this project, regarding coal occurrence. The Block also has the highest coal production projections among the four Blocks namely, A, B C, and D, (Foundation Piling, 2010). Within Block C, which is the target area, a number of target sites are identified namely, Foundation Piling 3 (FP 3), Foundation Piling 2 (FP 2), Kathonzweni 3 (Katz. 3), Commissioning Well (Comm. Well) and, Yoonye 2 (YO 2), from North to South, respectively (Figure 3.4).

The indicated mining zones 1 to 5 (Foundation Piling 2010) are the richest coal areas within Block C in Mui Basin.

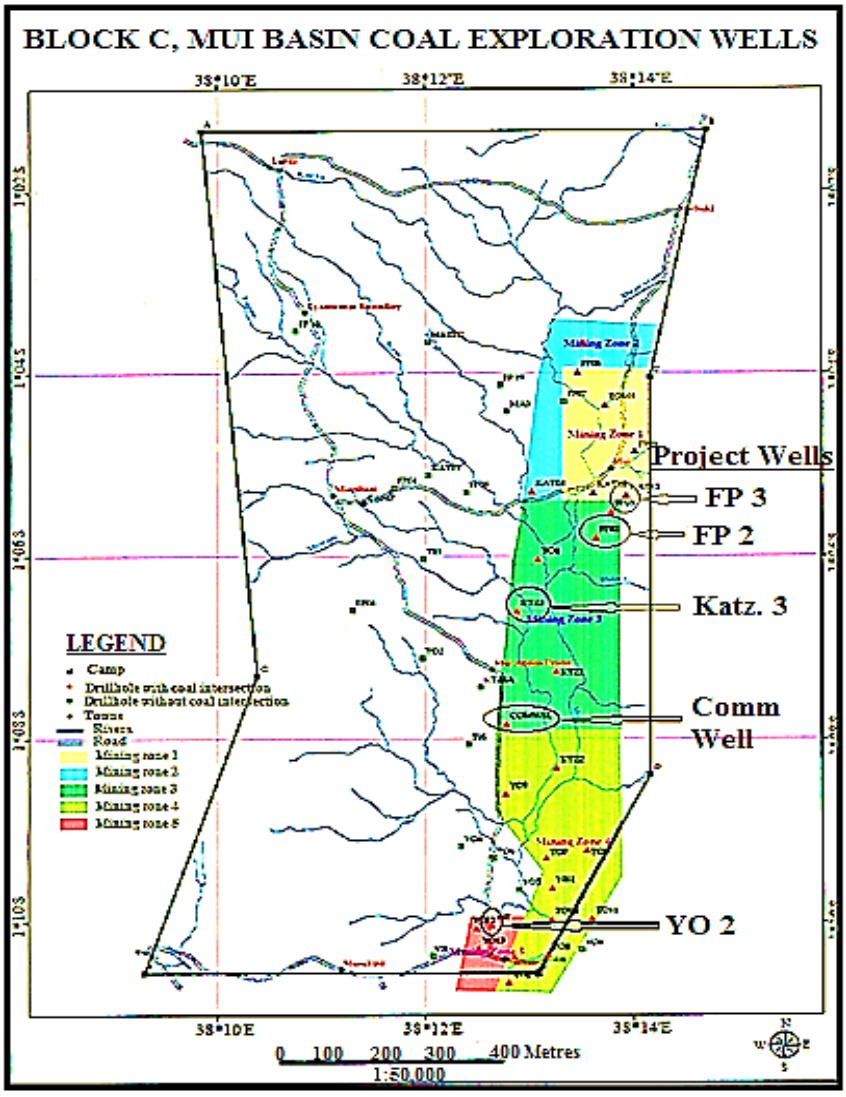

Figure 3.4: A map illustration for the project wells in Block C, Mui Basin in Kitui County, modified from, (Foundation Piling, 2010)

3.3 SAMPLING METHODS

It is essential to mention the sampling methods that were used in this project. Specimen population & size selection method and specimen sampling method have specifically been highlighted in Sections 3.3.1 and 3.3.2.

3.3.1 SPECIMEN POPULATION & SIZE SELECTION METHODS

Specimen population for this project described the whole set of drill core specimens from all the 56 (including the 32 with coal indications) drill wells that were obtained from Block C, Mui Basin. It was from this specimen population that a suitable specimen size was drawn based on the criteria indicated in Section 3.2. Specimen size referred to the drill well core specimens selected from specific drill-wells in Block C. These drill wells are FP 3, FP 2, Katz.3, Comm.Well, and YO 2.

Plate 3.1 shows semi-arid vegetation near Mathuki stores, North at Block C, Mui Basin in Kitui County. This photo was taken during the sampling session. Some of the core specimens sampled at the time are displayed in Plates 3.2 and 3.3. The rest of the plates on core specimens are included in Appendix A.1.

Plate 3.1: Semi-arid vegetation near Mathuki stores, North in B

Plate 3.2: Drill-core Specimen in box from Comm. well at depth of 239.83 metres bgl, muddy shales

Plate 3.3: Core specimen in box from Katz. 3 at depth of 321.0 metres bgl, muddy sandstones

Visual observations on Commissioning Well 239.83m specimen revealed that the drill core consisted of alternating dark-and-light-coloured laminations that occurred within the fine-grained rock as shown in Plate 3.2. Therefore, this rock is classified as muddy shales.

The framework members of Katz. 321.0m specimen comprised of lithified sand particles that were in-filled with conspicuous greyish clay minerals as shown in Plate 3.3. Therefore, this rock classified is as muddy sandstones.

3.3.2 SPECIMEN SAMPLING METHOD

Sampling is the process of selecting a number of cases from all the cases in a particular group or universe while sampling technique is the identification of the specific process by which entities of the sample are selected (Glossary of Statistical Terms, 2011).

This project used two techniques namely convenience sampling and quota sampling. Convenience sampling is described as the non-random selection of samples based on their convenient accessibility. Quota sampling is described as the non-random selection of samples based on the identification of specific characteristics to increase the sample's representativeness, (Kothari, 2003).

Convenience sampling was used for VES data in this project. This involved the selection of the readily available data from the project sites. Meanwhile, quota sampling was useful for both XRF and UCS tests. Selection of specimens that were used was from the selected wells and within them, from suitable strata.

Generally, for all tests, the following criteria applied. Firstly, the specimens were selected from boreholes only in Block C, which was the area of interest in this project, and in particular from within the area classified as mining zones (richest coal fields in Block C), (Foundation Piling, 2010). Secondly, the specimens further were selected from drill-wells, which already had results of earlier done VES survey. Thirdly, the specimens were selected only from wells with coal indications for the reason of maximizing on both coal-bearing and non-coal-bearing strata rather than the non-coal-bearing strata only.

Fourthly, the specimens were selected at well depth intervals based on the observed most representative mineralogy for the cores, so no regularity of strata interval was maintained. Fifth, the total numbers of specimens were limited in order to save time and resources while acquiring representative data. Lastly, only the strata with significant thicknesses were considered, for the sake of generating reliable results especially for VES measurements.

More details on sampling and sampling techniques for XRF, VES and UCS methods are shown in Sections 3.4.1 to 3.4.3 respectively.

3.4 DATA ACQUISITION METHODS

Specific data acquisition methods used in this project are, XRF data acquisition, VES data acquisition and UCS data acquisition methods as highlighted in Sections 3.4.1, 3.4.2 and 3.4.3.

3.4.1 XRF DATA ACQUISITION METHOD

Drill core specimens from coal exploration wells constituted the test materials used in this project for XRF testing.

XRF test used the same specimens that were used for UCS test. This was to take advantage of their already flattened ends after UCS testing to ease the process of stage centring. In addition, no chemical pre-treatments or special environments were required in this test as stated in Shimadzu (2011).

Plate 3.4: EDX-800HS spectrometer, a computer system, and a colour printer

XRF testing required a number of instruments. These included, the Shimadzu' EDX-800HS fluorescence spectrometer and a modern desktop computer system. The Shimadzu' energy dispersive X-Ray (EDX-800HS) fluorescence spectrometer was required for specimens' raw data collection. This specific spectrometer, being a light-element high-sensitivity model is also able to analyse regular materials (and defects). Elements from Carbon to Uranium of the Periodic Table are detectable a shown in Shimadzu (2011). The EDX-800HS fluorescence spectrometer system is in Plates 3.4 and 3.5.

Plate 3.5: 'Giant' 3-litre thermos flask to hold liquid nitrogen

Analysis also used a modern desktop computer system and an ink-jet colour printer. This computer system consisted of among other software, the proprietary bulk FP Method software for quantitative data analysis. Microsoft Windows XP^{TM} operating system hosted this software to give quantitative results as required and programmed.

A special 3-litre capacity thermos flask complete in its *rack-sack* was used to store the liquid nitrogen coolant that was used in EDX-800HS spectrometer.

The modern geochemical technology incorporated in the EDX-800HS fluorescence system simplified XRF measurements procedures. First, three litres of liquid nitrogen (instrument coolant with temperatures of about-186°C) were emptied into the instrument' cooling chamber which was then powered on. The machine was left to run idly for about 20 minutes in this state to sufficiently cool before the tests began.

The flattened ends surfaces of the cylindrical specimens centred on the testing stage of the EDX-800HS and the FP method analysis software's 'START TEST' button hit into action. The testing chamber, after this, automatically shut itself to start the data collection. Each specimen took about 10 minutes to test. Table 4.3 depicts a summarized compilation of XRF data set presented in the three columns entitled '*major analyte/oxide'*, '*Results (%)*' and '*Standard deviation*.' Chapter 4 presents these data sets alongside their analytic comments in the other three columns.

3.4.2 VES DATA ACQUISITION METHOD

During the VES survey, the ground was relatively dry (as most of all the months of December normally provide in Kitui County). This was convenient for the study because the resistivity values obtained were not influenced by climatically wet surface conditions. Clearing of ASAL-based bushes and thickets made straight pathways to allow the electrical lines to pass through unobstructed.

The survey lines ran N-S and E-W and for length intervals between 200m to 500m AB/2 and 1m to 100m MN/2.

VES data, in this project, were prepared by copy pasting from MS™ Excel 2013 into Notepad ™ for data formatting into (.dat) file format. Then, the formatted data sets were plotted on elog-log graph using RES 1-D.

Inversion is a mathematical technique, which is used in RES1D as a sub-routine. Here, least squares algorithms are used to modify the inputs automatically. User-provided constraints are used iteratively as stated in Rahim (2013). These constraints include, minimum and maximum damping factors (ideal for data of unknown noise are 0.15 and 0.03 respectively, in RES1-D). Other constraints included a number of iterations (usually 5-7 in RES1-D, but more are still OK) and convergence limits (in terms of RMS error percentage, say ideal is 0 percent but can go up to above 100% in RES1-D). This procedure is used to calculate the computer simulated initial model responses that translate into strata depths and corresponding apparent resistivities.

Lastly, curve fitting is done through user-provided parameters (as estimated from the calculated models) which then are processed in (.mod) file format to produce the forward models. It is from these results that apparent resistivity values at any strata-point can be read-off.

A modern SARIS Terrameter (Synthetic Aperture Radar Instrument Simulator) was used in VES raw data acquisition by the author and a colleague, Faith Wanjiru at Block C, as shown in Plates 3.6 and 3.7.

Plate 3.6: The author in a past (2010) VES Survey at Mui Basin, Kitui County

Plate 3.7: SARIS Terrameter (owned by the MoEP, GoK)

This meter operated under a resistivity accuracy of ±1 percentage (measured in 2,500Ω load) which applied for VES measurements as per instrument specification in Scintrex (2001). Further processing of this data required the use of a modern computer system. A laptop computer with modern features including; 15.6" LED monitor, core i3 processor, 2.4GHz clock speed, 8GB RAM and 1TB hard drive was used in this case. MS Excel ™ 2013 software, which was installed in a Windows 8 Pro™ operating system, was used for preliminary *cleaning* of the VES raw data in readiness for analysis using RES1-D. The resultant data were recorded on paper using ink-jet printer.

A compilation of the raw VES data sets from original data sheets for the five sites in Block C, which were used in this project, is shown in Table 3.3.

Table 3.3: Compilation of VES parameters for the five project wells areas

Well / VES Parameters		Comm. Well	Katz. 3	FP 2	FP 3	YO 2
AB/(m)	***MN/2 (m)***	***ρ_a (Ωm)***				
3	*1*	*67.6*	*92.7*	*60.7*	*313.8*	*25.9*
5	*1*	*41.2*	*64.9*	*50.1*	*457.2*	*11.9*
7	*1*	*26.2*	*14.3*	*39.2*	*536.0*	*6.1*
10	*1*	*13.4*	*15.3*	*26.4*	*518.3*	*5.1*
10	*2.5*	*18.1*	*12.7*	*24.8*	*491.6*	*4.3*
15	*2.5*	*8.4*	*8.1*	*15.6*	*371.9*	*4.7*
20	*2.5*	*7.4*	*8.1*	*12.8*	*224.9*	*5.5*
30	*2.5*	*6.4*	*8.7*	*9.7*	*78.2*	*6.3*
40	*2.5*	*4.8*	*6.4*	*9.1*	*29.9*	*6.6*
50	*2.5*	*3.3*	*7.3*	*8.2*	*12.6*	*6.8*
50	*10*	*4.3*	*5.6*	*9.4*	*10.6*	*5.7*
70	*2.5*	*2.9*	*9.8*	*11.5*	*8.2*	*6.7*
70	*10*	*1.8*	*4.3*	*10.5*	*9.9*	*7.0*
100	*10*	*4.1*	*8.1*	*15.6*	*14.7*	*11.2*
150	*10*	*2.6*	*2.2*	*19.5*	*13.1*	*11.5*
200	*10*	*3.5*	*4.2*	*11.2*	*12.7*	*11.7*
200	*40*	*24.6*	*4.6*	*18.9*	*21.3*	*12.9*
300	*40*	*4.2*	*11.9*	***End***	*13.9*	***End***
400	*40*	*6.3*	*6.2*		*11.9*	
500	*40*	*7.8*	*11.4*		*20.2*	
500	*100*	*18.9*	*182.0*		*21.8*	

3.4.3 UCS DATA ACQUISITION METHOD

Drill core specimens from coal exploration wells once again were used in this project to measure the strength property in UCS testing. These came in three standard sizes namely, BQ=36.5mm, NQ=47.6mm and HQ=63.5mm in diameter.

Sample sizes are shown clearly in specimens, which are stored in boxes at Mathuki Stores, Kitui County as shown in Plate 3.8.

Plate 3.8: Typical drill-cores store-house at Mathuki Stores, Block C, Mui Basin, Kitui County and two drilling personnel (to assist sort out heavy drill-cores boxes for this project)

These samples were then selected as drill-core specimens retrieved from their respective storage boxes while avoiding breakages and contaminations. It was very necessary to find some help from two drilling personnel to lift and sort the heavy (about 50-70Kgs each in weight) and heavily piled-one-on-top-of-the-other(s) drill core boxes.

In this project, quota selection for the specimens was used. This means that specimens were selected based on intactness in form, their lengths that must conveniently but not mandatorily, be more than 2.5 times their diameters. The preliminary measurements were estimated under this rule.

Next, the specimens were wrapped in clean, dry and new water-proof field bags, clearly labelled and sealed, for example, ‘‘Comm. well 30.14m’’. This label implies that this specimen originates from Comm. well and at depths of 30.14m bgl, which for this report is the depth from ground level to the middle (half-length) of the specimen.

Finally, the wrapped-up specimens were packed into extra-strong field nylon bags and then in turn these were packed into shock absorbent used paper boxes; one closely fitted into the other. These then were fastened using sisal ropes to avoid the specimens from playing inside

and hence breaking during transportation to the testing facilities in Nairobi (about 190km from Mathuki).

Various equipment was used in UCS tests. Stronger specimens were analysed using the Dennison compression machine, which was manufactured by Samil Dennison and Son Ltd, Moor Road, Leeds, England, Model TIB/MC; machine No.30034 with a maximum capacity of 2000kN as shown in Plates 3.9 to 3.11. A 1Newton dial-division on this machine equals to 0.0254mm of strain. This implies that this machine bears an accuracy of 0.0001mm in strain measurements. This accuracy was rated as good for this project's testing.

Plate 3.9: Dennison 2000kN compression machine in the background at Civil Engineering laboratories, University of Nairobi

The UNESCO special-fund flexural/transverse frame-loading machine was used to analyse weaker specimens as shown in Plate 3.10. A 1Newton dial-division on this machine is equal to 0.001inch, which also is equal to 44lbs. This one dial equals to 0.1298mm and bears an accuracy of 0.0001mm in strain measurements, which was rated as good for this project's testing.

Plate 3.10: UNESCO 50kN flexural loading/transverse frame loading machine in the background at Civil Engineering laboratories, University of Nairobi

An electric-powered stone saw type SS206 manufactured by Stone Machinery Co. Inc., Manlius N.Y, Plate 3.11 was used to cut flat ends on the specimens while maintaining specimens lengths of about twice the dimension of their diameters as required. A bench vise incorporated in this system was used to fasten the specimens before the cutting process could begin.

Plate 3.11: An electric-powered stone saw; showing mounted vise to the left-hand side

Two tools namely, the 5m measuring tape (longer measurements) and a Mitutoyo linear callipers 170mm, made in Japan, (shorter measurements) were used to measure all the other project measurements. Also, a square rule which was incorporated in the stone saw' bench vise was used to ensured that these flattened ends were parallel to each other as required.

Specimens' preparations were the first step in UCS measurements. This process entailed the flattening of one end of each of all the specimens through accurate cutting by use of the stone-saw. Then specimens' markings and taking of their linear measurements came next. The flat end acted as datums while taking the measurements. The diameters and lengths (in millimetres) of the specimens' then were recorded. Lastly, the specimens were centred, one by one, on the appropriate compression machine' stages. The loading platen gently was lowered to rest on top of the specimen, one at a time. Then axial force was applied evenly for acquisitions of nominal UCS values (as opposed to dynamic true values) until the specimen just begin to experience brittle failure. The final readings *froze* on the axial load dial from where they were read off and manually recorded. Plates 3.12, 3.13 shows how, using examples of UCS measurements were carried out. All the others are shown in Appendix A2.
From the two photographs, it is apparent that the specimens were trimmed evenly at both edges. The brittle failure was attained at approximately the expected angle of failure, 45° to the direction of the principle/deviator force (F). (Ramamurthy & Sitharam, 2011) have approved this phenomenon.
In this project, only the UCSs were sought to give the scientific and professional estimates for the coaly sediments.

P

late 3.12: Coherent characteristic brittle failure in marlstones at about 45° to horizontal plane

Plate 3.13: Excellent brittle failure at approximately 45° to horizontal plane in muddy sandstones so UCS result was accepted

3.5 RESULTS CORRELATION METHODOLOGY

Quantitative-based research methodology uses confirmatory statistical methods (Kombo & Tromp, 2011). This project also falls in this category. Various appropriate figures were used to plot the analysed data sets for XRF, VES, and UCS. Tables, column bars, (Andy & Karl, 2011) and ternary diagrams were suitable to display the data for subsequent discussions (on trends), conclusions (what the quantities say) and recommendations (measures to be taken based on conclusions). Each data type (XRF, VES and UCS) were not constrained to each other in an aim to acquire independent results that clearly indicated merits and demerits of each analytical methodology but still giving preliminary coalmines designs.

CHAPTER 4: DATA ANALYSIS AND RESULTS

4.1 DATA ANALYSIS

Analysis is the manipulation of collected raw data from complex initial to simplified final states with an aim to understand the associated phenomena pertaining to the object/stimuli (Collins Dictionary, 2010) and (The American Heritage Science Dictionary, 2005). In addition, raw data is unprocessed data (Siddhartha, 2009).

Various calculations in this project were used to achieve the analyses of specimens. These analyses were presented two-fold. For best results, the diagrams first were presented, followed by the explanations. For VES analyses, sample processed data were presented in form of graphs just as printed from the RES 1D software system.

4.1.1 XRF DATA ANALYSIS

XRF data analysis entailed the subjection of raw data sets to a set of geochemical algorithms and calculations with an aim to find their suitable applications in Engineering Geology, specifically coalmines in this project.

Two sets of algorithms were used to achieve the XRF data analysis and results, in this project. These comprised of; i) the use of CIPW norm to reconstruct the mineralogies and hence rock types from the oxide datasets for each of the project specimens and, ii) use of engineering geological knowledge on elemental oxides' characteristics and hence the prediction of typical rock types.

Further, these results complemented the visual observations using colours and fabrics of each specimen in an attempt to classify them into specific rock types. Processing in ED-XRF equipment acquired the constituent minerals and their corresponding rock types as reconstructed from their chemical oxide percentages. This used the knowledge on elemental oxides and their geochemical properties, specifically stability in nature to Engineering geologically assess the rocks as in this project.

4.1.2 VES DATA ANALYSIS

Two steps were used to accomplish these analyses. These were auto-inversion (using user-provided constraints that included damping factor, number of iterations and others) and, forward modelling (using user-provided inputs as strata thicknesses in metres and apparent resistivities (Ω-m) as were obtained from inverse modelling analyses. Specifically, the user-

provided constraints that were selected included a damping factor of 0.15, the number of iterations between 5 to 18 and the convergence limit as 2.00.

Data of resistivity surveys that trended N-S directions were not used in VES analyses, except for FP 3 where E-W trending survey data were missing. This was because most faults (including along Mui River), fissures and master joints (Sanders, 1954), trended approximately N-S and these readings most likely can cause errors in data analysis for this project. For example, VES survey lines data that cuts along the general trends of fractures in this region will result in relatively lower apparent resistivities (from the saline solutions within the fractures). The will be regionally false apparent resistivities and strata thicknesses than VES survey lines that cut across such fracture zones. Highly fractured rocks along fault lines have increased permeability as water normally percolates easier via the fracture channels and partly dissolves the rocks to form readily ionized solutions, which have low apparent resistivities.

4.1.3 UCS DATA ANALYSIS

Standard calculations, which involved collected data sets as the key inputs were used to achieve the UCS data analyses. These calculations were presented concisely in the self-explanatory (Figure 4.1).

The arrows in the flow chart point systematically to the direction from one analytical step to the next. All the raw data sets acquired in this project were analysed from the first through to the last step, whereby the strength values obtained were the results.

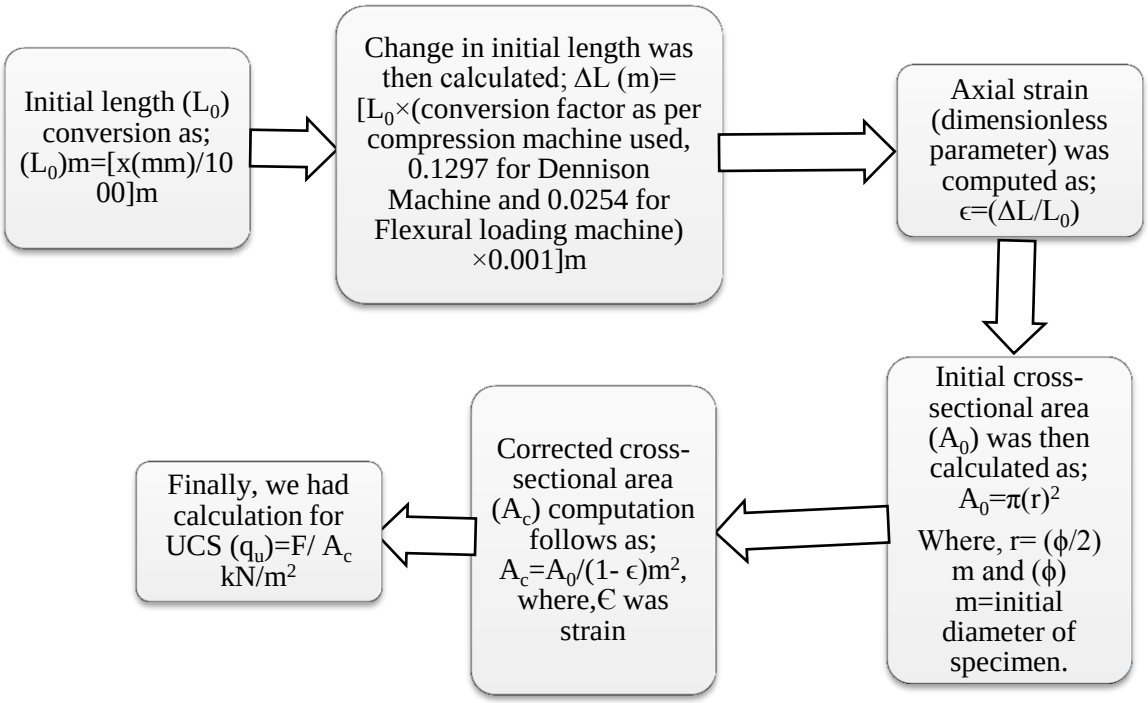

Figure 4.1: Flow-chart diagram illustration of steps undertaken in project analysis for UCSs

4.2 RESULTS

4.2.1 XRF RESULTS

4.2.1.1 CIPW RESULTS

As stated earlier in Section 4.1.1, this project also used CIPW norm classification to classify the thirteen project specimens. Comm. Well 3 and FP 2.1 specimens serve as examples of results as shown in Table 4.1.

Table 4.1 shows three columns; one lists normative 13 minerals, the second lists weight norms percentage and the third lists the volume norm percentage. At the bottom is a totals row for the analytic results that totalled to at least 100%. The more than 100% attributes to CIPW norm program error; this is rated as minimal (in the range of 0.01%) relative to the values for the norms percentage. The second row among the totals row indicates 2.73g/cm^3 as the calculated rock specimen density for Comm. Well 3 specimen and, 2.39g/cm^3 for FP 2.1 specimen. These values are quite typical to coal measure rocks. In addition, the third row among the aggregates rows contains the entry that indicates the proposed rock name as a result from the analysis. Comm. Well 3 specimens classified as marlstones while FP 2.1 specimen classified as muddy shales. Tabulation of the rest of the CIPW norm analytic results were in similar manner, Table 4.1 in Appendix B.2.

Table 4.1: CIPW norm classifications for Comm. well 3 and FP 2.1 specimens

Comm. Well 145.15 m specimen			**FP 2 49.4 m specimen**	
Normative Minerals	**Weight (%) Norm**	**Volume (%) Norm**	**Weight (%) Norm**	**Volume (%) Norm**
Quartz	0.00	0.00	72.63	76.64
Plagioclase	39.43	42.71	0.00	0.00
Orthoclase	0.00	0.00	2.01	2.19
Leucite	3.85	4.62	0.00	0.00
Corundum	0.00	0.00	13.99	9.83
Wollastonite	17.12	17.89	0.00	0.00
Larnite	24.65	22.53	0.00	0.00
Rutile	0.00	0.00	0.31	0.08
Ilmenite	0.24	0.15	0.13	0.08
Haematite	4.06	2.13	4.26	2.27
Apatite	9.24	8.64	0.00	0.00
Perovskite	1.03	0.77	0.00	0.00
Anhydrite	0.39	0.39	9.30	8.79
Total	100.01	100.01	102.63	100.01
Rock density (g/cm^3)	2.73		2.39	
Proposed rock name	Marlstone		Muddy shales	

4.2.1.2 XRF RESULTS USING TERNARY DIAGRAM

Generally, ternary diagrams display results of rock specimens by classification or grouping together of similar rock types. In this study, such classifications were based on inferred graphical relationship between the three pre-selected mineral oxides that were shared in various proportions within specimens' compositions. The final plot appears as a triangular-shaped figure with clusters of plotted results.

In Figure 4.2 are analyses of the thirteen project specimens plotted in terms of SiO_2 (at top apex), CaO (left-hand apex), and Al_2O_3 (at right-hand apex) in a ternary diagram. The rock specimens generally plotted notably into three clusters within the tri-graph. One that was nearest SiO_2 apex plotted Comm. Well 4 and FP 2.1 specimens and classified them as muddy shales. Secondly, two conspicuously anomalous plots represented YO 2.2 specimen (as Shaley ironstones) and Comm.Well 3 specimen (as marlstones). Finally, plots for the rest nine of the project specimens plotted at the left-hand side of marginal line in the ternary diagram. These generally were classified as sandstones.

ProSim™ computer software using normalized oxide proportions was used to draw, Figure 4.2.

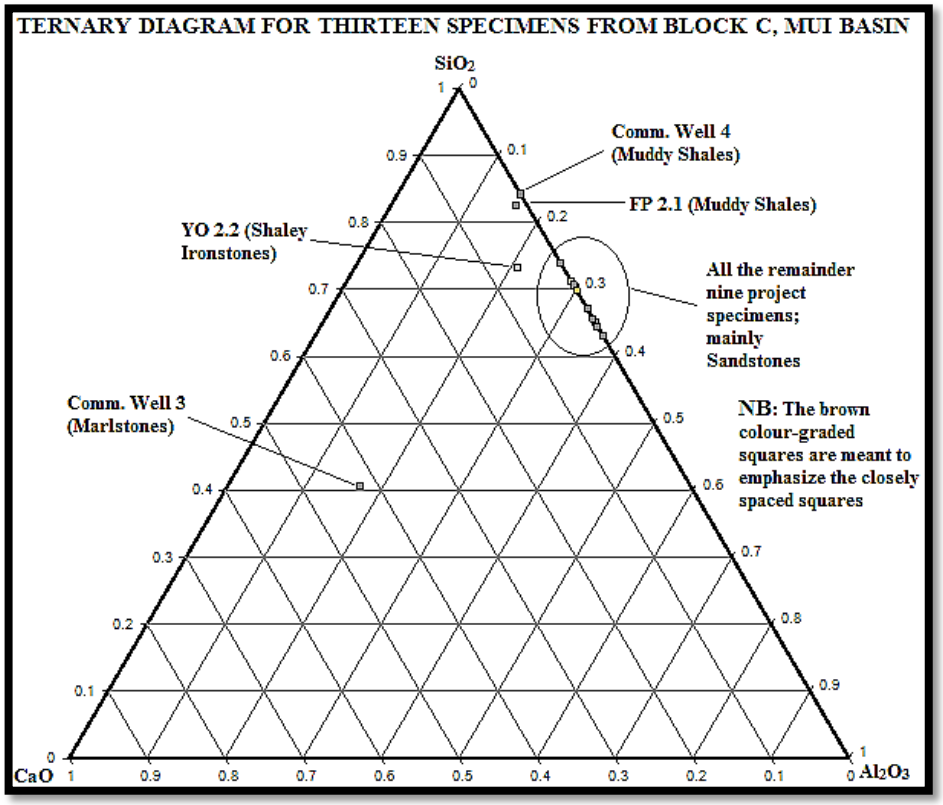

Figure 4.2: Ternary diagram on analyses for specimens from Block C, Mui Basin

Figures B.1, B.2, and B.3, Appendix B 6, offer auxiliary information to support these ternary diagram results (Figure 4.2).

Meanwhile, it was also necessary to ascertain the classification of the marlstones from additional sources. Figure B.4 shows the simplified classification of rocks that mainly comprise of CaO and clays. It was noted that Comm. Well 3 rock specimen matched the classification of marl/marlstone because it consists of 38% CaO (35 to 65% $CaCO_3$) and about 55% clays (35 to 65% clays). This verified that the specimen actually is a marlstone.

4.2.1.3 USE OF ELEMENTAL-OXIDES GEOCHEMISTRY TO BACK XRF RESULTS

Knowledge on elemental oxides and their geochemical properties, specifically stability in nature as shown in Figures B.2 and B.3, is important in engineering geological assessment in this project.

For more details, a number of common elemental oxides act as pointers to parent rock forming environments. In this project, these elemental oxides included SiO_2, Al_2O_3, K_2O, TiO_2, CO_3, $SO3$, and P_2O_5. First, silica (SiO_2), mainly in form quartz grains and siliceous matrix mineral, is relatively very stable against chemical weathering and therefore more commonly forms residual sandstones and shales.

In addition, alumina (Al_2O_3) mainly occur in sedimentary terrains as feldspars (terrigenous) in lithologies such as mudstones and claystones, corundum crystals and bauxite normally enriched in Fe-minerals. These are most stable in chemical weathering series, on the discontinuous branch **(**Figures B.2 and B.3). These normally occur as goethite, magnetite, and stained quartz and in bog-iron environments.

In addition, potash (K_2O) is a mineral that more commonly forms in sedimentary basins and is associated with green-colored and chemically unstable glauconite, mica, which often occurs with claystones, green sandstones, and shales. The other mineral cases, rutile, brookite, and anatase (TiO_2) are high P/T accessory minerals found after alteration especially of eclogites but also kimberites and lamprophyres. These accumulate in placer deposits always associated with iron suspected to form rutile, which mostly occurs with sandstones and shales. Others are calcite/lime, aragonite, siderite, and dolomite ($CaCO_3$) in calc-plagioclase feldspars and marl or argillaceous mudstones. These normally contain impurities such as barium and strontium and are associated with marlstones, mudstones, and sandstones. In this project, no Mg was noted, only some Mn. The Mn is normally associated with siderite and calcite because of cation replacement (Swaine, 1994). Further, chalk and marlstones are described as '….soft compact calcite….with varying amounts of silica, quartz, feldspar, or other mineral impurities, generally grey-white or yellow-white and is derived chiefly from fossil seashells' (Glossary of Statistical Terms, 2011). SO_3 rich minerals (anhydrite ($CaSO_4$) and wollastonite ($CaSiO_3$)) are associated with non-hydrous phases, without clays and muds and generally are associated with shales, which normally form sedimentary exhalative (SedEx.) ore deposits. While P_2O_5 (phosphate sedimentary rocks) is known to mainly consist of fluorapatite $Ca_5(PO_4)_3$ and hydroxyapatite $Ca_5(PO_4)_3OH$ minerals that often form in mudstones, sometimes interbedded in shales. In this project, boron was lacking in phosphates to form boron phosphate, which also sometimes deposits in coal boilers (Swaine, 1994).

4.2.1.4 XRF RESULTS USING BAR-COLUMN CHART

Composite bar-column charting method was used to present these project results (Figure 4.3**)**.

Silica was the most abundant elemental oxide at this project's sites followed by alumina and iron oxide while the least abundant were the carbonates.

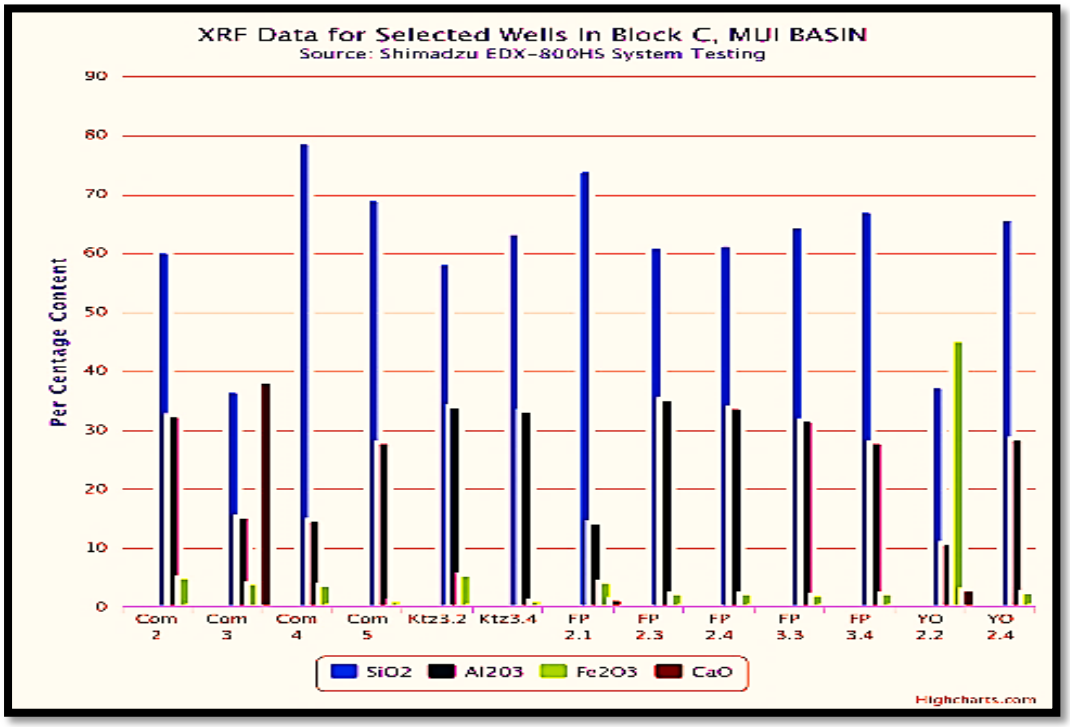

Figure 4.3: Bar-column presentation for summary of ED-XRF oxides results for project specimens (using a source code in java computer programming)

4.2.1.5 TABULAR SUMMARY OF XRF RESULTS

On the other hand, Table 4.2 depicts the summary of ED-XRF results for the thirteen project specimens. The first vital aspects about the data were the magnitudes of errors of chemical detection during analyses. These errors ranged from standard deviations 0.01 to 0.803. In addition, these errors were rated relatively well because they were quite small figures relative to the corresponding oxide per centages and they translated to equally good analytical results. This table generally showed that the project rocks chemically consisted essentially of SiO_2 in abundances ranging from lows of 36.568% (Comm. Well 3 specimen) to highs of 78.656% (Comm. Well 4). Al_2O_3 was the second highest in abundance with content range from lows of 10.646% (YO 2.2 specimen) to highs of 33.949% (Katz. 3.2 specimen). Fe_2O_3 and CaO occurred in lesser content per centages while anomalously high abundances occurred with contents of CaO (38.071% in Comm. Well 3 specimen) and Fe_2O_3 (45.108% in YO 2.2 specimen). The other oxide contents in this project rocks were minor and include K_2O, TiO_2, MnO, SO_3 and P_2O_5. Preliminary classification ignored the chemical type content that existed in trace per centages, in this project for the sake to simplify the classification.

The three approaches of analyses of XRF oxide data revealed interesting summary results. First, these revealed new rock classes. Comm. Well 3 where both CIPW norm classification and visual observation classification methods concluded that this rock specimen presumably was marlstones while MoEP geologists classified the same specimen as siltstones or silty sandstones. The other was YO 2.2, which classified as shaley ironstone (CIPW norm classification), muddy ironstone (visual observation classification) and mudstones or muddy shales (MoEP geologists).

In most of the other specimens' classification, the variations across the three classification schemes observed less discordant variance, for example FP3.3 (sandstones to muddy sandstones to clayey sandstones). However, class identity of the missing MoEP well logs for Comm. Well 4 specimen, (which had been marked as missing in this table**)** can be unruffled. These were interpreted to be muddy shales or muddy sandstones while Comm. Well 5 specimen can be muddy sandstones or clayey sandstones. YO 2.4 specimen similarly was interpreted to be muddy sandstones or clayey sandstones. See Table 4.2.

Table 4.2: Summary of ED-XRF results for project specimens at Block C, Mui Basin

	Specimen Name		Major oxide	Results (%)	Std. Dev.	Comments/analyses		
						MoEP loggers' classification	CIPW norm-ED-XRF classification	Visual classification
1	**Comm.Well 2 (137.43m)**	a.	SiO_2	60.248	0.309	Mudstones	Muddy sandstones	Muddy shales
		b.	Al_2O_3	32.34	0.455			
		c.	Fe_2O_3	4.924	0.012			
		d.	TiO_2	1.244	0.013			
2	**Comm.Well 3 (145.15m)**	a.	CaO	38.071	0.057	Siltstones or silty sandstones	Marlstones	Marlstones
		b.	SiO_2	36.568	0.324			
		c.	Al_2O_3	15.334	0.504			
		d.	P_2O_5	3.983	0.067			
		e.	Fe_2O_3	4.058	0.016			
3	**Comm.Well 4 (239.83m)**	a.	SiO_2	78.656	0.297	Missing well logs	Muddy shales	Muddy shales
		b.	Al_2O_3	14.663	0.285			
		c.	Fe_2O_3	3.656	0.01			
		d.	SO_3	1.726	0.019			
4	**Comm.Well 5 (279.35m)**	a.	SiO_2	68.963	0.2245	Missing well logs	Muddy sandstones	Clayey sandstones
		b.	Al_2O_3	27.803	0.305			
		c.	K_2O	1.042	0.006			
		d.	Fe_2O_3	1.014	0.006			
5	**Katz. 3.2 (141.13m)**	a.	SiO_2	58.212	0.322	Mudstones	Muddy sandstones	Muddy shales
		b.	Al_2O_3	33.949	0.473			
		c.	Fe_2O_3	5.49	0.013			
		d.	TiO_2	1.307	0.014			
6	**Katz. 3.4 (321.0m)**	a.	SiO_2	63.258	0.235	Mudstones	Muddy sandstones	Muddy sandstones
		b.	Al_2O_3	33.088	0.322			
		c.	K_2O	1.446	0.007			
		d.	Fe_2O_3	1.147	0.006			
7	**FP 2.1 (49.4m)**	a.	SiO_2	73.917	0.326	Shales and mudstones	Muddy sandstones	Muddy shales
		b.	Al_2O_3	14.359	0.333			
		c.	SO_3	5.472	0.036			
		d.	Fe_2O_3	4.255	0.012			
		e.	CaO	1.201	0.008			
8	**FP 2.3 (179.8m)**	a.	SiO_2	70.342	0.263	Mudstones	Muddy sandstones	Muddy sandstones
		b.	Al_2O_3	24.736	0.316			

		c.	Fe_2O_3	1.815	0.008			
		d.	K_2O	1.779	0.009			
9	**FP 2.4 (193.57m)**	a.	SiO_2	61.342	0.272	Granitoid gneiss	Muddy sandstones	Clayey sandstones
		b.	Al_2O_3	33.81	0.384			
		c.	Fe_2O_3	2.314	0.009			
		d.	K_2O	1.16	0.008			
		e.	TiO_2	1.005	0.014			
10	**FP 3.3 (158.54m)**	a.	SiO_2	64.423	0.27	Sandstones	Muddy sandstones	Clayey sandstones
		b.	Al_2O_3	31.517	0.359			
		c.	Fe_2O_3	2.135	0.009			
11	**FP 3.4 (258.47m)**	a.	SiO_2	67.018	0.27	Sandstones	Muddy sandstones	Clayey sandstones
		b.	Al_2O_3	27.825	0.345			
		c.	Fe_2O_3	2.293	0.009			
		d.	K_2O	1.505	0.008			
12	**YO 2.2 (21.53m)**	a.	Fe_2O_3	45.108	0.063	Mudstones and muddy shales	Muddy ironstones	Shaley ironstones
		b.	SiO_2	37.361	0.558			
		c.	Al_2O_3	10.646	0.803			
		d.	CaO	2.937	0.023			
		e.	MnO	2.244	0.015			
		f.	SO_3	1.549	0.042			
13	**YO 2.4 (43.10m)**	a.	SiO_2	65.753	0.276	Missing well logs	Muddy sandstones	Clayey sandstones
		b.	Al_2O_3	28.532	0.356			
		c.	Fe_2O_3	2.521	0.009			
		d.	K_2O	1.606	0.009			

4.2.2 VES RESULTS

4.2.2.1 AUTO-INVERSION AND FORWARD MODELS VES RESULTS

Comm. Well's E-W auto-inversion model and its forward model (Figure 4.4) serves as examples results at this point. These portray the inverse model to be calculated automatically at a best of 69.69% RMS error at 12 iterations (Table 4.3). This was considered a quite high value (ideal RMS error should be 0%) but is sufficient for use as estimates during this analysis. Therefore, the lower the RMS then the higher the accuracy was achieved in the results. Further, in Figure 4.4, results indicate the detection of three major strata. These results served as key inputs during the next stage of analysis, namely, forward modelling/curve fitting.

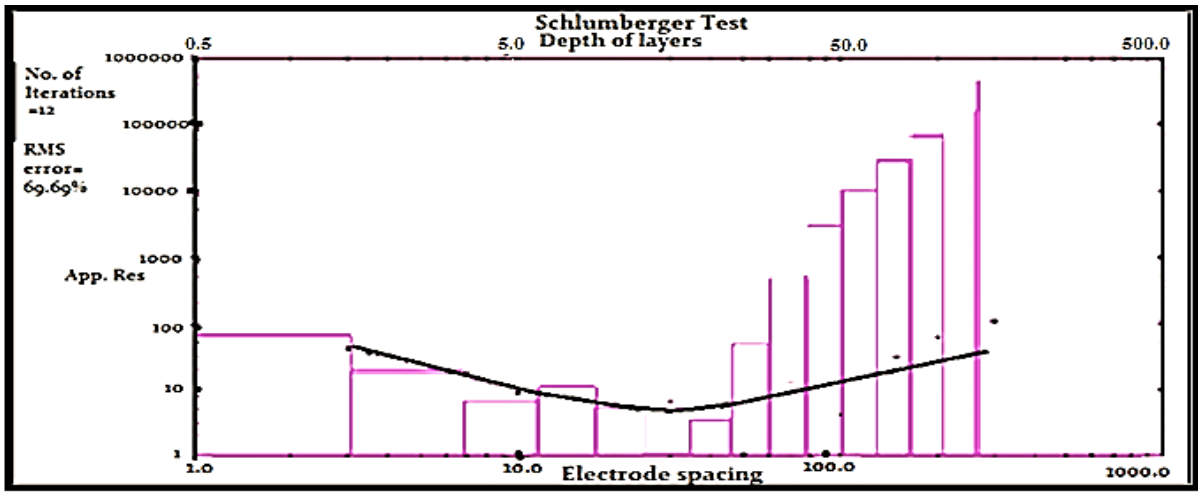

Figure 4.4: Comm. well E-W drill-well' auto-inversion geo-electric model

Figure 4.5 displays VES data analysis using the inversion results obtained from Figure 4.4, as input parameters for forward modelling. The obtained results consists of a best of 70.84% RMS error at 18 iterations. Therefore, the error for the measurement of three strata layers was relatively high. The rest of the project VES results of this type are in Appendix C.1.

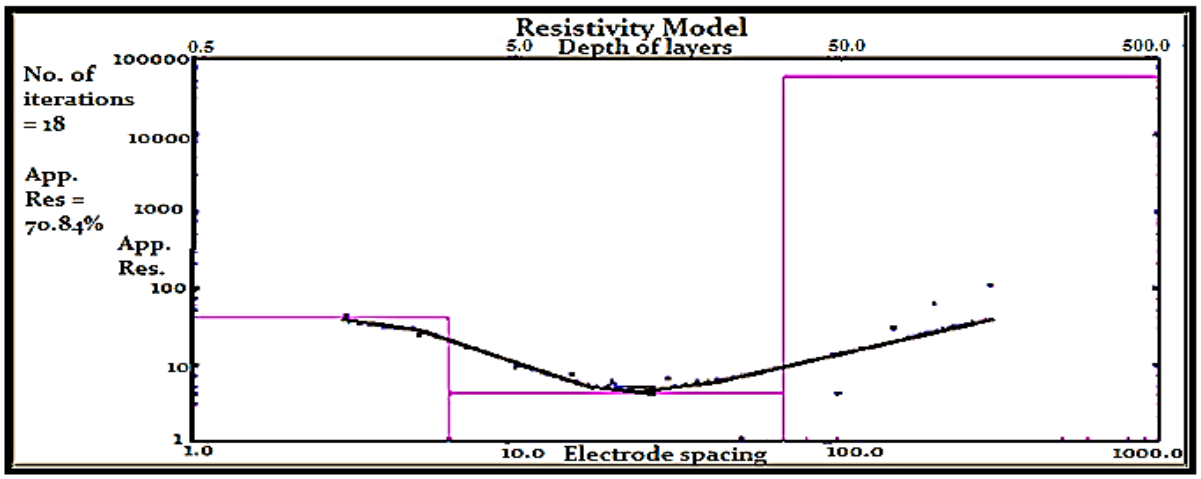

Figure 4.5: Comm. Well E-W drill-well' geo-electric forward model (user-provided parameters)

4.2.2.2 TABULATED SUMMARY OF VES RESULTS

Compilation of the analysed VES survey data were presented in Table 4.3. In this table, ten columns are listed. Two of these columns presents two groups namely auto-survey result (inverse model produced more number of layers than forward models) and user-provided survey result (forward model produced less number of layers and was suitable for this project because the results generalized the layers into more simplified strata).

The number of layers from auto-survey result ranged from 13 to 17 for 8 to 14 iterations (fell between the recommended 5 to 18 numbers of iterations as earlier stated). Therefore, the numbers of iterations for this experiment were acceptable. RMS error per centage ranged from high accuracy of 9.64% (FP 3 well area) to low accuracy of 102.57% (YO 2 well area).

User-provided survey result revealed that lesser number of strata (3 to 4) and for each of these and their corresponding apparent resistivities were also given (Ω-m) alongside with their thicknesses (m). The thinnest layer belonged to YO 2 stratum that measured 0.25m at 620Ω-m while the thickest measured 497.3m at 15Ω-m. In addition, the highest apparent resistivity measured 50,000Ω-m for Comm. Well' 457m stratum and the lowest measured 1.4Ω-m for YO 2' 1.25m thick stratum.

The user-provided survey results also revealed that the number of iterations ranged from 8 to 18 and RMS error (%) ranged from an accuracy of highest of 23.96 (FP 3) to lowest of 102.57 (FP2) as shown in Table 4.3. High RMS errors were noted in the results in most cases.

Table 4.3: Summary of VES analysis results for project' well areas at Block C, Mui Basin

Well	Auto-survey results			User-provided survey results					Conclusions
	No. of layers	No. of iterations	RMS error (%)	No. of layers	Apparent resistivity (Ω-m)	Layer thickness (m)	No. of iterations	RMS error (%)	All result-values Table 4.3 are good for basic modelling of subsurface for the sake of preliminary geo-design of proposed coalmines at Block C, Mui Basin in this project.
FP 2	13	8	94.42	3	3300 180 5.8	1.75 143.25 366	13	101.34	
FP 3	17	8	9.64	4	280 475 460 15	1.3 1.0 0.4 497.3	13	23.96	
Katz. 3	15	14	28.38	3	540 6.5 28	0.5 18.5 481	8	40.75	
Com. Well	15	12	69.69	3	2.5 36 50,000	40 3 457	18	70.84	
YO 2	13	12	102.57	4	620 1.4 750 0.45	0.25 1.25 6.00 492.5	9	102.57	

4.2.3 UCS RESULTS

4.2.3.1 TABULATED SUMMARY OF UCS RESULTS

Table 4.4 (attached to this report) was used to present a summary of UCS results. The column that is labelled *Sp'n depth* actually implies *Specimen Depth* gives the depth in any given drill-well from the ground level (GL) to the middle (half-length) of any given specimen. For example, in the fourth row, third column, the well depth was given as 137.43m from GL, which means that while the specimen length was given as 0.19m, then the depth range of the specimen from GL was 137.335-137.525m. This style of labelling was adopted to make the records easier to record.

Columns *L01* and *L02* represent the initial lengths (in meters) of the specimens, *1* and *2* apply only where specimens have 2 samples and likewise for *A01* and *A02*. *A01* and *A02* are also rated partly as raw data since the initial diameters (ϕ) are incorporated in their calculations. Specimens' *L01* ranged from 0.009m to 0.1m. Two specimens represented each of the five out of the thirteen specimens, an advantage for this project. The diameters ranged from standard sizes (but approximately shrunk) of BQ (36.5mm) for YO 2 specimens, NQ (47.6mm) for Katz. 3's specimens and HQ (63.5mm) for Comm. Well's specimens. Accuracy on measurements was inscribed on each machine's proving ring as 0.0001mm per strain measurement.

On the analysis part, columns ΔLA and ΔLB referred to the change in initial lengths of samples *A* and *B* whenever two samples occurred for a specimen from start of compression to just before brittle failure. ΔL ranged from 0.00015m (clayey sandstones from FP 2.3) to 0.01816m (muddy shales from FP2.1) as shown in Table 4.4 columns ϵ *(A)* and ϵ *(B)* depicted strain for samples *A* and *B* per specimen. Strain refers to stress per unit area and is a dimensionless parameter. This ranged from lows of 0.001604 (FP2.3 sample) to highs of 0.157896 (FP2.1 sample). *Ac1* and *Ac2* referred to the corrected surface areas for samples *1* and *2* of specimen as provided. The smallest Ac was 0.000888m^2 (YO2.4 specimen) and the highest was 0.024202m^2 (Comm.Well 2 specimen).

The magnitude of initial diameter of specimen influenced these readings. The principal forces (*FA* and *FB*) that caused specimen failure; in kilo-Newtons per square meter come next. The stronger specimens were compressed using the more powerful Dennison compression machine (for example, Comm. Well 3, which failed at F=68kN) while the Flexural loading compression machine was used on the weaker specimens (for example, YO 2.2 which failed at F =1.1748kN). Summary UCS (qu mean in kN/m^2) values were listed in the farthest right column of Table 4.4 (attached). The smallest recorded UCS value was 82.504kN/m^2

(Comm.Well 2 specimen) while the largest UCS value record was 37,211.91kN/m^2 (FP 2.1). The larger the UCS value implied the stronger the rock specimen.

On the other hand, the first row has the table title; the second row has the project area title while third row has UCS parameters. All the other rows have the names of the specimens and their specific attributes, for example, fourth row we have Comm. Well 2 specimen, third column is the Specimen depth.

The results from the project analyses were found to be substantial for discussion in Subchapter 4.3**.**

Table 4.4: Summary of computation results for UCS from project area

SUMMARY OF COMPUTATION RESULTS FOR UCS

PROJECT AREA: Block C, Mui Basin, Kitui County

	Well	Sp'n depth (m)	Visual classif'n	L01 (m)	L02 (m)	ΔLA (m)	ΔLB (m)	Strain (ϵA)	Strain (ϵB)	A01 (m2)	A02(m2)	AC1 (m2)	AC2 (m2)	FA (kN)	FB (kN)	quA (kN/m2)	quB (kN/m2)	qu mean (kN/m2)
1	**Com. Well 2**	137.43	Mudstones	0.16	None	0.000259	None	0.0016213	None	0.02420196	None	0.024241261	None	2	None	82.504	None	**82.504**
2	**Com. Well 3**	145.15	Siltstones	0.125	0.115	0.00882	0.01751	0.0705568	0.1522565	0.0031185	0.0031185	0.003355234	0.003679	68	135	20266.843	36698.865	**28482.85**
3	**Com. Well 4**	239.83	Muddy shales	0.1	0.1	0.009728	0.00843	0.097275	0.084305	0.007857142	0.007857142	0.008703804	0.008581	75	65	8616.922	7575.296	**8096.109**
4	**Com. Well 5**	279.35	Muddy sandstones	0.09	0.09	0.001067	0.00097	0.0118533	0.0107244	0.001591071	0.001591071	0.001610156	0.001608	8.2236	7.4404	5107.331	693.78	**2900.555**
5	**Katz. 3.2**	141.13	Mudstones	0.009	None	0.000254	None	0.0028222	None	0.001521142	None	0.001525447	None	1.958	None	1283.56	None	**1283.56**
6	**Katz. 3.4**	321	Muddy sandstones	0.1	None	0.000813	None	0.008128	None	0.00178024	None	0.001794828	None	6.2656	None	3490.92	None	**3490.92**
7	**FP 2.1**	49.4	Muddy shales	0.115	None	0.018158	None	0.1578957	None	0.003168196	None	0.003762236	None	140	None	37211.91	None	**37211.91**
8	**FP 2.3**	179.8	Clayey sandstones	0.095	0.09	0.000152	0.00025	0.0016042	0.0178246	0.0225	0.0225	0.022536152	0.022908	1.1748	1.958	52.13	85.47	**68.8**
9	**FP 2.4**	193.5	Weathered Basem't	0.087	None	0.000381	None	0.0043793	None	0.00178024	None	0.00178807	None	2.937	None	1642.55	None	**1642.55**
10	**FP 3.3**	158.54	Muddy sandstones	0.075	0.075	0.000737	0.00051	0.0098213	0.0067733	0.001591071	0.001591071	0.001606852	0.001602	5.6782	30916	3533.74	2444.56	**2989.15**
11	**FP 3.4**	258.47	Muddy sandstones	0.095	0.095	0.000457	0.00066	0.0048126	0.0069516	0.00178024	0.00178024	0.001788849	0.001793	3.5244	5.0908	1970.21	2839.74	**2404.975**
12	**YO 2.2**	21.53	Muddy shales	0.075	None	0.000152	None	0.002032	None	0.0009625	None	0.000964459	None	1.1748	None	1218.09	None	**1218.09**
13	**YO 2.4**	43.1	Muddy sandstones	0.075	None	0.000508	None	0.0067733	None	0.000881767	None	0.00088778	None	3.916	None	4411.003	None	**4411.003**

CHAPTER 5: DISCUSSIONS

In this chapter trends as to how rock strengths vary with depth per each major strata formed the larger part of discussion in this project. The classification of rocks in this project was achieved through XRF testing. Strata thicknesses were obtained from the apparent resistivities while the rock strengths were derived from the UCS measurements. Apparent resistivities also helped to obtain information on occurrences of potential aquifers. All the information derived in this way was used to assess the applicability of the various mining methods and the selection of the optimal coal mining method for each of the project sites.

In Figure 3.4 and Sections 5.1 to 5.5, each of the five key project sites was considered for discussions. The circumscribed information in Figures 5.1 to 5.5 represents the essentials of geo-design models that have been acquired in this project while the background logs represents auxiliary geological information from various MoEP well log reports for the purpose to independently compare and complement. This partly was because the VES results exhibited high RMS errors, which are suspected to have resulted from the functioning of the RES 1-D software, though we appreciate it as offered free by its developer. This discussion synthesized the project conclusions.

5.1 COMM. WELL SITE

Several facts came up from analyses of Commissioning Well's results as shown in Figure 5.1. Two new litho-stratigraphic units were identified from among the representative specimens. Through XRF analysis, it was revealed that several rock types occur in the sub-surface at Comm. Well's project site. Muddy sandstones and muddy shales that were classified using XRF occur at 137.44m and 239.83m depths bgl respectively. These muddy sandstones have apparent resistivity of 50,000Ω-m (for the 457m thick stratum using VES data) but greatly differ in strength as shown Figure 5.1. The top muddy sandstones rock unit indicated strength of 82.5kN/m^2 while the bottom unit indicated strength of up to 8,096.1kN/m^2. In addition, muddy sandstones occur at depths of 279.35m bgl and have apparent resistivity of 50,000Ω-m (part of the 457m thick VES stratum).

Marlstones occur at 145.15m depths bgl. These indicated great strength of about 28,482.91kN/m^2 and apparent resistivity of 50,000Ω-m (part of the 457m thick VES stratum).

Aquifers occur approximately at 25m, 75m, 150m, and 275m depths bgl. These comprise mainly of friable siltstones and sandstones (Mutunguti & Ndogo 2006). 1-D VES survey did not detect these aquifers. For this reason, they are assumed not to pose any significant

engineering geological problems during coalmines development. This is true especially during dry seasons.

These results show that at Comm. Well's area, the rocks occur in varying strength values ranging from 82.5kN/m^2 (muddy sandstones) to 28,482kN/m^2 (marlstones). General trends indicated increase in values at the middle of the rock profile upward than downward.

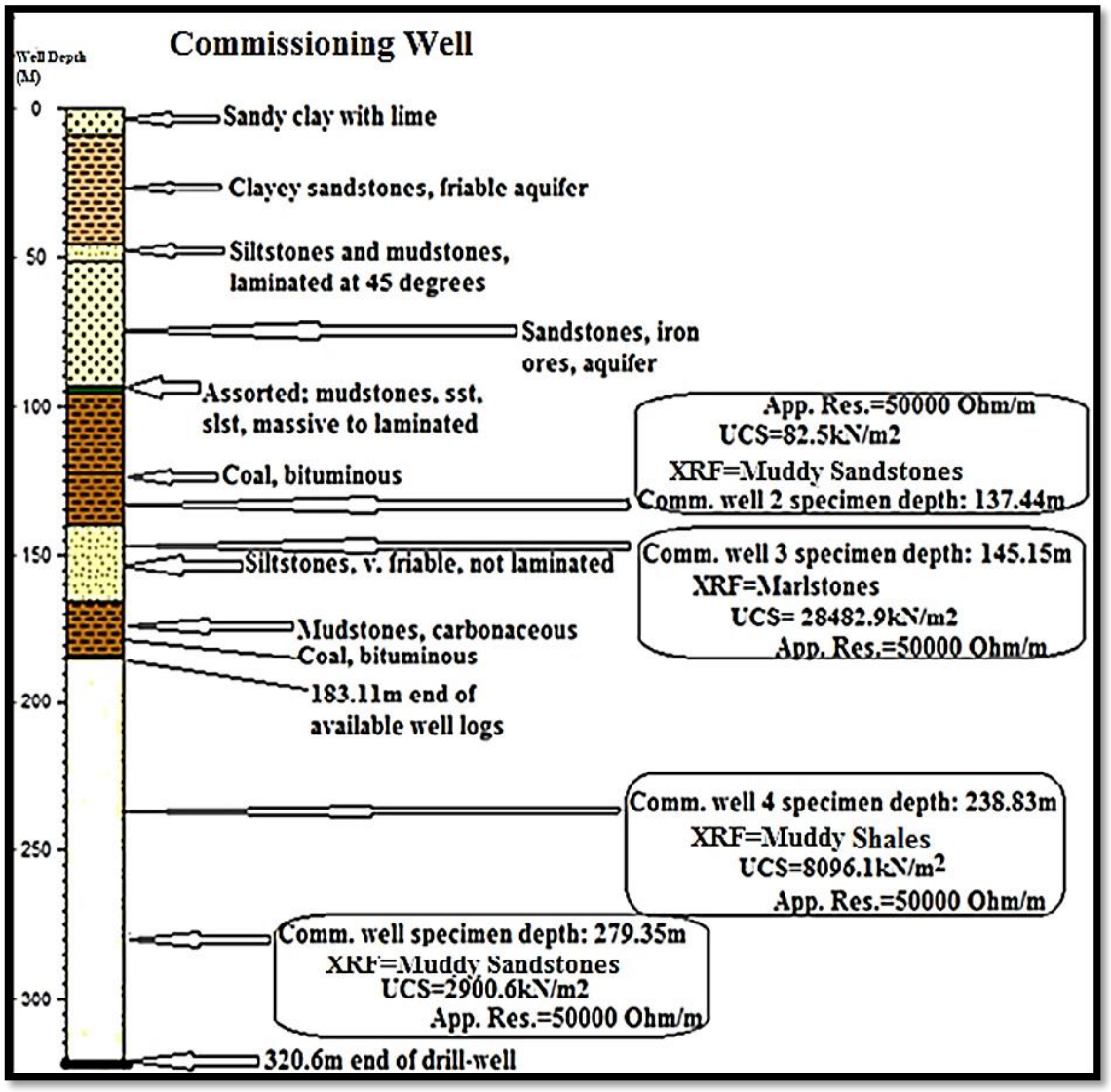

Not to scale

Figure 5.1: Schematic model for Comm. well area with geo-design parameters

5.2 FP 3 SITE

The geo-design for FP 3 (Figure 5.2) is based on the results of two specimens. XRF was used to classify both these litho-stratigraphic units as muddy sandstones at the depths of 158.54m and 258.47m bgl. These lithologies bore relatively low apparent resistivity of about 15Ω-m (part of the 497.3m thick VES stratum) and relatively low strength of 2,989kN/m^2 for top litho-stratigraphic unit and 2,405kN/m^2 for the bottom litho-stratigraphic unit. General

trends indicated that rock strengths increased anomalously downwards then decreased deeper in the well.

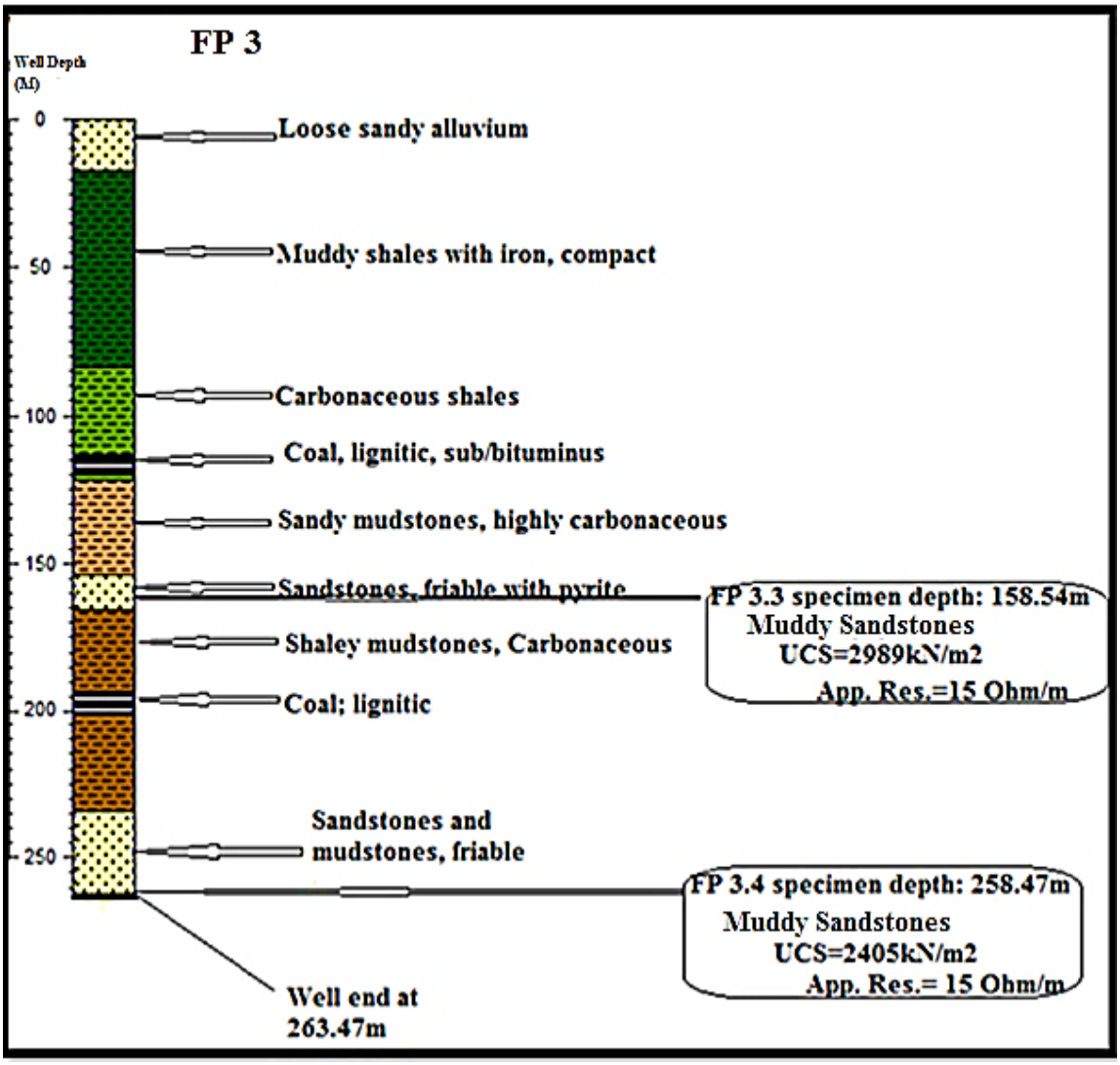

Not to scale

Figure 5.2: Schematic model for FP 3 well area with geo-design parameters

5.3 FP 2 SITE

In Figure 5.3, three specimens are discussed as representatives of FP 2 well area. One specimen was identified as muddy shales while the other two were identified as muddy sandstones. The specimen from well depth 49.4m depth bgl indicated relatively higher strength of about 37,211.9kN/m^2 and low apparent resistivity of about 180Ω-m (part of the 143.25m thick VES stratum). The specimen from 117.8m depth bgl indicated lower strength of about 972.94kN/m^2 and low apparent resistivity of about 5.8Ω-m and the specimen from 193.57m depth bgl has apparent resistivity as 5.8Ω-m (both are parts of the 366m thick VES stratum).

The trends indicated that rock strengths decreased downwards up to the middle of the well from where they increased slightly.

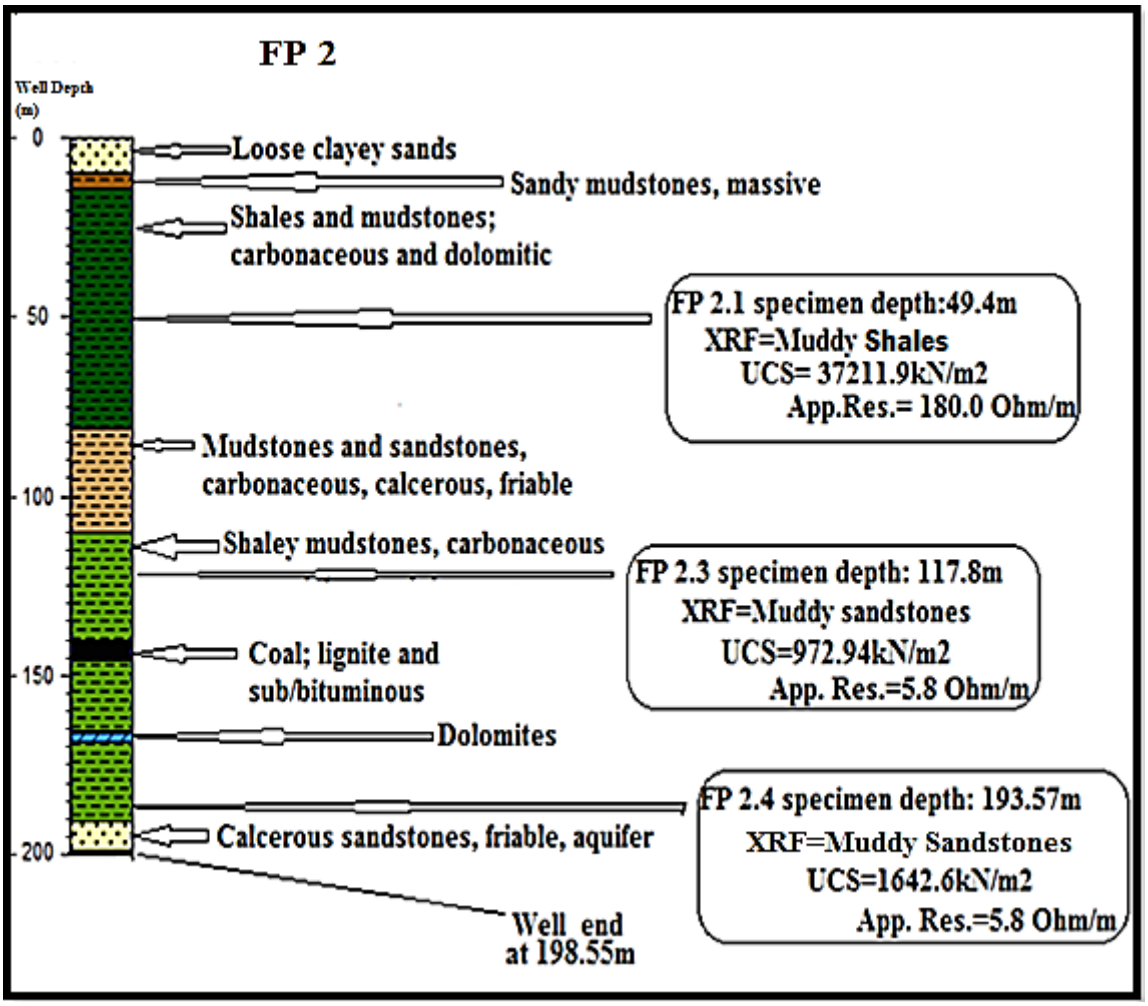

Not to scale

Figure 5.3: Schematic model for FP 2 well area with geo-design parameters

5.4 KATZ. 3 WELL SITE

At Katz. 3 drill-well, two specimens represented the strata for discussions in this project. At depths of 141.13m, XRF analysis was used to classify the rocks as muddy sandstones with apparent resistivity of 28Ω-m (part of the 481m thick VES stratum) and relatively low strength of 1,283.56kN/m^2.

Meanwhile, at the end of the well (321m depth bgl) there also occurs muddy sandstones of similar apparent resistivity (28Ω-m and is part of the 481m thick VES stratum) but with higher strength of 3,490.9kN/m^2 as shown in Figure 5.4.

General trends indicated that rock strengths increased downwards, which agree with the rule of consolidation.

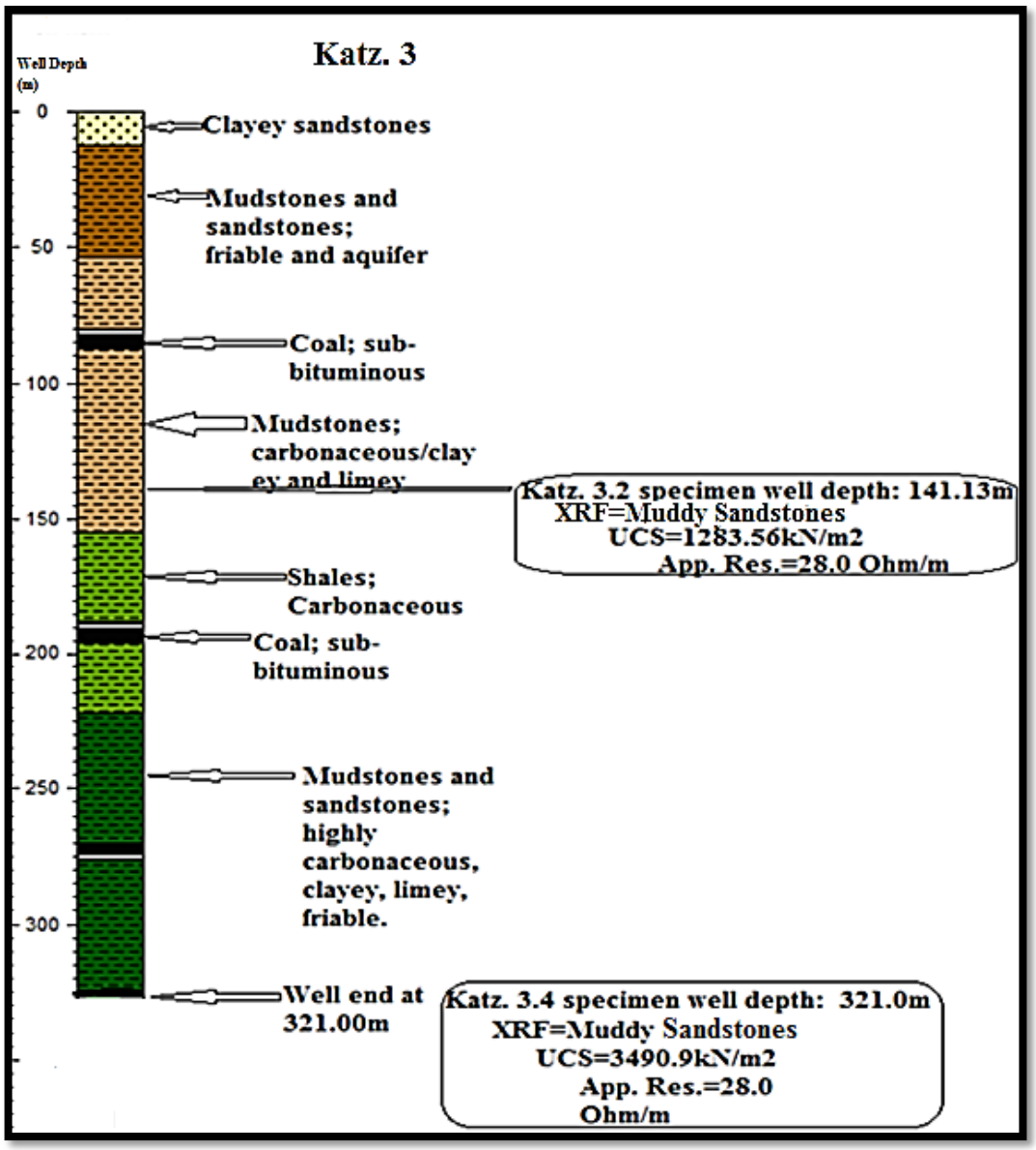

Not to scale

Figure 5.4: Schematic model for Katz.3 well area with geo-design parameters

5.5 YO 2 WELL SITE

Analyses results considered two specimens to represent the strata at YO 2 well as shown in Figure 5.5. At this well site, there was an acute unavailability of formly specimens on which to test both XRF and UCS as declared in Chapter 3, which posed challenges even during discussion stages in this project.

The specimen at 21.53m depth bgl was classified as muddy ironstones. This rock recorded strength value of 1,218.1kN/m^2 and apparent resistivity value of 0.45Ω-m (part of the 492.5m thick VES stratum). The other specimen at 43.1m depth bgl was classified as muddy sandstones of strength value of 4,411kN/m^2 and apparent resistivity value of 0.45Ω-m (part of the 492.5m thick VES stratum).

The presence of independent iron in the litho-units does not contribute to the very low apparent resistivities. Iron naturally occurred in this area mainly as compounds and not as an element. This cannot, in any major way have directly contributed to these very low apparent resistivities.

Additionally, it is important to discuss the effects of natural iron and silicon through comparison of strength in natural rocks. This effect is similar to the effects of iron in artificially simulated ferro-cement materials. In this project, this strength-boost effect is not remarkable in shaley ironstones (due to iron) as compared to marlstones and muddy shales (due to silicon through re-crystallization) as shown in Figures 5.1 and 5.5. Therefore, siliceous cementing is stronger than ferruginous cementing despite other factors. Further studies may be required to back up the explanation behind this observation.

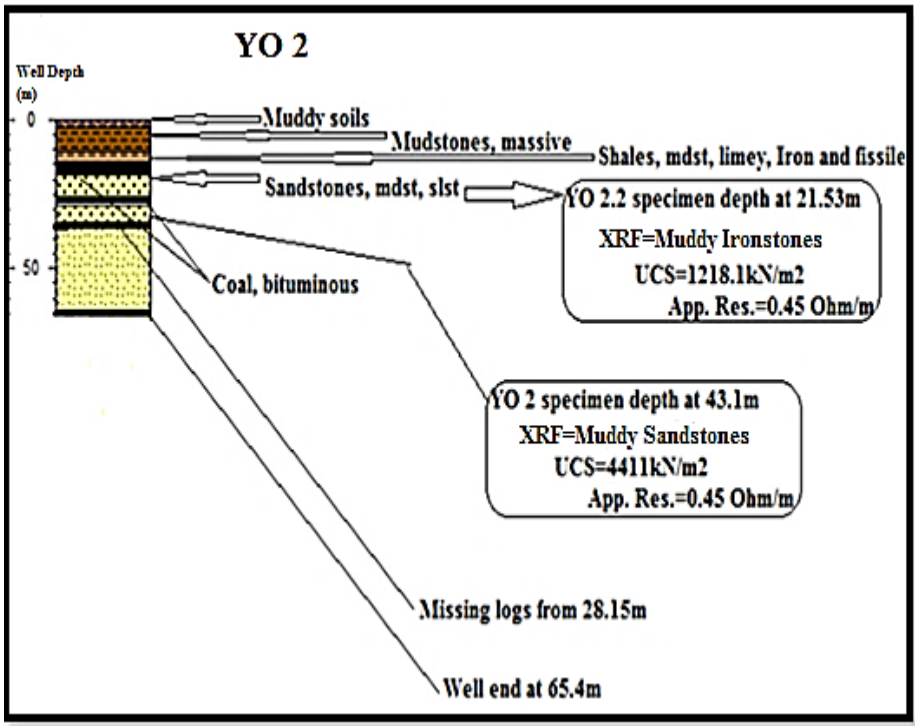

Not to scale

Figure 5.5: Schematic model for YO 2 well area with geo-design parameters

5. 6 PROJECT WELLS CORRELATION AND GENERAL OBSERVATION

Rock types, VES-derived strata thicknesses, and corresponding UCSs, all correlated established that no matching existed. For example, all the muddy sandstones varied in UCSs and strata thicknesses. At Comm. Well, specimens 2 (137.44m) had 82.5kN/m^2 while specimen 4 (238.83m) had 8,096.1kN/m^2. These muddy sandstones also varied in UCSs from the others in the rest of the wells. Examples include muddy shales from FP 3 well's specimen 3 (158.54m) has 2,989kN/m^2 and specimen 4 (258.47m) has 2,405kN/m^2.

Correlation between these properties was not possible due to lateral variations probably due to changing environments of formation and the use of analytical tools with varying accuracies. Notably, the VES 1-D software produced quite high RMS errors even with additions in the number of iterations.

In addition, it was difficult to tell what lithologies lie beyond the drilled depths based only on project results. Nevertheless, from the cross-section of a line cutting approximately NNE-SSW across this area in Figure 1.2, it is apparent that below the Mui sediments lie the MMB System rocks (which have no coal).

Regardless of the depths of strata and based on the average rock strengths and average VES results as shown in Table 5.1, the following was true. Comm. Well project site indicated relatively average strengths and relatively high apparent resistivities. All the other project sites had relatively lower resistivities despite relatively higher or sometimes lower strengths. In addition, the muddy shales, muddy ironstones, and marlstones are not included in this averaging since they occur as minor formations relative to the occurrences of muddy sandstones in the project area.

The averages of UCS rock strength and apparent resistivity are 5,272.05kN/m^2 and 10,009.85Ω-m respectively.

Despite the high RMS errors in VES analyses, the VES values tentatively compared to the classic values in Appendices C.2; generally, sandstones fall in the range of 1-740,000,000 Ω-m (project sandstones range from 0.45-50,000 Ω/m) while shales are in the range 20-2000 Ω-m (for project shales range from 28-180 Ω-m).

Table 5.1: Calculated averages of UCSs and apparent resistivities at the 5 project wells

Rock \ Well	Comm. Well		FP 3		FP 2		Katz. 3		YO 2	
Muddy Sandstones	UCS (kN/m^2)	App. Res. (Ohm-m)	UCS (kN/m^2)	App. Res. (Ohm-m)	UCS (kN/m^2)	App. Res. (Ohm-m)	UCS (kN/m^2)	App. Res. (Ohm-m)	UCS (kN/m^2)	App. Res. (Ohm-m)
	82.5	50,000	2,989	15			1,283.56	28		
	8,096.1	50,000	2,405	15	37,211.9	180			4,411	0.45
					1,642.6	5.8				
	2,900.6	50,000			972.4	5.8				
Averages	3,693.07	50,000	2,697	15	13,275.63	5.8	1,283.56	28	4,411	0.45
Combined Average	UCS (3,693.07+2,697+13,275.63+1,283.56+4,411)/5=**5,272.05 kN/m^2** App. Res.(50,000+15+5.8+28+0.45)/5=**10,009.85 Ω-m**									

CHAPTER 6: CONCLUSIONS AND RECOMMENDATIONS

6.1 CONCLUSIONS

The analysis of project results and subsequent discussions was used to reveal the geological information on ground conditions at project sites. These comprised of trends of strengths of rock strata and corresponding thicknesses at the project sites. Patterns as well as the geometries and depths of coal occurrence can guide on the applicability of either subsurface or open cast coal mining methods at each of these five project sites. In the end, the optimal mining method was be identified for each of the five project sites. The influence of aquifers on coalmine development at these sites has been also assessed.

Firstly, at Commissioning Well project site, UCS decreased either way from mid-depths (about 150m depth bgl). The whole litho-profile was dry and isotropic. Bituminous coal seams and carbonaceous matter in rocks occur approximately between 125m to 190m bgl. Aquifers at about 25m, 75m, 150m and 275m depths are highly saturated during the rainy seasons. These factors suggested that the most suitable coal mining method for Commissioning Well project site could be subsurface tunnelling, mainly during dry seasons. The use of this method can avoid the costly affair to strip the thick overburden that overlies the coal at this site. *In situ* underground coal gasification (UCG) using clean coal technology (CCT) can complement, specifically to extract the thin coal seams and other carbonaceous matter in the rocks at depths greater than 190m bgl.

Meanwhile, at FP 3 project site, the rock strengths trends generally indicated slight decreases downwards. The rockmasses at this project site are generally non-uniform and relatively weak. Quite low apparent resistivity (15Ω-m) for the 497.3m-thick bottom stratum reflects persistent ground water flows from potential aquifers (around 160m and 250m bgl). This reflects weakness. Therefore, large scaled open cast method can be used to extract the coal seams at the depths of 120m and 190m bgl as well as other carbonaceous matter in the rocks that generally occur at depths of about 90m to 200m bgl.

At FP 2 project site, the rockmasses trends in strengths indicated large increases upward but smaller increases downward from mid-well depths (about 110m bgl). The low resistivity values (180Ω-m) for mid-well stratum which is about 143.25m thick and (5.8Ω-m) for bottom stratum which is about 366m thick implies rock anisotropy while the very high strengths (up to 37,211.9kN/m^2) of the muddy shales indicates rock isotropy at the top section of the well. Based on these facts, the author suggests that the lignitc coal and sub-bituminous coal seams (at about 140m depths bgl) and carbonaceous matter in the

surrounding strata can be mined using subsurface tunnelling method. The *extra* strong muddy shales can offer enough support (as roofs) for the coalmine below. In addition, water pumping from the aquifers at about 100m and 200m can further facilitate coal mining at this site.

At Katz. 3 project site, the rock strengths trends showed increases downwards from (1283.56kN/m^2 and 3490.9kN/m^2). Relatively low apparent resistivity (28Ω-m) for the bottom stratum, which is 481m thick, reflects anisotropy in the rockmasses. Two strata (approximately 10m to 60m and 240m to 310m) are potential aquifers that comprise mainly of friable sandstones. Pumping out the water can be a solution. The safest coal mining method to extract the coal and carbonaceous matter (80m to 320m depth bgl) at this project site can therefore be large-scale open cast mining.

Finally, at YO 2 project site, the trends in strata strengths increased with depth (1218.1kN/m^2 to 4411.kN/m^2). Extremely low apparent resistivity (0.45Ω-m) for the bottom stratum that is 492.5m thick indicates high anisotropy. The bituminous coal (about 45m bgl) reported to measure about 6.50m in thickness occur at this project site. A lot of ground water can be expected to pool (about 30m to 40m depth bgl) during coalmining especially during wet seasons. This information suggests that the most suitable coal mining method can be large-scale open cast mining.

In general, the RMS error was great during processing of VES data. All, the other methodologies yielded more accurate results.

6.2 RECOMMENDATIONS

Recommendations in this project are as follows:

- Safe coal mining is feasible at project sites.
- Coal mining can proceed at project sites using the concluded mining methods (either open cast or tunnelling).
- Aquifers need to be observed when mining coal especially during the rainy seasons. Pumping out of pooled ground water can be done.
- For Comm. Well and FP 2 well sites where the recommended mining method is tunnelling, extensor-meters need be installed immediately above to monitor any potential coalmine subsidence.

- Also, during tunnelling, individual pillar designs need be done using rockmass rating (RMR) while coalmine roofing need to be appropriately propped and grouted to avoid caving-in.
- In future of coalmining in Kenya, it is also recommended that coalmines designs be based on more methods for comparative results, if finances, technology and time allows. For example, use XRF, XRD and petrography for rock classification, SARIS and ABEM Terrameters for VES, RES 1D and WINGLINK software for VES data analysis (which can avoid the great RMS errors that were observed in this study). Plate bearing and point load testing can be used for strength tests and fresh core specimens can be used in real-time testing to compare with the provided drying correctional ratios.

REFERENCES

Abraham, B, Gebrehiwot, G & Yirgale, G 2013, 'Application of Vertical Electrical Sounding and Horizontal Profiling Methods to Decipher the Existing Subsurface Stratification in River Segen Dam Site, Tigray, Northern Ethiopia,' *Journal of Environmental and Earth Science*, vol.3, no. 10, pp.42-54.

Adekoya, AT, Ehinola, OA, & Oluwajana, A 2012, 'Geophysical Investigation and Reserve Estimation of a Coal Seam in Ute Area, South-western Nigeria,' *Petroleum & Coal, International Journal for Petroleum Processing, Petrochemistry and Coal Processing,*' pp. 252-259.

Agioutantis, Z & Komnitsas, K 2004, 'Advances in Mineral Resources Management and Environmental Geotechnology (AMIREG 2004),' *Proceedings of the first International Heliotopos Conference,* pp. 25-27.

Aryberk, K, Ayhan, K & Kadir, K 2015, 'Use of Point Load Index in Estimation of the Strength Rating for the RMR System,' *Journal of African Earth Sciences*, Vol. 106, pp. 40-49.

Aydan, O & Tano, H 2011,'The Damage to Abandoned Mines and Quarries by the Great East Japan Earthquake on March 11, 2011,'*Proceedings of the International Symposium on Engineering Lessons Learned from the 2011 Great East Japan Earthquake*,' pp. 981-992.

Barker, RD 1992, 'Depth of Investigations of Collinear Symmetrical four-electrode arrays.' *Geophysics*, Vol. 54, No. 8 pp. 1031-1037

Best, MG 2002, *Igneous and Metamorphic Petrology,* 2nd Ed. John Wiley, & Sons Publishers. *pp. 616-619*

Best, MG, Christiansen EH, Gromme & Sherman 2013, 'Introduction: The 36-18 Ma Southern Great Basin, USA, Ignimbrite Province, and Flare-up: Swarms of Subduction-related Supervolcanoes', *Geosphere*, Vol. 9 Issue 2. pp. 260-274.

Cardimona, S 2002, 'Electrical Resistivity Techniques for Subsurface Investigation', *Geophysics 2002 Conference Proceedings*, pp.?

Chebet, ZK 2009, *FP02 Well Report; Lithostratigraphic and Stratigraphic Description*, *Mui Basin Coal Geo-exploration Project, Unpublished Report*. Available from: MoEP, GoK Library. [January 2009].

Chebet, ZK 2009, *FP 03 Well Report; Lithostratigraphic and Stratigraphic Description, Mui Basin Coal Geo-exploration Project, Unpublished Report*. Available from: MoEP, GoK Library. [March-April 2009].

Chebet, ZK & Otieno, JCO 2008, *Kathonzweni 3 Well Report; Lithostratigraphic and Stratigraphic Description*. *Mui Basin Coal Geo-exploration Project, Unpublished Report*. Available from: MoEP, GoK Library. [September 2008].

Culshaw M, Jefferson I & Yu MH 2006, 'Geohazards Caused by Rising Groundwater in Durham Coalfield, U.K,' *Proceeding of the International Association of Engineering Geology Congress*, pp. 367.

Debasis, D, Mark, C & Molinda, GM 2001, 'Using the coal mine roof rating (CMRR) to assess roof stability in U.S. coal mines,' *Journal of Minerals, Metallurgy and Fuel (India)*, Vol. 49, No.8-9, pp.314-321.

Debasis, D, Mark, C & Molinda, GM 2008, 'Effects of Specimen Age on the Uniaxial Compressive Strength and Moisture Content of Weak Coal Measure Rocks,' *A NIOSH (National Institute for Occupational Safety and Health) Study. Twenty-Seventh International Conference on Ground Control in Mining (ICGCM). Rock Mechanics*. pp. 51-61.

Droogers, P & Van Loon, A 2006, *Water Evaluation and Planning System (WEAP), Kitui, Kenya*. WatmanSup Netherlands Research Report No. 2. pp. 13.

Eke, KT & Igboekwe, MU 2011,' Geoelectric Investigation of Groundwater in Some Villages in Ohafia Locality, Abia State, Nigeria,' *British Journal of Applied Science & Technology*, vol.1, Issue 4, pp. 190-203.

Foundation Piling Limited 2010, *Mui Basin Coal Exploration Project. First draft Report*. Available from MoEP, GoK Library, Unpublished Report. pp. 37-39 [January 2010].

Goldich, SS 1938, 'A Study in Rock Weathering,' *Journal of Geology*, Vol. 46. pp. 17-58

Grotzinger, J & Jordan, TH 2010, *Understanding Earth*, Sixth Edition, W.H. Freeman & Company, New York, pp. 373.

Hess, PC 1989, *Origin of Igneous Rocks*, Harvard University Press. Pp275-285

Knott, DLPE 2012, *Assessment of potential subsidence impacts from coal mining using test borings, mine maps, and empirical methods*. HDR Engineering Incorporated, 3 Gateway Centre Pittsburgh, PA 15222. pp. 2-4.

Kombo, DK & Tromp, DLA 2006, *Research design, Proposal and Thesis Writing: An Introduction*. Pauline Publications Africa. Nairobi, Kenya.

Kothari, CR 2003, *Research design, Research Methods: Methods and Techniques*. Second Revised Edition, New Age International Publishers, New Delhi, India.

Lar, UA, Mohammed, ST, Oniku, SA & Yakubu, TA 2014, 'Geophysical Investigation of the Subsurface Fractures Zones Using Vertical Electrical Sounding in Kassa Volcanic

Field (KVF) on the Jos Plateau, North Central, Nigeria,' *Journal of Environmental and Earth Science.* Vol.4, No.10, 2014. pp. 150-160.

Liayang, Z 2010, 'Prediction of End-Bearing Capacity of Rock-Socket Shafts considering Rock Quality Designation (RQD),' *Canadian Geotechnical Journal*, Vol. 10, pp. 1071-1084.

Lokhande, RD, Prakash, A, Singh, KKK & Singh, KB 2004, **'**Multi-electrode resistivity imaging technique for the study of coal seam,' *Journal of Scientific & Industrial Research*, vol. 63, pp. 927-930.

Masibo, M 2009, *Legal Framework and Investment Opportunities in Kenya's Mineral Sector, Unpublished Report,* Available from: MoEMR, Mines and Geological Department Library, GoK. [2009].

Mathu, EM 1980, *Petrographic analysis of the metamorphic rock of the Migwani area.* MSc. Thesis. University of Nairobi.

Mathu, EM 1992, *The Mutito, and Ikoo faults of the Neoproterozoic Mozambique Belt, Kenya***.** Basement Tectonics. pp.7

Ministry of Energy 2011, *Updated Least Cost Power Development Plan Study for Period 2011-2031*. *Unpublished Report*. Available from: MoEP GoK Library. [March 2011].

Ministry of Energy 2011, *Coal Potential pamphlet*. *Unpublished Report.* Available from: MoEP, GoK, Libraries. [October 2011].

Ministry of Energy and Petroleum 2015, *Draft national energy and petroleum policy*. *Unpublished report.* Available from, MoEP, GoK Libraries. [January 2015].

Mutunguti, FN 2003, *The Lithologic Description of Yoonye 2 Well. Mui Basin Coal Exploration Project*. *Unpublished Report.* Available from: MoEP, GoK Library. [April 2003].

Mutunguti, FN & Ndogo, JM 2007, *The Lithologic Description of the Commissioned Well. Mui Basin Coal Exploration Project*. *Unpublished Report.* Available from: MoEP, GoK Library. [September 2008].

NCAPD, 2005, *Mwingi District Strategic Plan, 2005 to 2010, for Implementation of the National Population Policy for Sustainable Development*. Published by National Coordination Agency for Population and Development, Ministry of Planning and National Development. pp. 8

NDMA, 2014, *Kitui County, Larger Mwingi Sub-County, EWS Drought Monitoring Bulletin,* National Drought Management Authority, January, 2014. pp.3

Ndogo, J M & Omenge JM 2012, 'Drilling Challenges in Semi-lithified Sedimentary Formations of the Mui Basin, Kitui County, Kenya*', Presentations from the Ministry of Energy, Thirteenth International Geological Society of Kenya Conference*, Available from MoEP GoK Library. [21 – 23 March 2012].

Ndogo, J M & Omenge JM 2012, *Available Investment Opportunities in Coal Exploration in Mui Basin, Kitui County, Kenya, Unpublished Report*. Available from: MoEP GoK Library. [March 2012].

Nelson, AS 2012, *Subsidence: Dissolution and Human Related Causes. Natural Disasters,* Class Notes distributed at the Tulane University during 2012.

Nyamai, CM, Mathu, EM, Opiyo-Akech, N & Wallbrecher, E 2003, 'A Reappraisal of the Geology, Geochemistry, Structures and Tectonics of the Mozambique Belt in Kenya, East of the Rift System,' *African Journal of Science and Technology (AJST) Science and Engineering Series,* Vol. 4, No. 2, pp. 51-71.

Olson, RE & Lai, J 2004, *Unconfined Compression Test*, Class Notes distributed at the department of Construction Engineering at University of Chaoyang on 14 June 2013.

Onyancha, CK, Mathu, EM, Mwea & S, Ngecu, WM 2011, 'A Study on the Engineering Behaviour of Nairobi Subsoil', *Proceedings of the IEK Engineers International Conference*, pp. 104-121.

Orodho, A J 2003, *Essentials of Educational and Social Sciences Research Methods*, Masola Publishers, Nairobi.

Price, DG 2009, Engineering *Geology; Principles and Practice*, Springler-Verlag Berlin Heidelberg.

Rahim 2013, *Section 4a: Electrical Resistivity Surveying Lecture Notes* distributed at the Universiti Kebangsaan Malaysia (UKM) on 3 February 2013.

Ramamurthy, TN & Sitharam, TG 2011, *Geological Engineering: Soil Mechanics.* Revised Edition. S. Chand & Co, Ltd, pp. 213-214.

Rhett, H 2001, 'An Introduction to electrical resistivity in geophysics', *American Journal of Physics,* DOI: 10.1119/1.1378013, pp. 943-952

Rousseau, R 2013, 'How to apply the Fundamental Parameters Method to the Quantitative X-rays Fluorescence Analysis of Geological Materials,' *Journal of Geosciences and Geomatics* vol.1, no.1, pp. 1-7.

Sakamota, R & Shogaki, T 2003, 'Effect of Specimen Size on Unconfined Compressive Strength Properties for Natural Clay Deposits,' *Proceedings of the thirteenth International Offshore and Polar Engineering Conference,'* pp. 426-431.

Sanders, LD 1954, *Geology of the Kitui Area*, *Report No. 30*, *Geological Survey of Kenya*, Government Printer, Nairobi, pp.7-9.

Sqaysi, 2015, Chapter 5: *Electrical Resistivity Design Lecture Notes* distributed at the King Saud University (KSU) on 26 November 2015.

Thaxton, C & Courtier, A 2015, *Chapter 12: Resistivity Surveying Lecture Notes* distributed at the Appalachian State University (Appstate) on 26 November 2015.

Verwaal, W 2004, *Soil Mechanics Laboratory Manual*. Sixth Edition, Oxford University Press, pp. 40-45.

Xueyi Y, Zhao B, & Zhao G 2008, 'Damage Controls Mode of Mining Subsidence about Shaanbei-Jurassic Coalfield in China. Session 12: Risk Management & Subsidence Engineering,' *Paper presented at the World Mining Congress in Tehran,* pp. 52.

Zipf, Jr, RK 2006, 'Numerical Modelling Procedures for Practical. Coal Mine Design, NIOSH Pittsburgh Research Laboratory, Pittsburgh, PA, USA,' *Proceedings of the forty-first U.S. Rock. Mechanics Symposium, Golden, CO, Paper no. 06-1119,* [20 July2013].

INTERNET REFERENCES

Andy, B & Karl, W 2011, *X-Ray Fluorescence (XRF). Geochemical Instrumentation and Analysis*. Available from: <http://serc.carleton.edu/research_education/geochemsheets/techniques/XRF.html>. [1May 2013].

Gainouscr 2008, *Method for Determining the Unconfined Compressive Strength of Intact Rock Core Specimens*, South Carolina Department of Transportation Website. Available from; <http://www.scdot.org/doing/technicalpdfs/materialsresearch/testprocedure/soils/sct39.pdf>. [12 April 2013].

Infotrack, EA Ltd 2014, *General information for Mwingi East Constituency; in Kitui County,* Available from: <http://www.infotrackea.co.ke/services/leadership/constituencyinfo.php?cinf=wards&t=168>. [5 August 2014].

Scintrex 2001, *Operations Manual: Scintrex Automated Resistivity Imaging System (SARIS)*. Available from: < http://www.scintrexltd.com>. [12 April 2013].

Shimadzu 2011, *EDX Series: EDX-720/800HS Shimadzu Energy Dispersive X-Ray Fluorescence Spectrometry, Operations Manual*. Available from

<http://www.ssi.shimadzu.com/products/productpage2011.cfm?product=EDX>. [12 April 2013].

Siddhartha, K 2009, *Raw Data Processing*. Available from; <http://explorable.com/raw-data-processing.html>. [12 April 2014].

Swaine, DJ 1994, *Some Aspects of Basic Geochemistry in Coal Science*. Available from: <http://web.anl.gov/PCS/acsfuel/preprint%20archive/Files/Merge/Vol-39_2-0002.pdf>. pp. 482-485, [20 July 2013].

Van Der Murwe, JN 2001, *Develop international links for cooperative research in coal mining with special emphasis on interaction with international experts for developing industry guidelines for the design of pillars in coal mines*. Available from: Safety in Mines Research Advisory Committee Libraries, COL 815 electronically as <http://www.iea.org/ciab/papers/coal.pdf>. [20 July 2013].

Vulcanhammer 2001, *Soil Mechanics; Unconfined Compression Test*. Available from<http://www.vulcanhammer.net/utc/ence361/f2001/361ll8.pdf#page=1&zoom=auto, 620,7920.2>. [1 May 2013].

APPENDICES

APPENDIX A

UNCONFINED COMPRESSIVE STRENGTH (UCS) TEST INFORMATION

Complementary information on sampled specimens and data collection through testing regarding unconfined compressive strength (UCSs) are shown in *Appendix A.1* to *A.3*.

APPENDIX A.1: PHOTOGRAPHS OF SPECIMENS

The other 11 project specimens, as sampled from Mathuki stores, Block C, Mui Basin for testing in this project are shown in Plates A.1.1 to A.1.11.

All the numerical values in both the pink labels and the captions signify the well lengths from ground level (GL) up to the middle (half-length) of any given specimen.

Plate A.1.1: Drill-core specimen in box from Comm. well at depth of 137.43 metres bgl; muddy sandstones

Plate A.1.2: Drill-core specimen in box from Comm. well at depth of 145.15 metres bgl; Marlstones

Plate A.1.3: Drill-core specimen in box from Comm. well at depth of 279.35 metres bgl; muddy sandstones

Plate A.1.4: Drill-core specimen in box from Katz. 3 at depth of 141.13 metres bgl; muddy sandstones

Plate A.1.5: Drill-core specimen in box from FP 2 at depth of 49.4 metres bgl; muddy shales

Plate A.1.6: Drill-core specimen in box from FP 2 at depth of 179.80 metres bgl; muddy sandstones

Plate A.1.7: Drill-core specimen in box from FP 2 at depth of 193.57 metres bgl; Muddy sandstones

Plate A.1.8: Drill-core specimen in box from FP 3 at depth of 158.54 metres bgl; muddy sandstones

Plate A.1.9: Drill-core specimen in box from FP 3 at depth of 258.47 metres bgl; muddy sandstones

Plate A.1.10: Drill-core specimen in box from YO 2 at depth of 21.53 metres bgl; muddy ironstones

Plate A.1.11: Drill-core specimen in box from YO 2 at depth of 43.1 metres bgl; muddy sandstones

APPENDIX A.2: UCS LABORATORY DATA COLLECTION

UCS laboratory tests results of the remainder 11 specimens for this project are shown in Plates A.2.1 to A.2.11.

Plate A.2.1: Brittle failure, through crumbling, is at a vague approximate of 45° to horizontal plane, characteristic of muddy sandstones so UCS result was accepted, Ramamurthy and Sitharam (2010)

Plate A.2.2: Another display of brittle failure in muddy sandstones, so UCS result was accepted

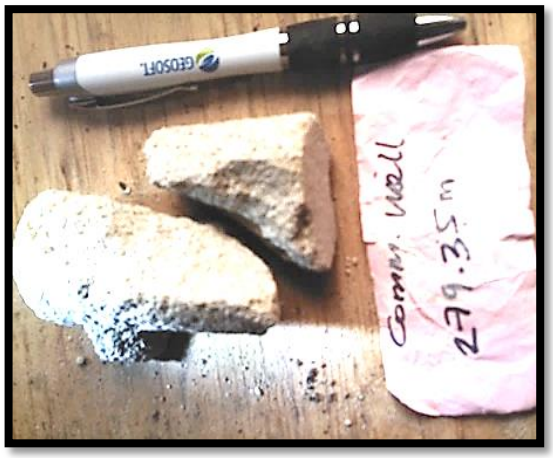

Plate A.2.3: Exhibition of brittle failure in muddy sandstones, so UCS result was accepted

Plate A.2.4: Brittle failure, through crumbling, is at a vague approximate of 45° to horizontal plane, characteristic of muddy shales so UCS result was accepted

Plate A.2.5: Good display for brittle failure in muddy sandstones so UCS result was accepted

Plate A.2.6: Excellent brittle failure at approximately 45° to horizontal plane in muddy sandstones so UCS result was accepted

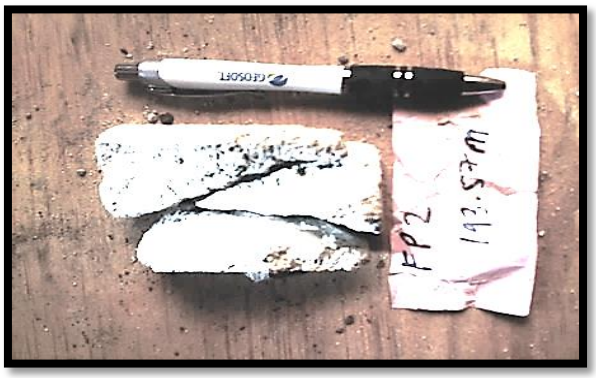

Plate A.2.7: Excellent brittle failure at approximately 45° to horizontal plane in muddy sandstones so UCS result was accepted

Plate A.2.8: Good brittle failure at approximately 45° to horizontal plane in muddy sandstones so UCS result was accepted

Plate A.2.9: Excellent brittle failure at approximately 45° to horizontal plane in muddy shales so UCS result was accepted

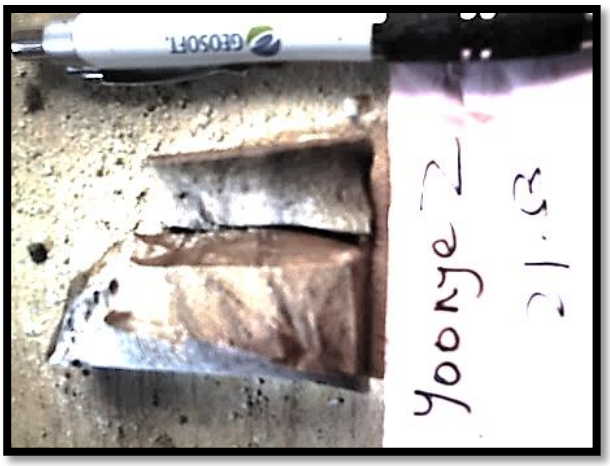

Plate A.2.10: Good brittle failure at approximately 45° to horizontal plane in muddy ironstones so UCS result was accepted

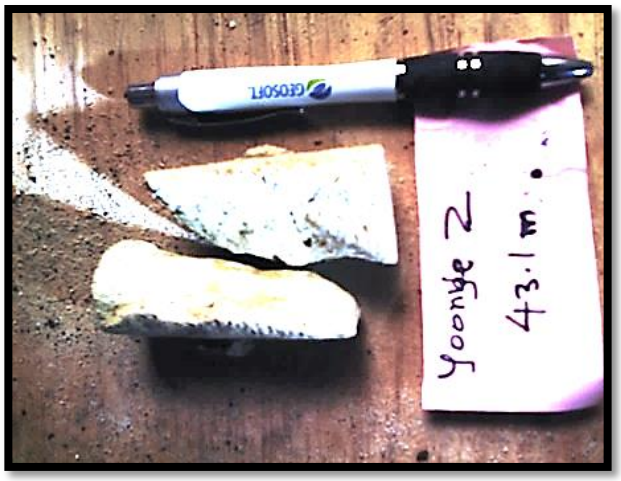

Plate A.2.11: Good brittle failure at approximately 45° to horizontal plane in muddy sandstones so UCS result was accepted

APPENDIX A.3: COMPUTATIONAL RESULTS OF UCSs

This project' calculations results for UCSs per specimens are presented bulkily in Appendix A.3 (1-13),

1. Comm. well 2 specimen

   Initial length (L_0) conversion, (160mm/1000) =0.16m

   Change in initial length, (ΔL) m= (0.1297×0.001×2) =0.0002594m

   Axial strain, (ϵ) = ($\Delta L/L_0$) = (0.0002594/0.16)=0.00162125

   Initial cross-sectional area, $A_0=\pi(r)^2$, where, r= ($\phi c/2$) and, ϕ=55.5mm×0.001=0.0555m

   Therefore, A_0= (22/7) × $(0.0555/2)^2$=0.02420196m^2

   Corrected cross-sectional area, $A_c=A_0/(1-\epsilon)$ = (0.02420196/ (1-0.00162125) =0.024241216m^2

   UCS (q_u) =F/A_c= (2/0.024241216)=82.504 kN/m^2

2. Comm. well 3 specimen

Initial lengths conversion; L_0A (125mm/1000) =0.125m and L_0B= (115mm/1000) =0.115m

Change in initial lengths, ΔLA (m) and ΔLB (m); ΔLA (m) = (0.1297×0.001×68) =0.0088196m and ΔLB (m) = (0.1297×0.001×135) =0.0175095m

Axial strains, $(\epsilon A)=(\Delta LA/L_0A)=(0.0088196/0.125)=0.070568$ and axial strain, $(\epsilon B)=(\Delta LB/L_0B)=(0.0175095/0.115)=0.1522565217$

Initial cross-sectional areas; $A_01=\pi(rA)^2$, where, $rA=(\phi A/2)$ and $\phi=(63\times0.001)=0.063m^2$ and $A_02=\pi(r)^2$, where $rB=(\phi B/2)$ and $\phi=(63\times0.001)=0.063m^2$.Therefore, $A_01=(22/7)\times(0.063/2)^2=0.0031185m^2$ same as $A_02=0.0031185m^2$

Corrected cross-sectional areas, A_c1 and A_c2; $A_c1=A_01/(1-\epsilon A)=(0.0031185/(1-0.0705568)=0.0033552341m^2$ and, also $A_c2=A_02/(1-\epsilon B)=(0.0031185/(10.15225621)=0.003678587m^2$

UCS (q_uA) and UCS (q_uB) in (kN/m^2) and the average UCS (q_U av.) in (kN/m^2) UCS (q_uA) $=FA/A_c1=(68/0.003355234)=20,266.843kN/m^2$ and UCS (q_uB)$=FB/A_c2=(135/0.003678587)$

$=36,698.865kN/m^2$

Average UCS ($q_u$av.)= (20,266.843+36,698.865)/2 $kN/m^2=28,482.854kN/m^2$

3. Comm. well 4 specimen

Initial length (L_0A) conversion, (100mm/1000) =0.1m and L_0B= (100mm/1000) =0.1m

Change in initial length, (ΔLA) m= (0.1297×0.001×75) =0.0097275m

Change in initial length, (ΔLB) m= (0.1297×0.001×65) =0.0084305m

Axial strain, $(\epsilon A) = (\Delta LA/L_0A) = (0.0097275/0.1)=0.097275$

Axial strain, $(\epsilon B) = (\Delta LB/L_0B) = (0.0084305/0.1)=0.084305$

Initial cross-sectional area, $A_01=\pi\ (rA)^2$, where, $rA= (\phi A/2)$ and, $\phi= (100\times0.001) =0.1m^2$

And, $A_02=\pi(r)^2$, where $rB= (\phi B/2)$ and $\phi= (100\times0.001) =0.1m^2$

Therefore, $A_01=(22/7)\times(0.05)^2=0.007857142m^2$ and $A_02=22/7\times(0.05)^2=0.007857142m^2$Corrected cross-sectional area, $A_c1=A_01/(1-\epsilon A)=(0.007857142/(1-0.097275)=0.008703804m^2$ and $A_c2=A_02/(1-\epsilon B)=(0.007857142/(1-0.084305)=0.008580522m^2$

UCS (q_uA)$=FA/A_c1=(75/0.008703804)=8,616.922kN/m^2$ and

UCS (q_uB)$=FB/A_c2=(65/0.008580522)=7,575.296kN/m^2$

Average UCS ($q_u$av.)= (8,616.922+7,575.296)/2kN/m^2=8,096.109kN/m^2

4. Comm. well 5 specimen

Initial length (L_0A) conversion, (90mm/1000) =0.09m and L_0B= (90mm/1000) =0.09m

Change in initial length, (ΔLA) m= (0.0254×0.001×42) =0.0010668m

Change in initial length, (ΔLB) m= (0.0254×0.001×38) =0.0009652m

Axial strain, (ϵA) = (ΔLA/L_0A) = (0.0010668/0.09)=0.011853333

Axial strain, (ϵB) = (ΔLB/L_0B) = (0.0009652/0.09)=0.010724444

Initial cross-sectional area, $A_0$1=π (rA)^2, where, rA= (ϕA/2) and ϕ=45×0.001=0.045m^2

And, $A_0$2=π(r)^2, where rB= (ϕB/2) and ϕ=45×0.001=0.045m^2

Therefore, $A_0$1=(22/7)×(0.00225)^2=0.001591071m^2 and

$A_0$2=22/7× (0.225)^2=0.001591071m^2

Corrected cross-sectional area, A_c1=$A_0$1/(1-ϵA)=(0.001591071/

(1-0.0011853333)=0.001610156m^2 and A_c2=$A_0$2/ (1-ϵB)=(0.001591071/

(1-0.0010724444) =0.001608319m^2

UCS (q_uA)=FA/A_c1=(42divisions×0.1958)/0.00160156=5107.331kN/m^2 and UCS (q_uB) =FB/A_c2=(38 divisions×0.1958)/0.010724444)=693.780kN/m^2

Average UCS ($q_u$av.)= (5,107.331+693.780)/2kN/m^2=2,900.555kN/m^2

5. Katz 3.2 specimen

Initial length (L_0) conversion, (90mm/1000) =0.09m

Change in initial length, (ΔL) m= (10×0.0254) = (0.254×0.001) =0.000254m

Axial strain (ϵ) =ΔL/L_0= (0.000254/0.09)=0.00282222

Initial cross-sectional area, A_0=π(r)^2, where, r= (ϕ/2) and ϕ= (44mm×0.001) =0.044m

Therefore, A_0= (22/7) × (0.044/2)^2=0.001521142m^2

Corrected cross-sectional area, A_c=A_0/ (1-ϵ) = (0.01521142/

(1-0.00282222) =0.001525447m^2

UCS (q_u) = (F/A_c) = (10divisions×1.958)/0.001525447) = 1,283.56 kN/m^2

6. Katz 3.4 specimen

Initial length (L_0) conversion, (100mm/ (1000) =0.1m

Change in initial length (ΔL) m= (32×0.0254 ×0.001) =0.0008128m

Axial strain (ϵ) =ΔL/L_0= (0.0008128/0.1)=0.008128

Initial cross-sectional area, A_0=π(r)^2, where, r= (ϕ/2) and ϕ= (47.6mm×0.001) =0.0476m

Therefore, A_0= (22/7) × (0.0476/2)^2=0.00178024m^2

Corrected cross-sectional area, A_c= (A_0/ (1-ϵ) = (0.00178024/

(1-0.008128) =0.001794828m²

UCS (q_u) =F/A_c= (32divisions×0.1958)/0.001794828)=3,490.92kN/m²

7. FP 2.1 specimen

Initial length (L_0) conversion L_0= (115mm/ 1000) =0.115m

Change in the initial length, ΔL (m) = (140×0.1297 ×0.001) =0.018158m

Axial strain (ϵ) = (ΔL/L_0) = (0.018158/0.115=0.157895652)

Initial cross-sectional area A_0=π(r) ²; where, r= (ϕ/2) and ϕ= (63.5mm×0.001) =0.0635m and A_0= (22/7) × (0.0635/2)²=0.003168196m²

Corrected cross-sectional area, A_c=A_0/(1-ϵ)=(0.003168196/

(10.1567895652) =0.003762236m²

UCS (q_u) =F/A_c= (140/0.003762236)=37,211.91kN/m²

8. FP 2.3 specimen

Initial length (L_0A) conversion, (95mm/1000) =0.095m and L_0B= (90mm/1000) =0.09m

Change in initial length, (ΔLA) m= (0.0254×0.001×6) = 0.0001524m

Change in initial length, (ΔLB) m= (0.0254×0.001×10) = 0.0002540m

Axial strain, (ϵA) = (ΔLA/L_0A) = (0.0001524/0.095)=0.00160421

Axial strain, (ϵB) = (ΔLB/L_0B) = (0.0002540/0.09)=0.017824561

Initial cross-sectional area, $A_0$1=π (rA) ², where, rA= (ϕA/2) and ϕ=45×0.001=0.045m²

And, $A_0$2=π(r) ², where rB= (ϕB/2)] and, ϕ=45×0.001=0.045m²

Therefore, $A_0$1= (22/7) × (0.0225)²=0.001591071m² and

$A_0$2=22/7× (0.0225)²=0.001591071m²

Corrected cross-sectional area,

A_c1=$A_0$1/(1-ϵA)=(0.001591071/(10.00160421)=0.0015936275131929m² and

A_c2=$A_0$2/(1-ϵB)=(0.001591071/(1-0.017824561)=0.0016199458231413m²

UCS (q_uA) =FA/A_c1= (6divisions×0.1958)/0.0015936275131929=737.19kN/m² and

UCS (q_uB) =FB/A_c2= (10divisions×0.1958)/ 0.0016199458231413)=1,208.68kN/m²

Average UCS (q_u av.)= (737.19+1208.68)/2kN/m²=972.94kN/m²

9. FP 2.4 specimen

Initial length (L_0) conversion, (87mm/ 1000) =0.087m

Change in initial length (ΔL) m= (15×0.0254 ×0.001) =0.000381m

Axial strain (ϵ) = (ΔL/L_0) = (0.000381/0.087)=0.00437931

Initial cross-sectional area, A_0=π(r) ², where, r= (ϕ/2) and ϕ= (47.6mm×0.001) =0.0476m

Therefore, A_0= (22/7) × (0.0476/2)²=0.00178024m²

Corrected cross-sectional area, $A_c=A_0/(1-\epsilon)$ = (0.00178024/ (1 0.00437931)=0.00178807m^2

UCS (q_u) = (F/A_c) = (15divisions×0.1958)/ 0.00178807)=1,642.55kN/m^2

10. FP 3.3 specimen

Initial length (L_0A) conversion, (75mm/1000) =0.075m and, L_0B= (75mm/1000) =0.075m

Change in initial length, (ΔLA) m= (0.0254×0.001×29) = 0.0007366m

Change in initial length, (ΔLB) m= (0.0254×0.001×20) = 0.000508m

Axial strain, (ϵA) = ($\Delta LA/L_0A$) = (0.0007366/0.075)=0.009821333

Axial strain, (ϵB) = ($\Delta LB/L_0B$) = (0.000508/0.075)=0.006773333

Initial cross-sectional area, $A_01=\pi (rA)^2$, where, rA= ($\phi A/2$) and, ϕ=45×0.001=0.045m^2

And, $A_02=\pi(r)^2$, where rB= ($\phi B/2$) and ϕ= (45×0.001) =0.045m^2

Therefore, A_01= (22/7) × $(0.0225)^2$=0.001591071m^2 and,

A_02=22/7× $(0.0225)^2$=0.001591071m^2

Corrected cross-sectional area,

$A_c1=A_01/(1-\epsilon A)$=[(0.001591071/(10.009821333)=0.001606852m^2 and

$A_c2=A_02/(1-\epsilon B)$=(0.001591071/(1-0.006773333)=0.001601921m^2

UCS (q_uA) =FA/A_c1= (29divisions×0.1958)/0.001606852=3,533.74kN/m^2 and, UCS (q_uB) =FB/A_c2= (20divisions×0.1958)/0.001601921)=2,444.56kN/m^2

Average UCS ($q_u$av.)= (3,533.74+2,444.56)/2kN/m^2=2,989.15kN/m^2

11. FP 3.4 specimen

Initial length (L_0A) conversion, (95mm/1000) =0.095m and L_0B= (95mm/1000) =0.095m

Change in initial length, (ΔLA) m= (0.0254×0.001×18) =0.0004572m

Change in initial length, (ΔLB) m= (0.0254×0.001×26) =0.0006604m

Axial strain, (ϵA) = ($\Delta LA/L_0A$) = (0.0004572/0.095)=0.004812631

Axial strain, (ϵB) = ($\Delta LB/L_0B$) = (0.0006604/0.095)=0.0006604

Initial cross-sectional area, $A_01=\pi (rA)^2$, where, rA= ($\phi A/2$) and, ϕ= (47.6×0.001) =0.0476m^2

And, $A_02=\pi(r)^2$, where rB= ($\phi B/2$) and ϕ= (47.6×0.001) =0.0476m^2

Therefore, A_01= (22/7) × $(0.0238/2)^2$=0.00178024m^2 and,

A_02=22/7× $(0.0238)^2$=0.00178024m^2

Corrected cross-sectional area,

$A_c1=(A_01/(1-\epsilon A)$=(0.00178024/(1-0.004812631)=0.001788849m^2 and

$A_c2=(A_02/(1-\epsilon B)=(0.00178024/(1-0.0069551578)=0.001792702m^2$

$UCS(q_uA)=(FA/A_c1)=(18divisions\times0.1958)/0.001788849=1,970.21kN/m^2$ *and*

$UCS\ (q_uB)=(FB/A_c2)=(26divisions\times0.1958)/0.001792702)=2,839.74kN/m^2$

Average UCS $(q_uav.)= (1,970.21+2,839.74)/2kN/m^2=2,404.975kN/m^2$

12. YO 2.2 specimen

Initial length (L_0) *conversion, (75mm/ (1000) =0.075m*

Change in initial length, (ΔL) $m= (6\times0.0254\times0.001) =0.0001524m$

Axial strain, $(\epsilon) = (\Delta L/L_0) = (0.0001524/0.075)=0.002032$

Initial cross-sectional area, $A_0=\pi(r)^2$, *where,* $r= (\phi/2)$ *and* $\phi= (35mm\times0.001) =0.035m$

Therefore, $A_0= (22/7) \times (0.035/2)^2=0.0009625m^2$

Corrected cross-sectional area, $A_c= (A_0/ (1-\epsilon)) = (0.0009625/ (1-0.002032) =0.000964459m^2$

UCS $(q_u) =F/A_c= (6divisions\times0.1958)/0.000964459)=1,218.09kN/m^2$

13. YO 2.4 specimen

Initial length (L_0) *conversion, (75mm/1000) =0.075m*

Change in initial length, (ΔL) $m= (20\times0.0254\times0.001) =0.000508m$

Axial strain, $(\epsilon) = (\Delta L/L_0) = (0.000508/0.075)=0.00677333$

Initial cross-sectional area, $A_0=\pi(r)^2$, *where,* $r= (\phi/2)$ *and* $\phi= (33.5mm\times0.001=0.0335m$

Therefore, $A_0= (22/7) \times (0.0335/2)^2=0.000881767m^2$

Corrected cross-sectional area, $A_c=A_0/ (1-\epsilon)$

$= (0.000881767/ (1-0.00673333) =0.00088778m^2$

$UCS(q_u) = (F/A_c) = (20divisions\times0.1958)/0.00088778)=4,411.003kN/m^2$

APPENDIX B

ED-XRF TEST ANALYSIS QUANTITATIVE RESULTS

APPENDIX B.1: QUANTITATIVE ED-XRF DATA SETS

Quantitative ED-XRF data sets collected for this project are shown in Tables B.1 to B.5.

Table B.1: ED-XRF quantitative results for Comm. well drill-core specimens at various depths

ED-XRF TEST RESULTS				
Comm. Well				
Well depth (m)	137.43	145.15	239.83	279.35
SiO_2	60.248	36.568	78.656	68.963
Al_2O_3	32.340	15.334	14.663	27.838
Fe_2O_3	4.924	4.058	3.656	1.814
TiO_2	1.244	0.729	0.290	0.774
CaO	0.450	38.071	0.673	0.325
K_2O	0.441	0.833	0.246	1.642

Table B.2: ED-XRF quantitative results for Kathonzweni 3 and FP 2 drill-core specimens at various depths

ED-XRF TEST RESULTS					
Kathonzweni 3			**FP 2**		
Well depth (m)	141.13	321.0	49.4	179.8	193.57
SiO_2	58.212	63.258	73.917	70.242	61.348
Al_2O_3	33.949	33.088	14.359	24.736	33.810
Fe_2O_3	5.490	1.147	4.255	1.815	2.314
TiO_2	1.307	0.236	0.381	0.745	1.005
CaO	0.405	0.168	1.201	0.345	0.243
K_2O	0.446	1.446	0.335	1.778	1.160

Table B.3: ED-XRF quantitative results for FP 3 and YO 2 drill-core specimens at various depths

ED-XRF TEST RESULTS				
FP 3			**YO 2**	
Well depth (m)	158.54	258.41	21.53	43.1
SiO_2	64.423	67.018	37.361	65.753
Al_2O_3	31.517	27.825	10.646	28.532
Fe_2O_3	2.135	2.293	45.108	2.521
TiO_2	0.593	0.711	0.000	0.757
CaO	0.414	0.435	2.937	0.566
K_2O	0.774	1.505	0.155	1.606

Table B.4: CIPW norm classification for FP 2, FP 3 and YO 2 Well specimen at various depths

Weight (%) Norm						
Normative Mineral	**FP 2 (179.8m)**	**(193.57m)**	**FP 3 (158.47m)**	**(258.47m)**	**YO 2 (21.53m)**	**(43.1m)**
Quartz	62.95	56.47	60.77	60.54	32.77	33.55
Plagioclase	1.74	1.19	1.69	1.77	9.20	9.39
Orthoclase	10.52	6.86	4.55	8.92	0.95	0.95
Corundum	22.24	32.16	30.08	25.57	7.11	7.27
Rutile	0.75	1.01	0.59	0.71	0.00	0.00
Haematite	1.82	2.32	2.14	2.30	47.38	46.14
Anhydrite	0.00	0.00	0.17	0.20	2.69	2.69
Total (%)	100.02	100.01	99.99	100.01	100.05	99.99
Density (g/cm^3)	2.42	2.47	2.45	2.44	2.86	2.83

Table B.5: CIPW norm classification for Comm. Well and Katz. 3 Well specimens at various depths

Weight (%) Norm					
Normative Mineral	**Comm. Well** (137.43m)	(239.35m)	(279.35m)	**Katz.3** (141.13m)	(321.0m)
Quartz	57.92	77.70	64.32	55.84	57.52
Plagioclase	1.76	0.00	1.64	1.62	0.53
Orthoclase	2.60	1.48	6.15	2.66	8.57
Corundum	31.28	14.39	26.10	32.89	31.35
Rutile	1.25	0.38	0.77	1.31	0.74
Haematite	4.93	3.66	1.01	5.49	1.15
Anhydrite	0.26	2.94	0.00	0.20	0.15
Total (%)	100.00	100.00	100.01	100.01	100.01
Density (g/cm^3)	2.49	2.38	2.43	2.50	2.45

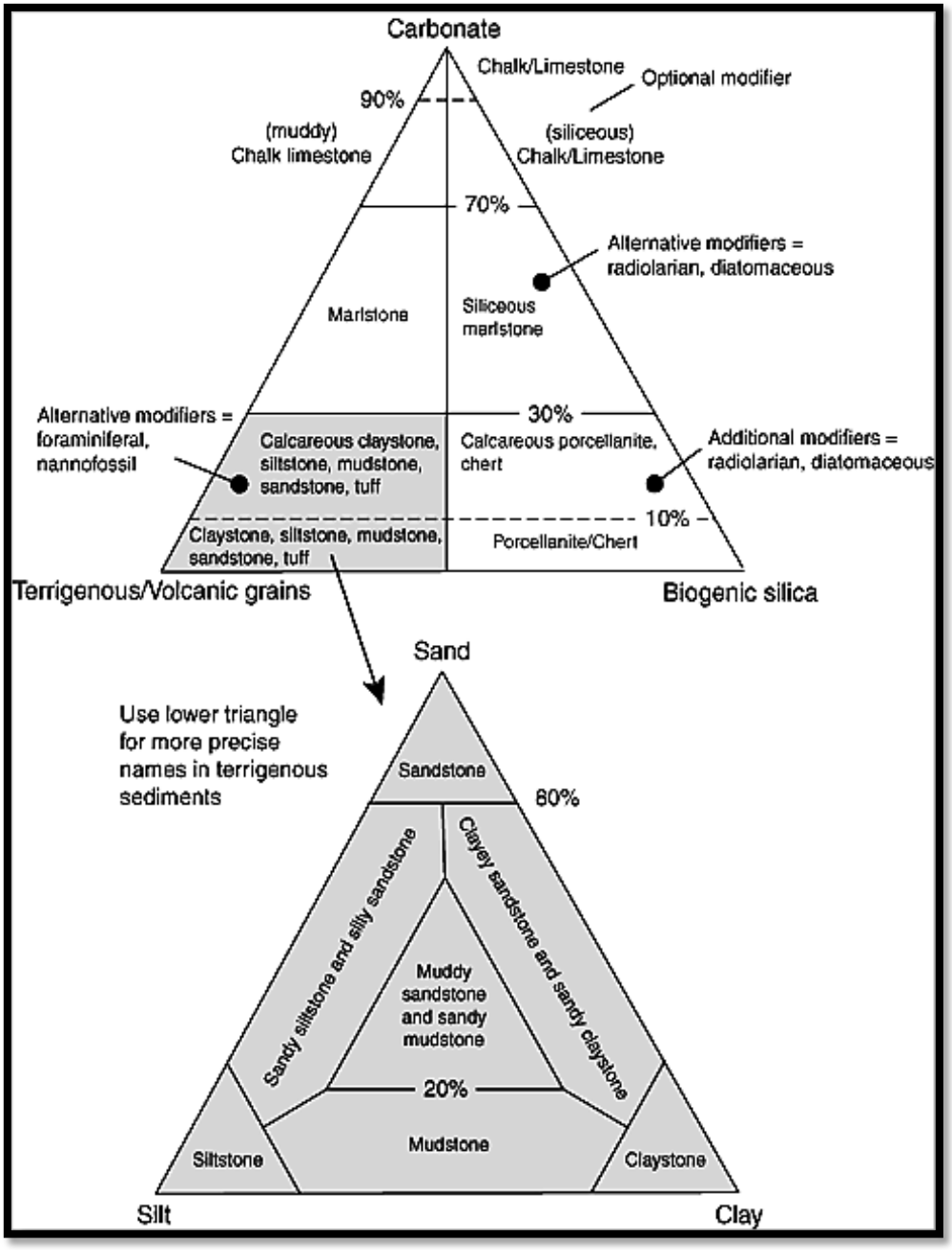

Figure B.1: Ternary diagram classification for marlstones, sandstones, claystones, mudstones, siltstones, and other intermediate sedimentary rocks (Internet Google picture-illustrations for classification of sedimentary

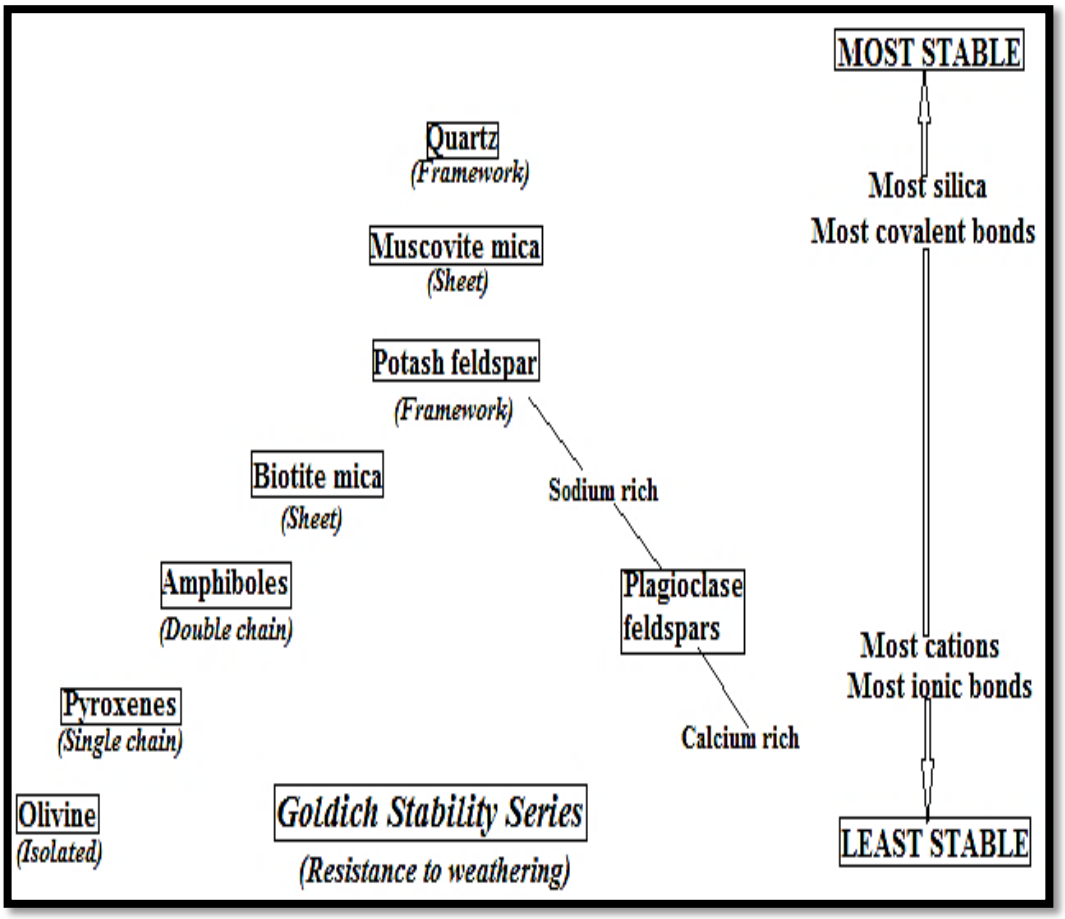

Figure B.2: Illustration for generalized mineral-stabilities during chemical weathering of granitoid gneisses, modified from (Goldich, 1938)

Stability of common minerals under weathering conditions compared with Bowen's reaction series				
Stability of minerals	Bowen's reaction series			
Most stable				
Iron oxide (hematite)				
Aluminum hydroxide (gibbsite)	Last to crystalize			
Quartz	Quartz			
Clay minerals				
Muscovite mica	Muscovite	Mafic minerals		Plagioclase feldspars
Potassium feldspars (orthoclase)	Orthoclase			
Biotite mica	Biotite			
Sodium-rich feldspar (albite)			Albite	
Amphibole	Amphibole		⇧	
Pyroxene				
Calcium-rich feldspars (anorthite)	⇧		Anorthite	
Olivine	Olivine			
Calcite				
Halite				
Least stable	First to crystalize			

Figure B.3: Illustration for generalized mineral-stabilities during chemical weathering of igneous and metamorphic rocks, re-drawn from (Grotzinger & Jordan, 2010)

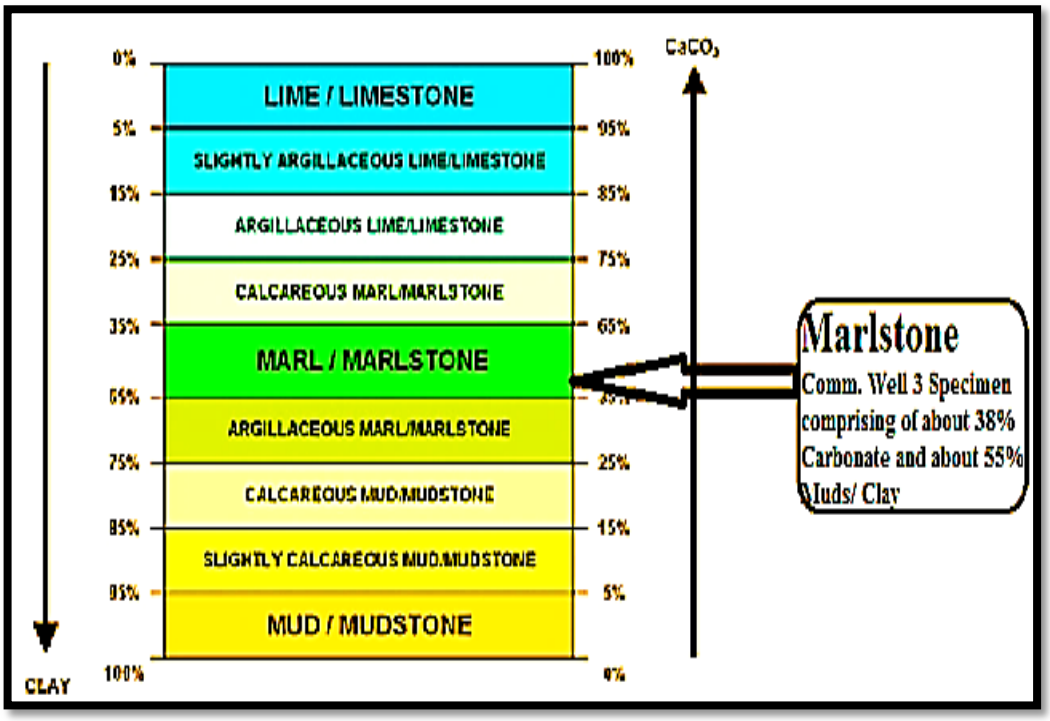

Figure B.4: Illustration for classification of Comm. well 3 marlstones specimen, modified from (The American Heritage Dictionary of the English Language 5th Ed, 2011)

VES ANALYSES RESULTS

APPENDIX C.1: VES ANALYSES RESULTS

The other four sets of VES analyses results for this project are presented as printouts from RES1-D analysis software as shown in Figures C.1.1 to C 1.8.

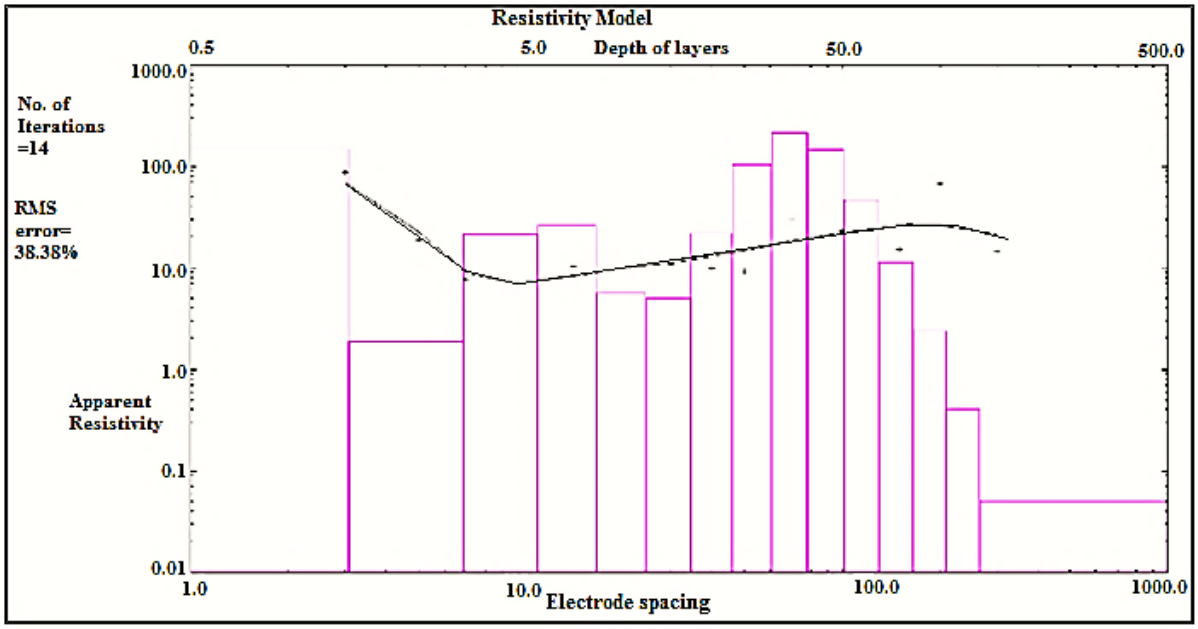

Figure C.1.1: Katz E-W drill-well auto-inversion resistivity model

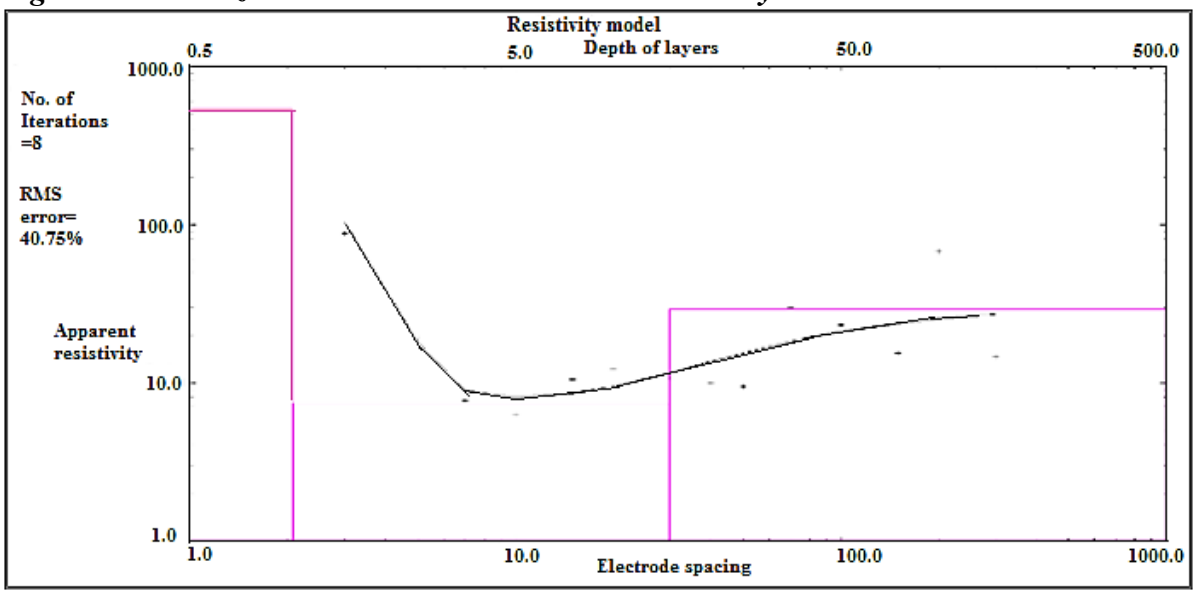

Figure C.1.2: Katz E-W drill-well forward model (user-provided parameters)

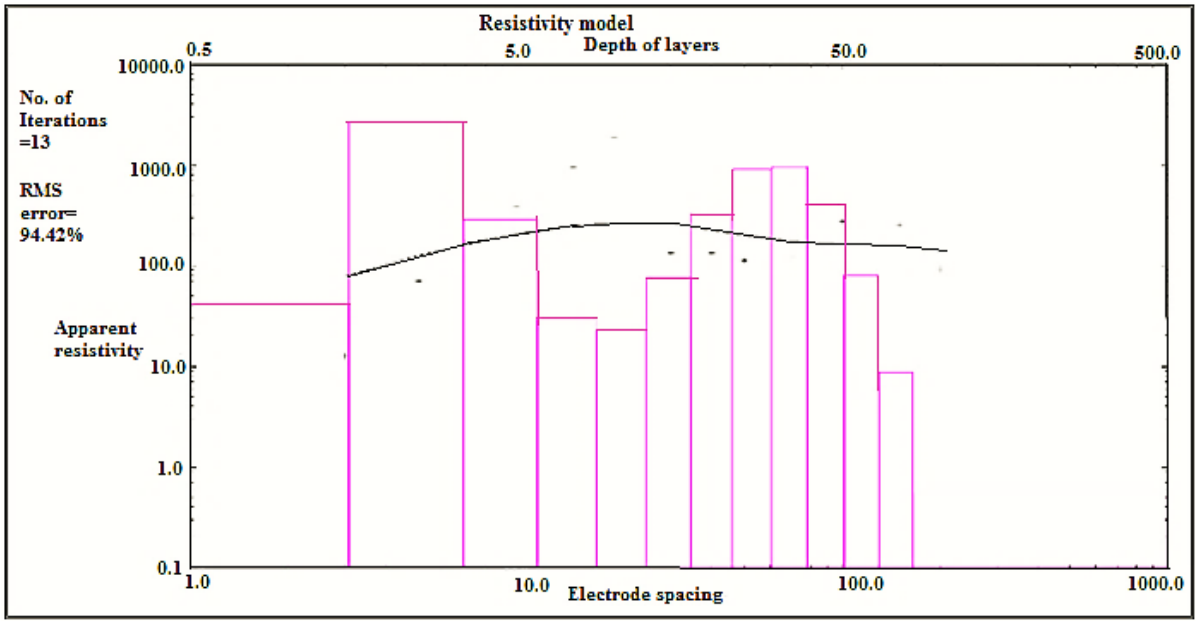

Figure C.1.3: FP 2 E-W drill-well auto-inversion resistivity model

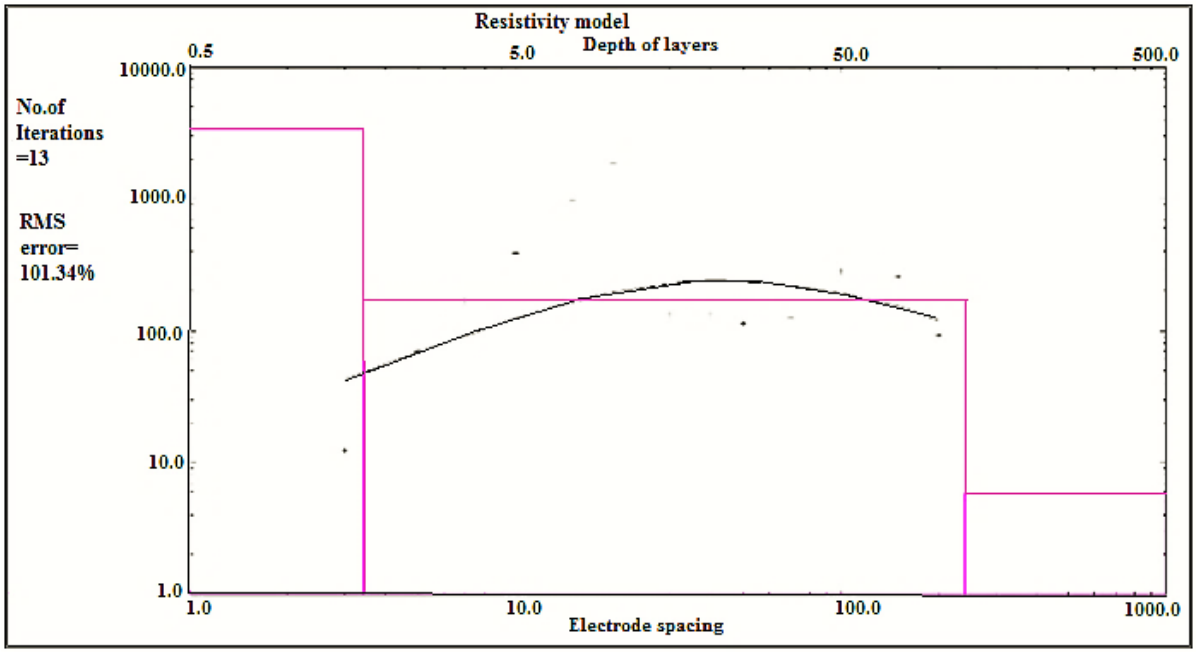

Figure C.1.4: FP 2 E-W drill-well forward model (user-provided parameters)

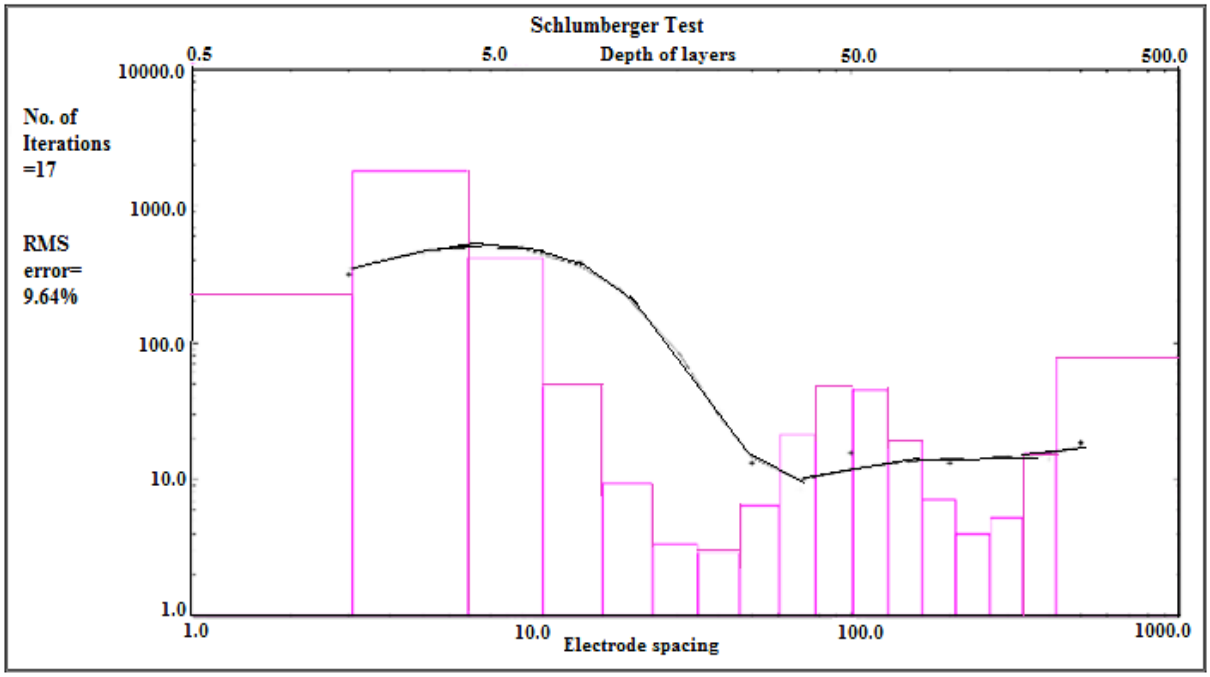

Figure C.1.5: FP 3 N-S drill-well auto-inversion resistivity model

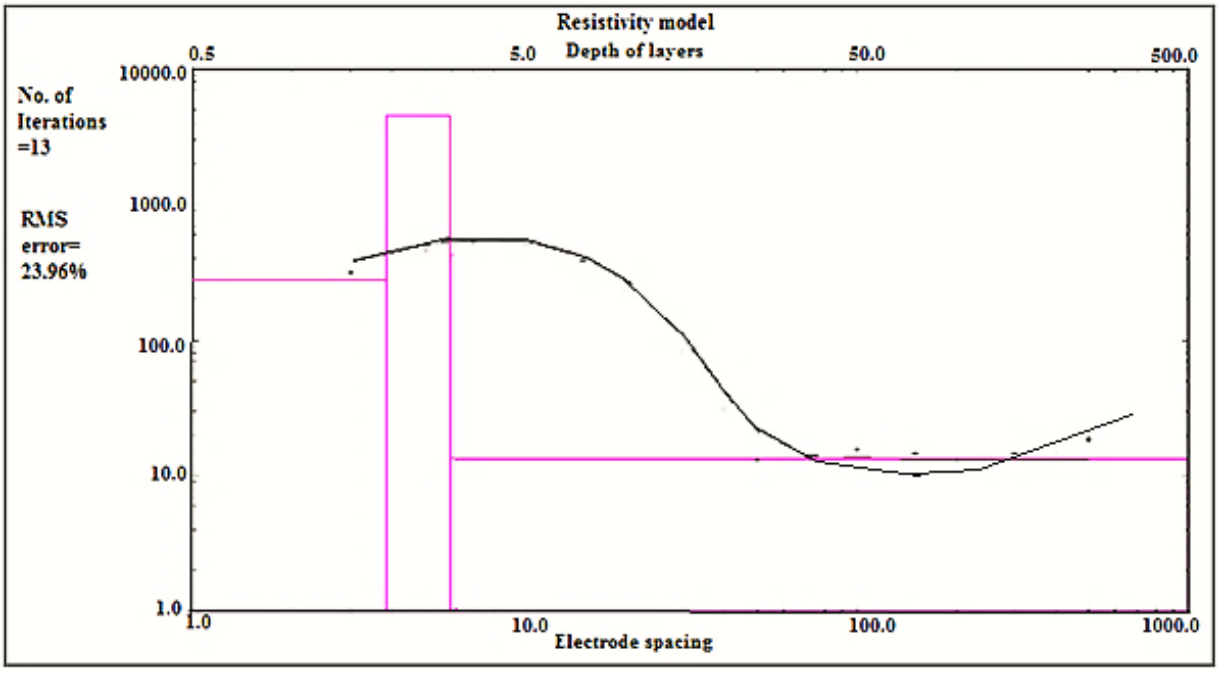

Figure C.1.6: FP 3 N-S drill-well forward model (user-provided parameters)

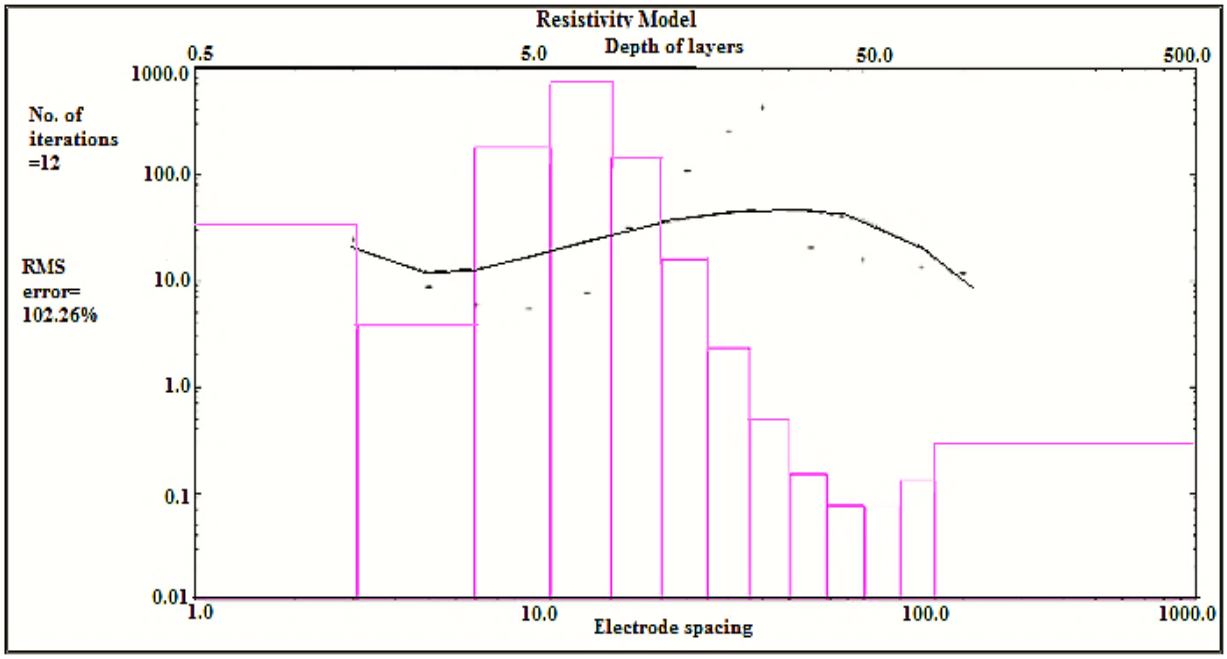

Figure C.1.7: YO 2 E-W drill-well auto-inversion resistivity model

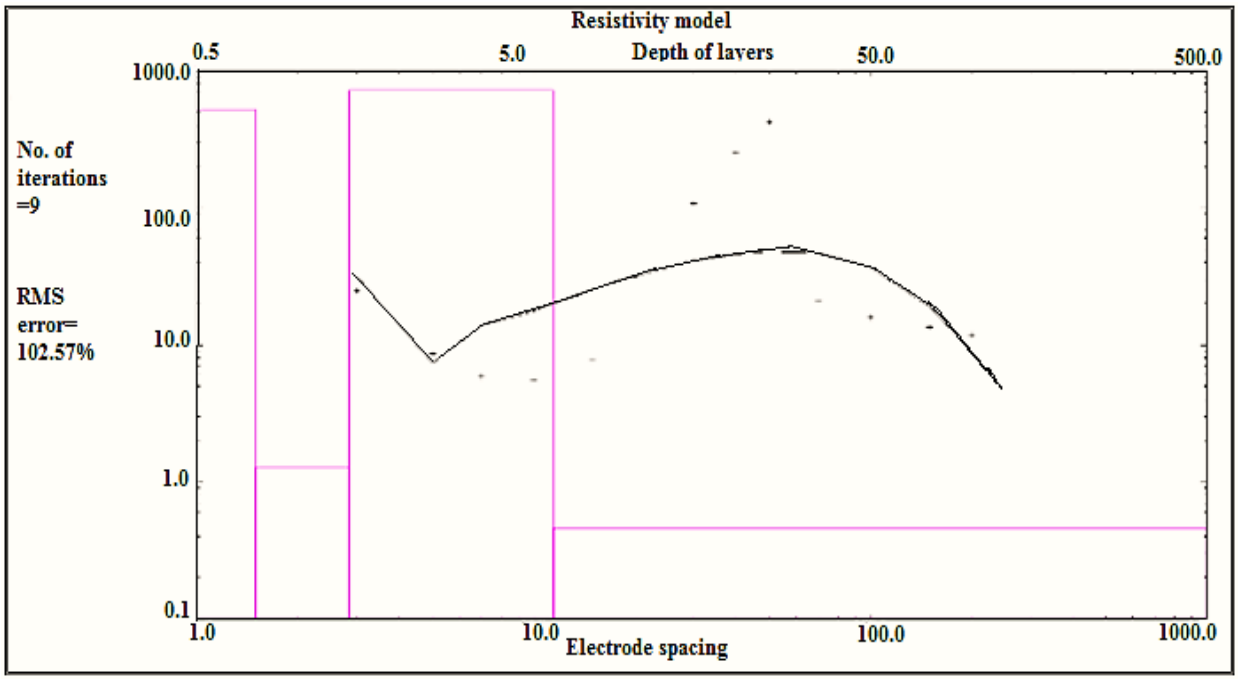

Figure C.1.8: YO 2 E-W drill-well forward model (user-provided parameters)

APPENDIX C.2: NOMINAL RESISTIVITIES FOR COMMON EARTH MATERIALS

Table C.2, shows the nominal apparent resistivities for common earth materials. The list has apparent resistivities for this project's rock types including sandstones and coal.

Table C.1: Nominal resistivities for common earth materials, after (Rahim. 2013)

Material	Nominal resistivity (Ωm)
Sulphides:	
Chalcopyrite	1.2×10^{-5}–3×10^{-1}
Pyrite	2.9×10^{-5}–1.5
Pyrrhotite	7.5×10^{-6}–5×10^{-2}
Galena	3×10^{-5}–3×10^{2}
Sphalerite	1.5×10^{7}
Oxides:	
Hematite	3.5×10^{-3}–10^{7}
Limonite	10^{3}–10^{7}
Magnetite	5×10^{-5}–5.7×10^{3}
Ilmenite	10^{-3}–5×10
Quartz	3×10^{2}–10^{6}
Rock salt	3×10–10^{13}
Anthracite	10^{-3}–2×10^{5}
Lignite	9–2×10^{2}
Granite	3×10^{2}– $\times 10^{6}$
Granite (weathered)	3×10–5×10^{2}
Syenite	10^{2}–10^{6}
Diorite	10^{4}–10^{5}
Gabbro	10^{3}–10^{6}
Basalt	10–1.3×10^{7}
Schists (calcareous and mica)	20–10^{4}
Schist (graphite)	10–10^{2}
Slates	6×10^{2}–4×10^{7}
Marble	10^{2}–2.5×10^{8}
Consolidated shales	20–2×10^{3}
Conglomerates	2×10^{3}–10^{4}
Sandstones	1–7.4×10^{8}
Limestones	5×10–10^{7}
Dolomite	3.5×10^{2}–5×10^{3}
Marls	3–7×10
Clays	1–10^{2}
Alluvium and sand	10–8×10^{2}
Moraine	10–5×10^{3}
Sherwood sandstone	100–400
Soil (40% clay)	8
Soil (20% clay)	33
Top soil	250–1700
London clay	4–20
Lias clay	10–15
Boulder clay	15–35
Clay (very dry)	50–150
Mercia mudstone	20–60
Coal measures clay	50
Middle coal measures	>100
Chalk	50–150
Coke	0.2–8
Gravel (dry)	1400
Gravel (saturated)	100
Quaternary/Recent sands	50–100

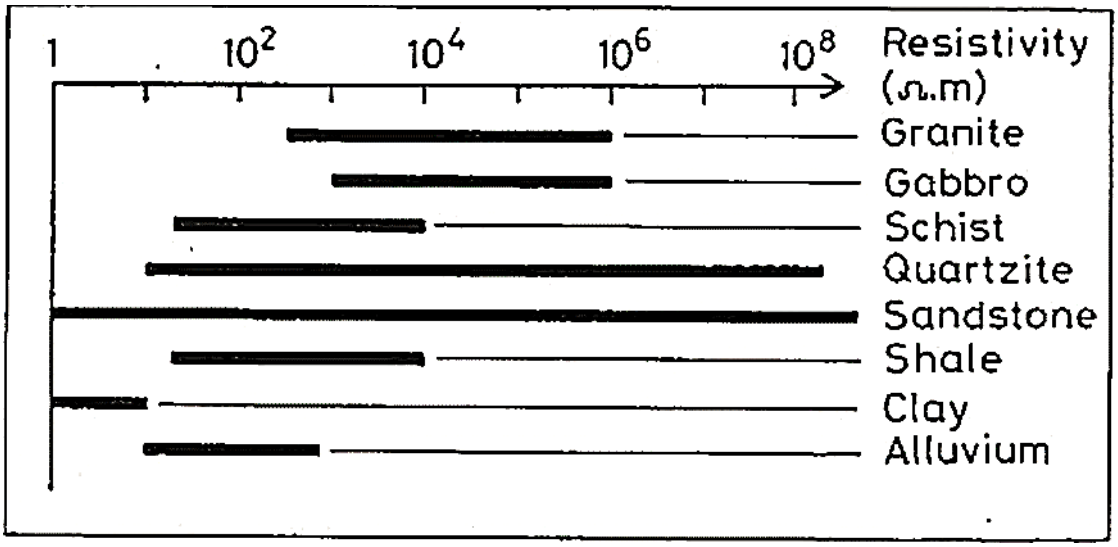

Figure C.1: Graphical representation for ranges for apparent resistivities for common rock types, after (Rahim, 2013)